BASIN-FILL STRATIGRAPHY, QUATERNARY HISTORY, AND PALEOMAGNETICS OF THE EAGLE FLAT STUDY AREA, SOUTHERN HUDSPETH COUNTY, TEXAS

by

M. L. W. Jackson, R. P. Langford, and M. J. Whitelaw

Final Report prepared for

Texas Low-Level Radioactive Waste Disposal Authority
under Interagency Contract Number IAC(92-93)-0910

Bureau of Economic Geology
W. L. Fisher, Director
The University of Texas at Austin
Austin, Texas 78713-7508

November 1993

QAe7704

CONTENTS

Appendices

Figures

Tables

Plates (in pocket)

EXECUTIVE SUMMARY

Data and analyses of basin-fill stratigraphy, paleomagnetics, Quaternary history, and pseudo-fissures/fissures were acquired and interpreted by the Bureau of Economic Geology (BEG) in the Eagle Flat study area in southern Hudspeth County, Texas. These investigations were funded by the Texas Low-Level Radioactive Waste Disposal Authority (the Authority) as part of the evaluation of a proposed site for the Texas low-level radioactive waste repository. Data and information developed as a result of these investigations will be used to evaluate the proposed waste repository site and surrounding region and to provide data for performance assessment, design, and licensing activities.

Basin-fill sediments are composed predominantly of sandy mud and mud; sands are abundant at the surface in the vicinity of the proposed repository site, and gravels are abundant at the base of the basin fill adjacent to the bedrock. Basin-fill thickness ranges from 163 ft (50 m) on the southeast side of the proposed site to 715 ft (218 m) on the northeast side of the proposed site. Basin-fill thickness is approximately 200 ft (61 m) on the west side of the proposed site. Coarser basin-fill deposits are interpreted as proximal alluvial fans and colluvium, and finer sands and muds are interpreted as ephemeral stream, distal alluvial fan, alluvial flat, and eolian deposits. At the proposed site, near-surface fine gravel and coarse to fine sand deposits exhibit characteristics consistent with fluvial deposition. Some well-sorted fine-grained sands have textures consistent with eolian sediments. Fine-grained sands and muds are interpreted as distal alluvial fan and ephemeral stream deposits.

Buried soils are nearly ubiquitous throughout the basin fill. They commonly exhibit vertisol characteristics such as mud- and sand-filled cracks and slickensides. Calcic horizons, characteristic of semiarid soils, are also common. Sediment texture varies locally in the near surface at the proposed site, and correlation of individual units is difficult beyond a few thousand feet. Channel complexes are from 1 to over 20 ft (0.3 to 6 m) thick and may contain pebble and, less commonly, cobble lenses interbedded with fine to medium sands.

Paleomagnetic analyses of 648 samples from 9 cores and a trench allow correlation between cores and estimates of the ages of the basin-fill sediments. Strong average magnetic susceptibility (MS) measurements suggest that magnetite is an important magnetic mineral in these cores. Magnetic polarity stratigraphic studies generated relatively complete magnetostratigraphies. Core YM-17/53 (672 ft, 205 m) preserves the longest sedimentary record and indicates that sedimentation was initiated in this part of the basin approximately 12 mya. Cores YM-4 and YM-6 preserve records of the Brunhes, Matuyama, Gauss, and Gilbert Chrons, indicating that sediments that now lie 250 ft (76 m) below land surface were deposited about 5.0 mya, and perhaps as early as 5.5 mya. Thickness variations of characteristic magnetozones preserved within the nine cores suggest that sediment accumulation rates averaged 26 to 29 ft per m.y. (8 to 9 m/m.y.) during the last 2.6 m.y. of the Brunhes and Matuyama Chrons. Sediment accumulation during the Gauss Chron (2.65 to 3.55 mya) averaged 79 ft per m.y. (24 m/m.y.), and accumulation during the Gilbert Chron averaged 43 ft per m.y. (13 m/m.y.).

Cores from the north Faskin Ranch area record the gradual burial of a hillside forming part of the south margin of the basin during the Pliocene and Quaternary. The oldest Tertiary sediments were deposited approximately 12 mya. These sediments were cored in YM-17 and YM-63 at the north end of Faskin Ranch. Gravels and sands form the lowest 150 ft (50 m), having accumulated at the base of a steep slope lying along the trend of an inferred normal fault. The gravel clasts are assumed to have formed in alluvial fans that formed along the slope. No evidence, either from seismic data or cores, indicates whether the fault was active (Raney and Collins, 1993) during the period of gravel accumulation, 12 to approximately 5 to 6 mya.

During the succeeding Gauss, Matuyama, and Brunhes Chrons, the basin floor aggraded and expanded to the south, burying the Cretaceous hills and the previously deposited alluvial fans. By 4.5 mya, in the Early Pliocene, deposition had filled NW Eagle Flat basin to an elevation of 4,000 to 4,100 ft. Near the proposed repository site, a low-relief basin floor formed, bounded to the south, near the present trend of the Southern Pacific Railroad tracks, by a series of alluvial fans, inset into a hilly, gently sloping bedrock terrain.

By 2.6 mya, at the end of the Gauss Chron, the basin fill had aggraded to elevations ranging from 4,170 ft (1,270 m) in YM-7 beneath the present-day floor of Grayton Lake, to 4,300 ft (1,310 m) in YM-3 north of Devil Ridge in the west part of Faskin Ranch. Basin-floor sediments had been deposited all the way to the south of the Southern Pacific Railroad tracks. The present-day site of Grayton Lake was an alluvial fan, forming part of a series of fans that extended westward along the present-day course of Blanca Draw.

Little change is recorded in the Faskin Ranch cores during the succeeding Matuyama Chron (2.6 mya to 780,000 mya). The most significant change was the appearance of Grayton Lake, which was probably established about 780,000 yr ago, at the end of the Matuyama Chron, according to the influx of muds recorded at this time in YM-7.

During the Brunhes normal polarity Chron, which has extended from 780,000 yr ago to the present and covers the middle and late Pleistocene, approximately 20 to 30 ft (7 to 10 m) of basin-fill sediments accumulated in northern Faskin Ranch. The basin-floor environment covered the entire proposed repository site, and drainage was generally from northwest to southeast along the present course of Blanca Draw.

Two axes of braided-stream channel have been mapped. One ran from north to south along the east margin of the repository site. A second axis of channel-fill sediments runs north-northwest to south-southeast through the center of the proposed repository site approximately 10 to 20 ft (3 to 6 m) below the surface. Deposition on the proposed repository site was generally sandier in the upper 15 to 20 ft (5 to 7 m), largely as the result of the presence of these braided-channel fills and associated deposits. This period of slow sediment accumulation probably terminated about 100,000 to 300,000 yr ago, when the landscape stabilized and soil-forming processes commenced. The gravel channels probably do not crop out in the basin floor, except where they are incised by the Blanca Wash drainage, because they are everywhere buried beneath the surface on north Faskin Ranch, and because the low-relief, gentle slope of the basin floor is only disturbed by the Blanca Draw drainage.

Eagle Flat Basin sediments are a uniform brown, in contrast to the more variegated colors of the Hueco Basin and Red Light Draw sediments. Eagle Flat sediments, more silt- and sand-rich than those of the Fort Hancock Formation, contain less sand and gravel than these of the Camp Rice Formation.

Surface collapse features in wash-fill deposits on Faskin Ranch, characterized by linear patterns of holes, pipes, and elongate depressions at the surface are believed to be pseudo-fissures, similar to hydrocompaction features by other researchers (Phil Pearthree, personal communication, 1993). The pseudo-fissures occur entirely within the floors of Blanca Draw and its tributaries. No cracks were visible below the pseudo-fissures on Faskin Ranch, and no pseudo-fissures or earth fissures have been identified on the proposed repository site. Surface or near-surface desiccation or hydrocompaction are possible origins for the pseudo-fissures on Faskin Ranch. Cracks formed in the shallow subsurface may concentrate the piping processes and produce the surface depressions.

An earth fissure, called Hoover fissure, is a 0.75-mi (1.2-km) linear group of surface depressions on the northeastern side of the ranch, east of Sand Mountain, that is marked clearly by vegetation on aerial photographs and is longer and wider than the pseudo-fissures. The fissure was trenched in two locations; no extensional crack was recognized below the ground surface. Two calcic horizons that are continuous to the east of the fissure are disrupted below the fissure depressions. The horizons appear to have been dissolved and reprecipitated below the fissure area.

Possible origins of Hoover fissure include desiccation, differential compaction of basin-fill sediments over a bedrock escarpment, faulting, and ground-water withdrawal. Although Hoover fissure is linear and not polygonal, desiccation of clay at depth cannot be ruled out as a cause of the fissure. A difference in compaction rates on two sides of a postulated buried bedrock knob beneath the fissure area could also have caused its formation. Hoover fissure does not appear to have been caused by fault activity, because there is no vertical offset of adjacent walls. A resistivity survey run perpendicular to the fissure showed no fault signature, and no Quaternary

faults are known in the area. Hoover fissure could not be caused by overpumping of aquifer zones in the region, since this type of pumping has not occurred, but tensional cracking at depth due to subsidence caused by natural ground-water withdrawal related to incision of the Rio Grande drainage as it was integrated into the Gulf of Mexico about 2.1 mya cannot be precluded.

INTRODUCTION

Purpose and Location of Study

The four sections of this report, basin-fill stratigraphy, paleomagnetics, Quaternary history, and pseudo-fissures/fissures, concern data acquired and interpretations made by the Bureau of Economic Geology (BEG) in the Eagle Flat study area in southern Hudspeth County, Texas, during 1992 and the first 8 months of 1993 (fig. 1). These investigations were funded by the Texas Low-Level Radioactive Waste Disposal Authority (the Authority) as part of the characterization of a proposed site for the Texas low-level radioactive waste repository. Data and information developed as a result of these investigations will be used to evaluate the proposed waste repository site and surrounding region and to provide data for performance assessment, design, and licensing activities.

The proposed site, located on the northern part of Faskin Ranch near Sierra Blanca, Texas (fig. 2), was the focus of most of the study. However, this report also includes the results of investigations on other parts of the ranch and in the adjacent region.

Geologic Setting

The regional geologic setting of the Eagle Flat study area was discussed by Raney and Collins (1993), and the summary given here is taken from that report. Eagle Flat Basin and the surrounding area are located within the Basin and Range geologic province in Trans-Pecos

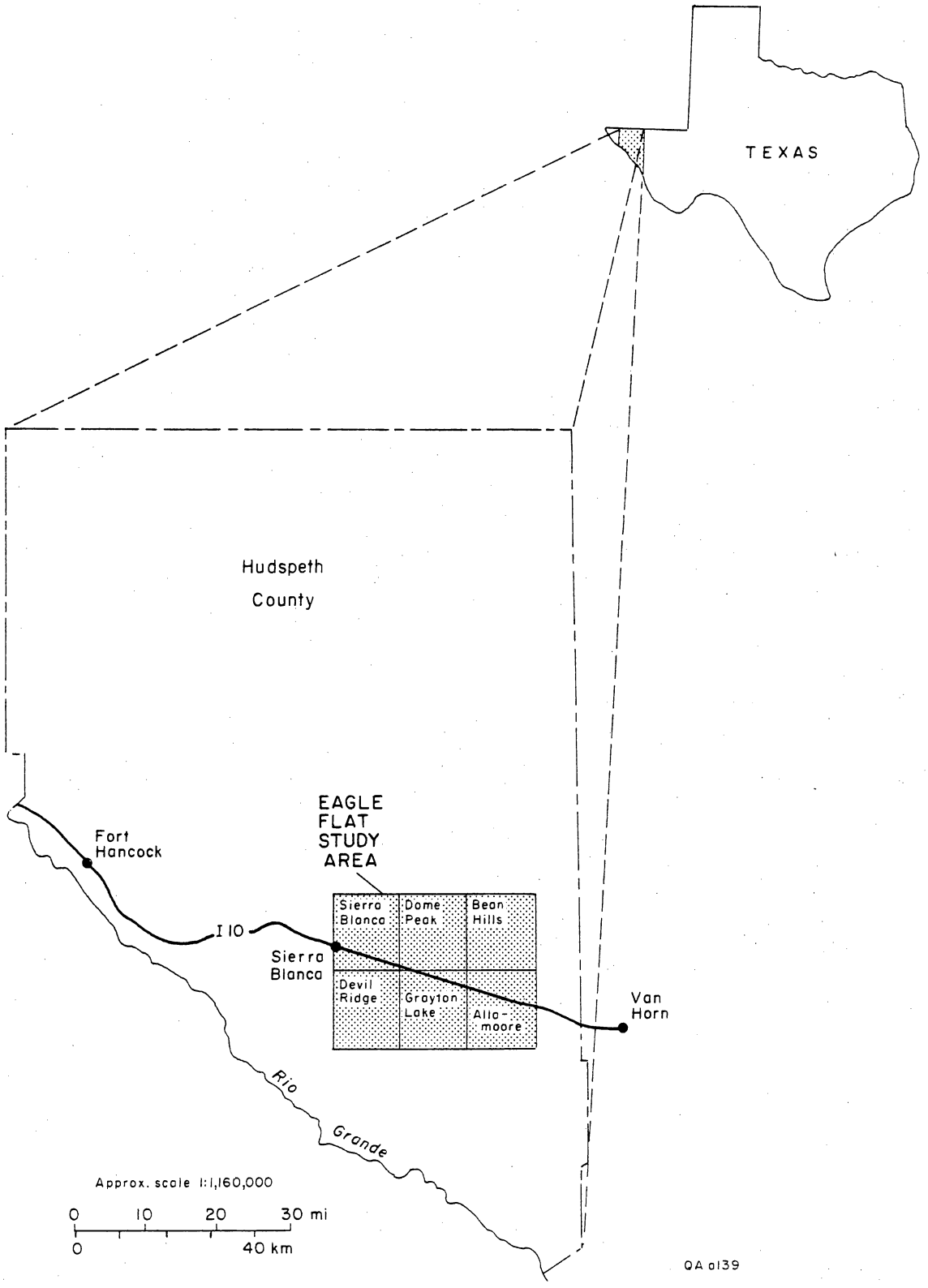

Figure 1. Map showing area designated by the Texas Legislature, the Eagle Flat study area, in Hudspeth County, Texas, and the six U.S. Geological Survey topographic quadrangle maps (1:24,000 scale) that comprise the area.

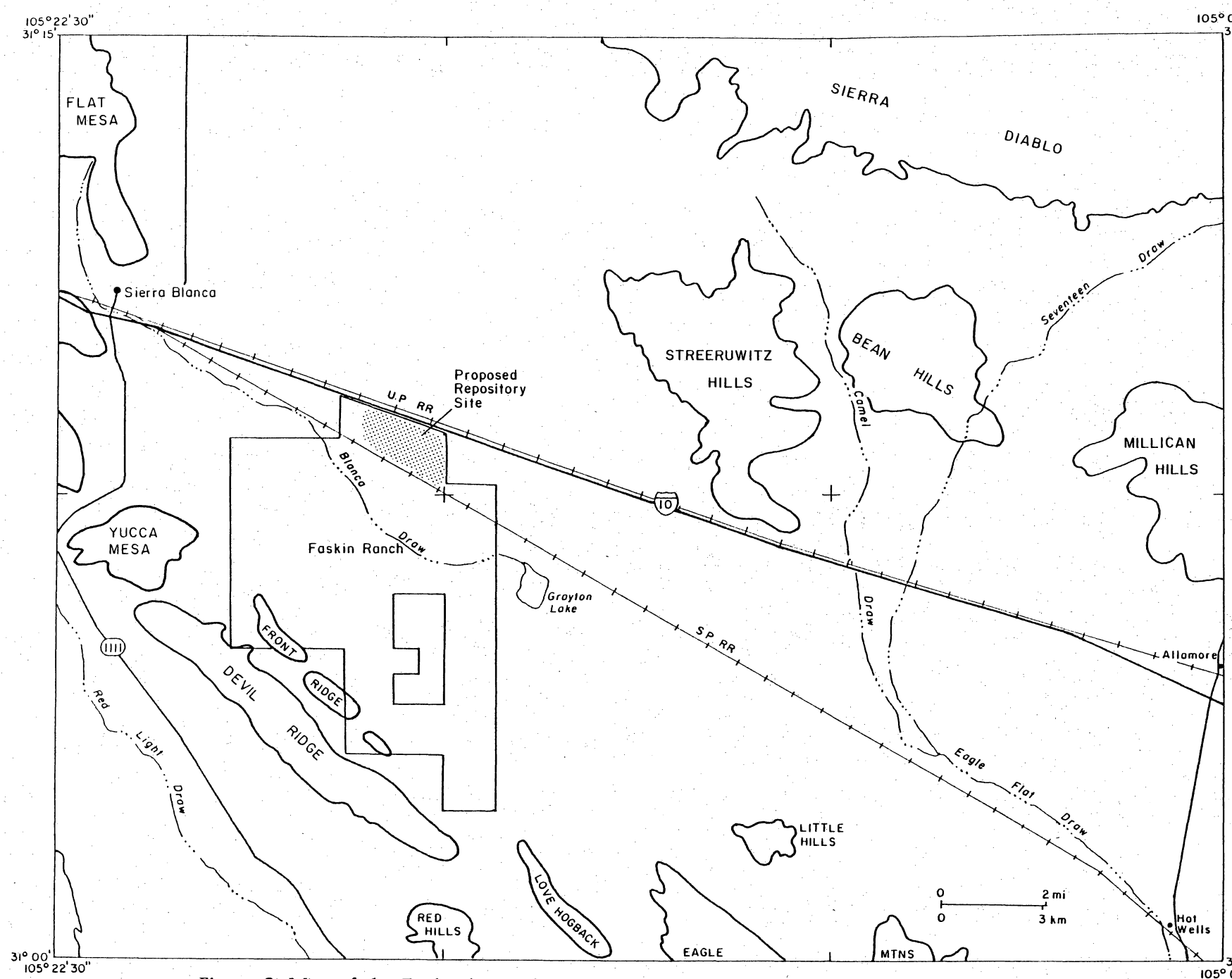

Figure 2. Map of the Eagle Flat study area showing major physiographic and cultural features, approximate boundary of Faskin Ranch, and the proposed repository site.

QA al41

Texas. The geologic features of the area record a long history of geologic events, beginning with the Precambrian, more than 570 mya.

The oldest rocks in the Faskin Ranch area occur in the southern Streeruwitz Hills about 6 mi (15 km) east of the proposed site. These rocks, called the Carrizo Mountain Group, are metasedimentary and metaigneous rocks that may be 1,200 to 1,300 mya (Denison, 1980). Orogenic activity in the region, designated as the Grenville event, may have occurred from 1,000 to 1,135 mya (Copeland and Bowring, 1988; Denison and Hetherington, 1969) and probably established a northwest structural grain that was reactivated in the late Cretaceous and late Tertiary periods of deformation (King and Flawn, 1953; Muehlberger, 1980).

The Paleozoic (570 to 250 mya) era is represented in the region by marine sedimentation and periods of mild uplift and subsidence. During the Late Paleozoic, the Diablo Platform, located north of the proposed site, was uplifted in the foreland of the Ouachita-Marathon structural orogenic belt. In the Mesozoic (250 to 63 mya), the Chihuahua Trough developed as a large depositional basin to the southwest of the Diablo Platform, and was subsequently folded and faulted by the Laramide orogeny during late Cretaceous and early Tertiary time. At about 30 mya the regional stress regime became extensional. Eagle Flat and other Cenozoic basins in the region formed in response to this extension (see Raney and Collins [1993] for details). Magmatism, which began prior to extension, continued through 17 mya. Although some of the adjacent basins, such as the Hueco Bolson, have continued to subside in the Quaternary, there is no evidence of Quaternary fault movement in northwest Eagle Flat Basin (Collins and Raney, 1993).

The proposed waste repository site lies within a 200 mi^2 (520 km^2) closed drainage basin that is drained by Blanca Draw and its tributaries into Grayton Lake playa. Tertiary and Quaternary basin-fill sediments attain more than 715 ft (218 m) of thickness in northwest Eagle Flat Basin and overlie Lower Cretaceous, predominantly limestone rocks (see Raney and Collins, 1993). This report discusses the thickness, sedimentary characteristics, age estimates, and proposed origins of the Miocene and Pliocene basin-fill deposits beneath Faskin Ranch.

Basin physiography and drainage characteristics are discussed in the "Quaternary History" section of this report. An analysis of surface-collapse features, known as pseudo-fissures and fissures, is also included.

Climate

Present Climate

The climate at Faskin Ranch is subtropical-arid (Larkin and Bomar, 1983). Average annual rainfall at the nearby town of Sierra Blanca from 1961 to 1990 was 12 inches (30.7 cm) (Owenby and Ezell, 1992). Average annual temperature is 62°F (17°C); the average summer high is 92°F (33°C) and the average winter low is 28°F (–2°C) (Owenby and Ezell, 1992). Average pan evaporation in nearby Ysleta, Texas, is 84 inches/year (213 cm/yr), approximately 8 times the average precipitation (Larkin and Bomar, 1983). Evaporation exceeds average precipitation throughout the year, with winter evaporation rates averaging 3.25 inches (8.3 cm) per month and summer rates averaging 10.25 inches (26 cm) per month. Rainfall is concentrated between July and October and largely occurs as convective thunderstorms. For this reason, precipitation probably increases with elevation, as has been demonstrated in other areas of southern New Mexico and West Texas (Gile and others, 1981). Wind and water are the major active erosive agents in the region.

Climatic History

The climate in southern New Mexico and Trans-Pecos Texas has been relatively arid since at least the late Pliocene. Bedded gypsum in ephemeral lake and saline playa deposits and well-developed calcic soils in both Pliocene and early Pleistocene units in the Hueco Bolson indicate an arid to semiarid climate during deposition of these units (Gustavson, 1991). The presence of calcic soils and nodules locally throughout the Eagle Flat Basin fill similarly suggest an arid to

semiarid climate for the last 10 to 12 Ma. Axelrod and Bailey (1976) and Wells and others (1982) reported that pollen typical of arid desert plant species has not been found the southern Basin and Range Province and inferred that an arid climate did not develop until 8,000 to 10,000 yr ago. Gustavson (1991) reconciles these observations with an interpretation of a semiarid to subhumid climate during the Pliocene.

During the early Pleistocene, the climate of the southwestern United States was cooler and more moist than that at present (Hall, 1985). The Late Wisconsinan glacial period extended from 25,000 to 14,000 yr ago (Wells and others, 1982; Hall, 1985). From 14,000 yr ago, at the end of the Wisconsinan, to 10,000 yr ago, the climate became warmer and drier, although somewhat cooler and more moist than that of the present, and a gradual transition occurred from glacial to post-glacial vegetation (Wells and others, 1982; Hall, 1985). Dry woodlands of juniper lasted in the present-day deserts of the Southwest until 8,000 to 10,000 yr ago (Axelrod and Bailey, 1976; Van Devender and Spaulding, 1979; Wells and others, 1982). Woodlands persisted in the Hueco Basin, immediately west of Eagle Flat, until 8,000 to 4,000 yr ago, when they were replaced by grasses (Horowitz and others, 1981). Because the Eagle Flat and Red Light Draw Basins are at higher elevations than the Hueco Bolson, dry woodlands should have persisted near the proposed site for a length of time at least equal to that in the Hueco Basin. To the north, wetter climatic regimes and woodlands persisted even longer, to about 5,000 yr ago in the San Augustin Plains of New Mexico (Markgraf and others, 1984) and to about 5,800 yr ago in Chaco Canyon (Hall, 1977).

A long-lasting hot and dry period is recorded in much of the Southwest from approximately 7,000 to 5,000 yr ago (Antevs, 1948). After that, desert shrubs and grasslands alternated as the climate alternated between wetter and drier periods (Freeman, 1972; Horowitz and others, 1981; Hall, 1985). The climate was arid from 8,000 to about 4,000 to 3,000 yr ago, and from 2,200 yr ago to the present (Freeman, 1972; Van Devender and Spaulding, 1979; Horowitz and others, 1981; Hall, 1985). The climate was wetter from about 2,500 to 2,200 yr ago (Bryant and Holloway, 1985). Within the current arid climatic regime,

short periods of slightly more moist conditions have occurred. Horowitz and others (1981) describe a wetter period from 1,000 to 500 yr ago and then a brief moist period from 1,610 to 1,660 yr ago.

Methods

To characterize the basin-fill stratigraphy, approximately 9,384 ft (2,860 m) of core and cuttings from 88 stratigraphic and hydrologic boreholes and 1,317 ft^2 (122 m^2) of section in 8 trenches on the Faskin Ranch property were described, photographed, and sampled (plate 1a and 1b, fig. 3, table 1, app. A). Core recovery averaged 95 percent, with the greatest losses being concentrated in sand and gravel zones. Grain size was visually estimated and confirmed by laboratory analyses of representative samples. For the Quaternary history of the region, surficial deposits of the six-quadrangle area that includes the proposed site were mapped and described (see Langford, 1993). Core, trench, and outcrop samples were analyzed for grain size using sieve, rapid sediment analyzer, Coulter counter, and hydrometer methods described in the Quality Assurance manuals of the Bureau of Economic Geology. Mineralogy of clays was determined by X-ray diffraction, and soil structures were examined in thin section.

BASIN-FILL STRATIGRAPHY

Characterization of basin-fill stratigraphy was determined from examination of continuous cores from surface to bedrock distributed throughout the area on and near the proposed site (fig. 4). Shallow basin-fill characteristics in the vicinity of the proposed waste repository were determined from closely spaced boreholes to a depth of 34 ft (10 m) (fig. 5). Most of the basin-fill sediments are sandy mud and mud (see appendix A); sands are most abundant near and at the surface in the vicinity of the waste repository (see Langford, 1993), and gravels are most abundant at the base of the basin fill adjacent to the bedrock.

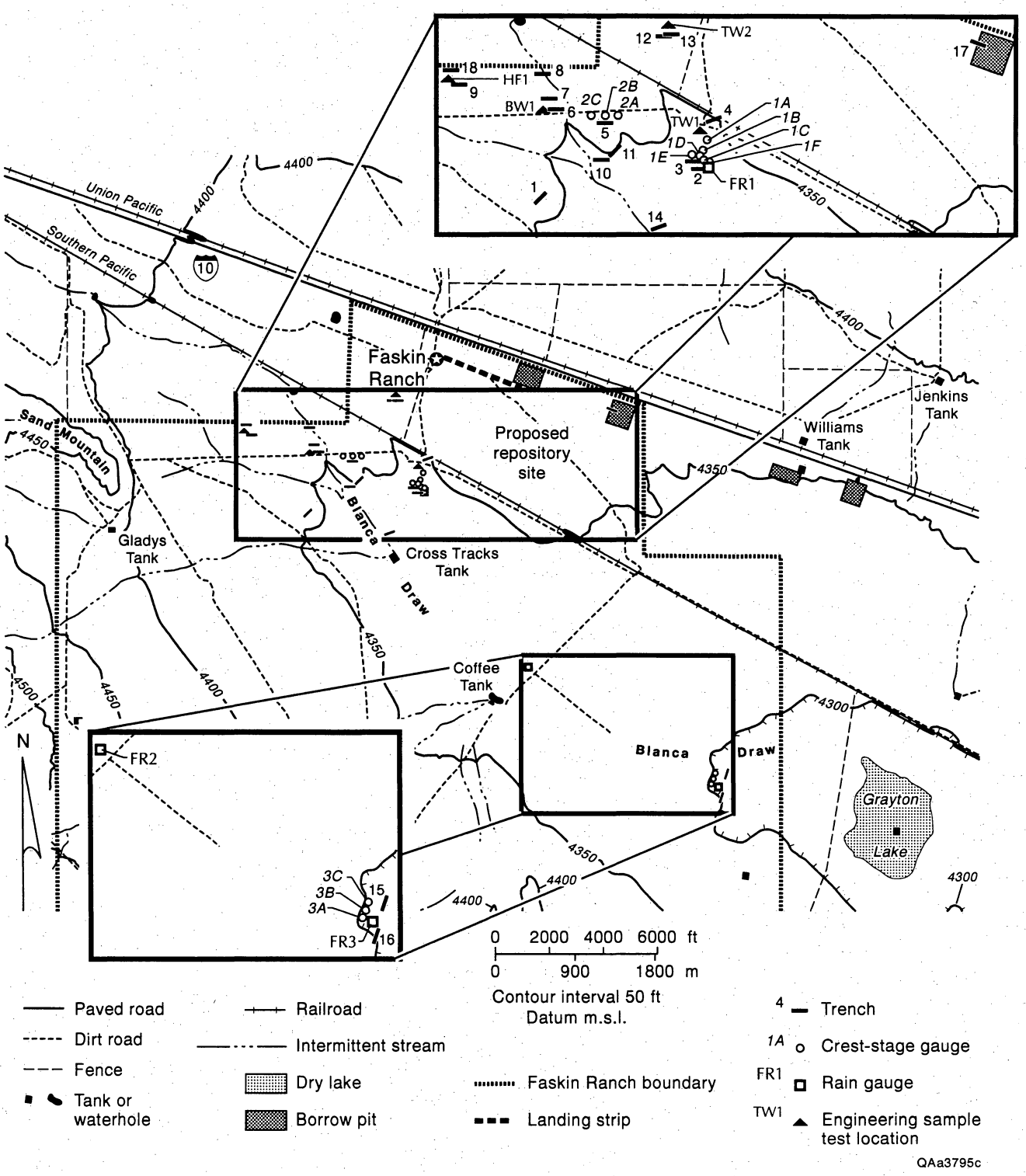

Figure 3. Northern portion of Faskin Ranch showing locations of trenches, crest-stage gauges, rain gauges, and engineering test sample locations.

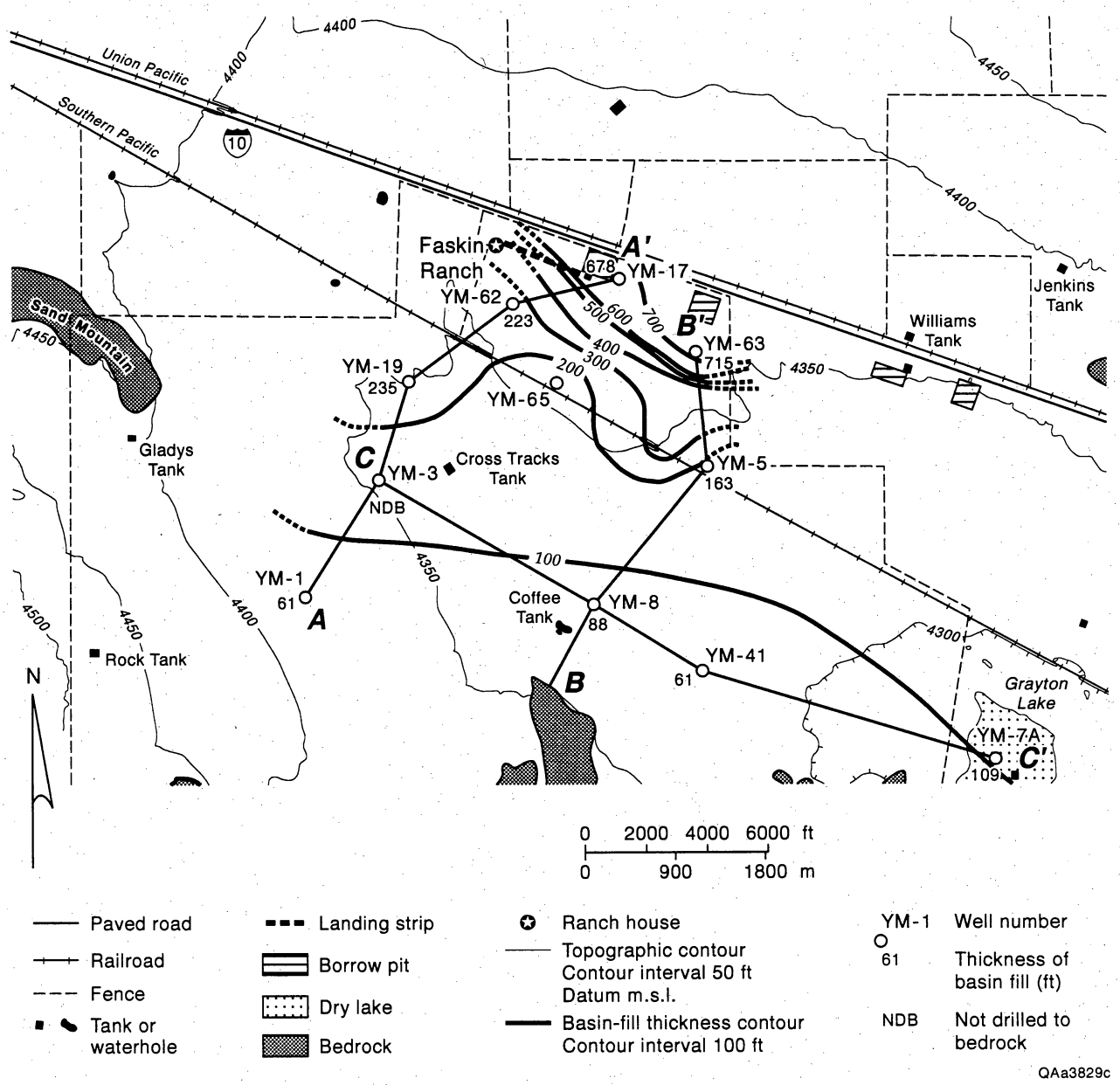

Figure 4. Isopach map of basin-fill sediments and cross section locations, northern Faskin Ranch. Contours based on data shown and data given in Paine and others (1993).

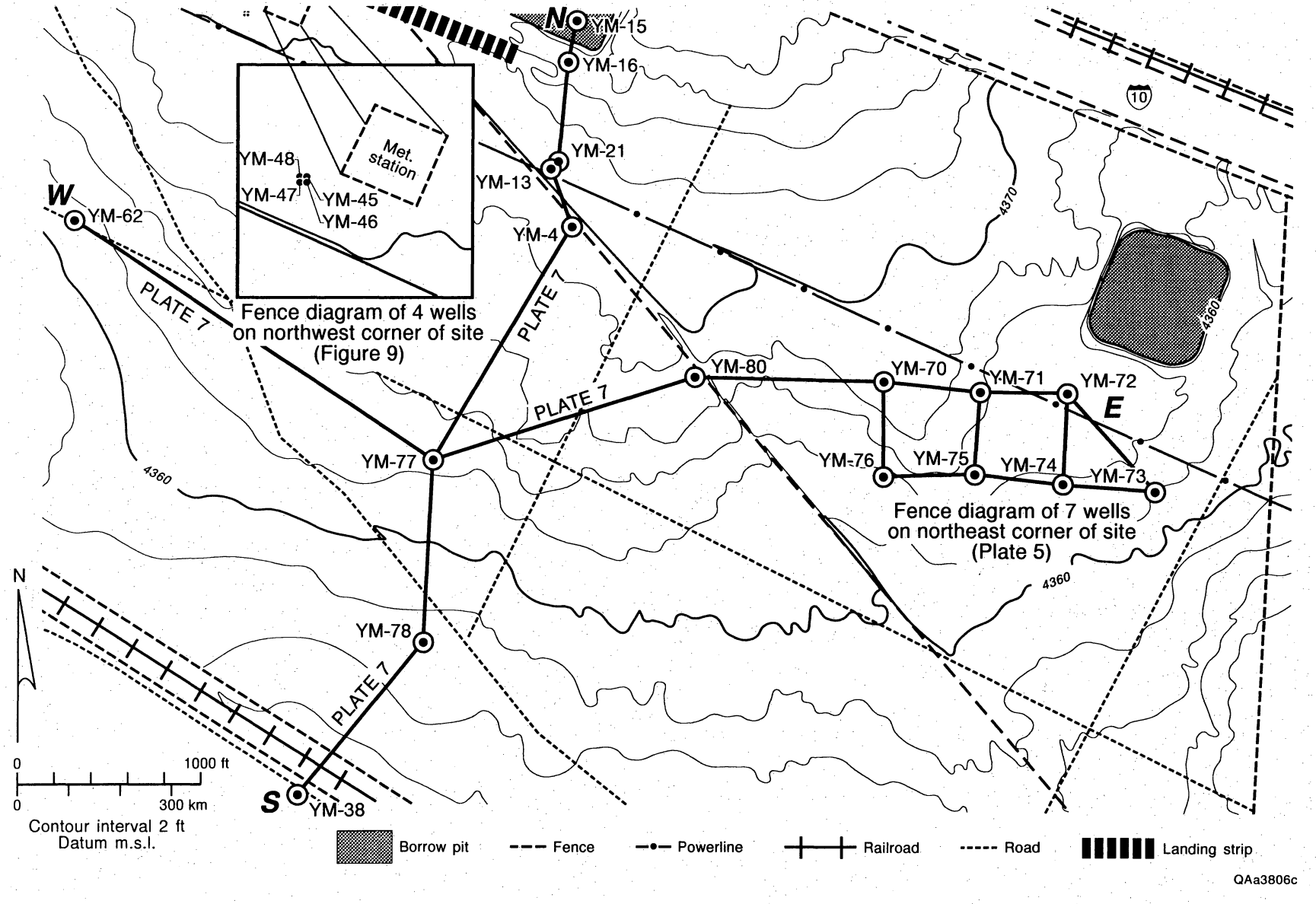

Figure 5. Location map of cross sections on the proposed repository site, northern Faskin Ranch.

Table 1. Eagle Flat and Faskin Ranch borehole summary.

Hole number	Total depth (ft)	Core (ft)	Primary purpose[1]	Depth to bedrock (ft)	Depth to P.S.[2] (ft)	Company or agency	Analyses[3]	Location
YM-1	150	150	S	61		BEG	Paleomag., Text.	Southern Faskin Ranch
YM-2	100	100	S	67		BEG	Paleomag., Text.	Southern Faskin Ranch
YM-3	151	151	S			BEG	Paleomag., Text.	Southern Faskin Ranch (near draw)
YM-4	250	250	S			BEG	Paleomag., Text.	Footprint
YM-5	201	201	S	163		BEG	Paleomag., Text.	Footprint (south)
YM-6	251	251	S			BEG	Paleomag., Text.	N. Faskin Ranch (W of house)
YM-7	612	612	S	109		BEG	Paleomag., Text.	Grayton Lake
YM-7A	880	C[4]	M		657	BEG	Monitor well	Grayton Lake, hole 7 twin
YM-8	1018	135[5]	M	88	672	BEG	Monitor well	Coffee Tank
YM-9	48	48	V			BEG	Moist., WatPot., Text., Chl.	Coffee Tank (bank scarp)
YM-10	34	34	V			BEG	Moist., WatPot., Chl.	Coffee Tank (bank scarp)
YM-11	31	31	V			BEG	Moist., WatPot., Text., Chl.	Coffee Tank (draw)
YM-12	19	19	V			BEG	Moist., WatPot., Text., Chl.	Coffee Tank (draw)
YM-13	37	37	V			BEG	Moist., WatPot., Text., Chl.	Power line (Qe_2)
YM-14	31	31	V			BEG	Moist., WatPot., Text., Chl.	Met. station (Qe_1)
YM-15	54	54	V			BEG	Moist., WatPot., Text., Chl.	West borrow pit (inside)
YM-16	48	48	V			BEG	Moist., WatPot., Text., Chl.	West borrow pit (outside)
YM-17	695	695	S	678		BEG	Paleomag., Text.	East of West borrow pit
YM-18	835	C[4]	M		747	BEG	Monitor well	East of West borrow pit, hole 17 twin
YM-19	822	285[5]	M	235	725	BEG	Monitor well	S. of tracks between draws
YM-20	14	14	S			BEG	(Descriptive log only)	Met. station (Qe_1) hole 25 twin
YM-21	29	29	S			BEG	(Descriptive log only)	Met. station (Qe_1) hole 20 twin
YM-22	29	29	S			BEG	(Descriptive log only)	Power line (Qe_2) hole 23 twin
YM-23	14	14	S			BEG	(Descriptive log only)	Power line (Qe_2) hole 24 twin
YM-24	16	0	VM			BEG	Neutron Probe	Power line (Qe_2) hole 14 twin
YM-25	17	0	VM			BEG	Neutron Probe	Met. station (Qe_1) hole 13 twin
YM-26	26	0	VM			BEG	Neutron Probe	West borrow pit (inside) hole 15 twin
YM-27	14	14	S			BEG	(Descriptive log only)	S. Faskin Ranch (near draw) hole 28 twin
YM-28	90	90	V			BEG	Moist., WatPot., Text., Chl.	S. Faskin Ranch (near draw) hole 3 twin
YM-29	14	14	S			BEG	(Descriptive log only)	S. of tracks between draws, hole 19 twin
YM-30	46	0	VM			BEG	Neutron Probe	West borrow pit (outside) hole 16 twin

Table 1 (cont.)

Hole number	Total depth (ft)	Core (ft)	Primary purpose[1]	Depth to bedrock (ft)	Depth to P.S.[2] (ft)	Company or agency	Analyses[3]	Location
YM-31	13	13	S			BEG	(Descriptive log only)	Rock Tank (alluvial fan) hole 32 twin
YM-32	9	9	V			BEG	Moist., WatPot., Text., Chl.	Rock Tank (alluvial fan)
YM-33	9	9	S			BEG	(Descriptive log only)	Faskin Well (slope deposits) hole 34 twin
YM-34	9	9	V			BEG	Moist., WatPot., Text., Chl.	Faskin Well (slope deposits)
YM-35	70	70	V			BEG	Moist., WatPot., Text., Chl.	Hoover fissure (outside)
YM-36	101	101	V			BEG	Moist., WatPot., Text., Chl.	Hoover fissure (inside)
YM-37	14	14	S			BEG	(Descriptive log only)	Hoover fissure (outside)
YM-38	14	14	H			BEG	(Descriptive log only)	S. of tracks, S. of footprint (Qe_1)
YM-39	29	29	S			BEG	(Descriptive log only)	S. of tracks, S. of footprint (Qe_2)
YM-40	14	14	S			BEG	(Descriptive log only)	E. of Coffee Tank (mesquite) hole 41 twin
YM-41	79	79	V	61		BEG	Moist., WatPot., Text., Chl.	E. of Coffee Tank (mesquite)
YM-42	14	14	S			BEG	(Descriptive log only)	E. of Coffee Tank (grass flats) hole 43 twin
YM-43	81	81	V			BEG	Moist., WatPot., Text., Chl.	E. of Coffee Tank (grass flats)
YM-44	24	24	S			BEG	Text.	E. of footprint, hole DMB-29 twin
YM-45	39.2	39.2	V			BEG	H_2O Sat.	Near Met. Station
YM-46	31	31	V			BEG	H_2O Sat.	Near Met. Station
YM-47	24.1	24.1	V			BEG	H_2O Sat.	Near Met. Station
YM-48	13.7	13.7	V			BEG	H_2O Sat.	Near Met. Station
YM-49	47	0	VM			BEG	Psychrometers	Near Met. Station
YM-50	47	0	VM			BEG	Psychrometers	Near Met. Station
YM-51	34.1	34.1	S			BEG	(Descriptive log only)	South of tracks between draws, SW of 19
YM-52	34.2	34.2	S			BEG	(Descriptive log only)	South of tracks between draws, NE of 19
YM-53	34.1	34.1	S			BEG	Paleomag.	North of runway, east of hole 17
YM-54	77.6	77.6	V			BEG	Moist., WatPot., Text., Chl.	NE of Coffee Tank, by hole 11
YM-55	28.15	0	VM			BEG	Neutron Probe	Hoover Fissure (inside)
YM-56	27.75	0	VM			BEG	Neutron Probe	Hoover Fissure (outside)
YM-57	16.8	0	VM			BEG	Neutron Probe	E. of Coffee Tank (mesquite), near hole 40
YM-58	16.7	0	VM			BEG	Neutron Probe	E. of Coffee Tank (grass), near hole 42
YM-59	90.2	90.2	V			BEG	Moist., WatPot., Text., Chl.	Hoover fissure (outside)
YM-60	57.7	0	V			BEG	Moist., Text., Chl., ^{36}Cl	Near Met. Station
YM-61	69.8	0	V			BEG	Moist., Text., Chl., ^{36}Cl	Near Met. Station
YM-62	339	339	S	223		BEG	(Descriptive log only)	West side of footprint, at seismic line loc.
YM-63	1004	1004	H	715	735	BEG	Monitor well	East side of footprint, south of borrow pit

Table 1 (cont.)

Hole number	Total depth (ft)	Core (ft)	Primary purpose[1]	Depth to bedrock (ft)	Depth to P.S.[2] (ft)	Company or agency	Analyses[3]	Location
YM-64	48.2	48.2	V			BEG	Stable isotopes, Tritium	Near Met. Station
YM-65	not drilled yet		S			BEG	(Descriptive log only)	South of footprint, north of tracks
YM-66	44	44	V			BEG	Moist., WatPot., Text., Chl.	Near Met. Station
YM-67	60.7	0	VM			BEG	Psychrometers	Near Met. Station
YM-68	28.4	0	VM			BEG	Neutron Probe	North of Cross Tracks Tank
YM-69	28.2	0	VM			BEG	Neutron Probe	North of Cross Tracks Tank
YM-70	34.1	34.1	V			BEG	Moist., WatPot., Text., Chl.	East side of footprint, near borrow pit
YM-71	34.1	34.1	V			BEG	Moist., WatPot., Text., Chl.	East side of footprint, near borrow pit
YM-72	34.2	34.2	V			BEG	Moist., WatPot., Text., Chl.	East side of footprint, near borrow pit
YM-73	34.2	34.2	V			BEG	Moist., WatPot., Text., Chl.	East side of footprint, near borrow pit
YM-74	34.3	34.3	V			BEG	Moist., WatPot., Text., Chl.	East side of footprint, near borrow pit
YM-75	34	34	V			BEG	Moist., WatPot., Text., Chl.	East side of footprint, near borrow pit
YM-76	34.2	34.2	V			BEG	Moist., WatPot., Text., Chl.	East side of footprint, near borrow pit
YM-77	34.2	34.2	V			BEG	Moist., WatPot., Text., Chl.	West side of footprint
YM-78	34.2	34.2	V			BEG	Moist., WatPot., Text., Chl.	Southwest side of footprint
YM-79	59.6	59.6	V			BEG	Stable isotopes, Tritium	Near met station
YM-80	34.1	34.1	V			BEG	Moist., WatPot., Text., Chl.	North central footprint, by road
YM-81	34.2	34.2	V			BEG	Moist., WatPot., Text., Chl.	Central part of footprint
YM-82	27.85	0	VM			BEG	Neutron Probe	Near Coffee Tank, by hole 11
YM-83	28.05	0	VM			BEG	Neutron Probe	Near Coffee Tank, by hole 12
YM-84	44.4	44.4	V			BEG	Moist., WatPot., Text., Chl.	E. of Coffee Tank (grass flats), hole 42 twin
YM-85	58.6	58.6	V			BEG	Moist., WatPot., Text., Chl.	E. of Coffee Tank (mesquite), hole 40 twin
YM-86	67.7	67.7	V	61		BEG	Moist., WatPot., Text., Chl.	E. of Coffee Tank, adjacent to psuedofissure
YM-87	72	72	V	59		BEG	Moist., WatPot., Text., Chl.	E. of Coffee Tank, in psuedofissure
YM-88	43.7	43.7	V			BEG	Moist., WatPot., Text., Chl.	Hoover fissure (inside)
YM-89	39.4	39.4	V			BEG	Moist., WatPot., Text., Chl.	NE of Coffee Tank, by hole 12
DMB-1	100	0[6]	E			D&M	Geotech.	West side of footprint
DMB-2	100	0	E			D&M	Geotech.	North side of footprint
DMB-3	100	0	E			D&M	Geotech.	West side of footprint
DMB-4	100	0	E			D&M	Geotech.	West side of footprint
DMB-5	25	0	E			D&M	Geotech.	North side of footprint
DMB-6	25	0	E			D&M	Geotech.	North side of footprint
DMB-7	25	0	E			D&M	Geotech.	North side of footprint

Table 1 (cont.)

Hole number	Total depth (ft)	Core (ft)	Primary purpose[1]	Depth to bedrock (ft)	Depth to P.S.[2] (ft)	Company or agency	Analyses[3]	Location
DMB-8	25	0	E			D&M	Geotech.	North side of footprint
DMB-9	25	0	E			D&M	Geotech.	North side of footprint
DMB-10	25	0	E			D&M	Geotech.	North side of footprint
DMB-11	25	0	E			D&M	Geotech.	North side of footprint
DMB-12	25	0	E			D&M	Geotech.	North side of footprint
DMB-13	25	0	E			D&M	Geotech.	North side of footprint
DMB-14	25	0	E			D&M	Geotech.	North side of footprint
DMB-15	25	0	E			D&M	Geotech.	West side of footprint
DMB-16	25	0	E			D&M	Geotech.	West side of footprint
DMB-17	25	0	E			D&M	Geotech.	West side of footprint
DMB-18	100	0	E			D&M	Geotech.	East side of footprint
DMB-19	100	0	E			D&M	Geotech.	Center of footprint
DMB-20	35	0	E			D&M	Geotech.	Center of footprint
DMB-21	35	0	E			D&M	Geotech.	Center of footprint
DMB-22	25	0	E			D&M	Geotech.	South side of footprint
DMB-23	35	0	E			D&M	Geotech.	South side of footprint
DMB-24	35	0	E			D&M	Geotech.	East side of footprint
DMB-25	35	0	E			D&M	Geotech.	East side of footprint
DMB-26	25	0	E			D&M	Geotech.	West side of footprint
DMB-27	100	0	E			D&M	Geotech.	South side of footprint
DMB-28	100	0	E			D&M	Geotech.	East side of footprint
DMB-29	100	0	E			D&M	Geotech.	East side of footprint
DMB-30	35	0	E			D&M	Geotech.	Center of footprint
DMB-31	35	0	E			D&M	Geotech.	Center of footprint
DMB-32	35	0	E			D&M	Geotech.	South side of footprint
DMB-33	35	0	E			D&M	Geotech.	West side of footprint
DMB-34	35	0	E			D&M	Geotech.	West side of footprint

[1] S=Stratigraphic, M=Hydrologic, saturated zone monitor well, E= Engineering, V=Vadose zone sampling, VM=Vadose zone monitoring
[2] Potentiometric Surface
[3] Paleomag.=Paleomagnetic stratigraphy, Moist.=Moisture content, WatPot.=Water potential, Text.=Texture (grain size), Chl.=Chloride, Geotech.=geotechnical, H_20 Sat.=Volumetric moisture content, ^{36}Cl=^{36}Cl
[4] Cuttings were collected from base of cored interval to total depth
[5] Cuttings were collected for entire hole.
[6] Samples for geotechnical testing were collected every 5 ft. No other core or cuttings were taken.

Faskin Ranch (Eagle Flat Study Area)

Thickness

Basin fill thickens from the Cretaceous outcrops to the south, west, and northeast of Faskin Ranch into the center of northwest Eagle Flat Basin (fig. 4 and plate 2). Although Grayton Lake is topographically the lowest point in the basin, boreholes and gravity surveys indicate that the thickest basin fill is located north and northwest of the ranch (Julie Whitelaw, written communication, 1993). Basin-fill thickness can vary rapidly over short distances (fig. 4 and plate 3). From a thickness of 715 ft (218 m) on the northern side of Faskin Ranch, the basin-fill sediment thins southward to 163 ft (50 m) at the railroad tracks, over a distance of 0.75 mi (1.2 km). The basin fill pinches out against bedrock farther to the south and east at the Grayton Lake, Front Ridge, and Sand Mountain bedrock exposures (fig. 4) and against bedrock covered by a thin residuum over much of the area south of Blanca Draw.

Textures, Environments of Deposition, and Mineralogy

The most common grain size of the basin fill is silt and clay (finer than 250-mesh sieve) (plate 4, sandy mud and mud unit, fig. 6). A typical core (fig. 7) contains an upper section, tens to hundreds of feet long, of alternating units of sandy mud and mud from inches to feet in thickness. Sediment having little or no sand fraction (0.015 inches or 0.6 mm in diameter, passing the 250-mesh sieve) was classified as mud. Sediment having more than 50 percent silt and clay, but an appreciable amount of sand was classified as sandy mud. Sediment having 20 to 50 percent silt and clay and 50 to 80 percent sand-sized clasts or larger was classified as muddy sand. Sediment having 80 percent or more sand-sized clasts was classified as sands. Deeper in the core, nearer the top of bedrock, muddy sands and sands from a few inches to 1 or 2 ft thick are more common. At the base of the basin-fill deposits, silty gravel and gravel units become abundant. The gravels commonly contain clasts derived from the underlying bedrock. At the

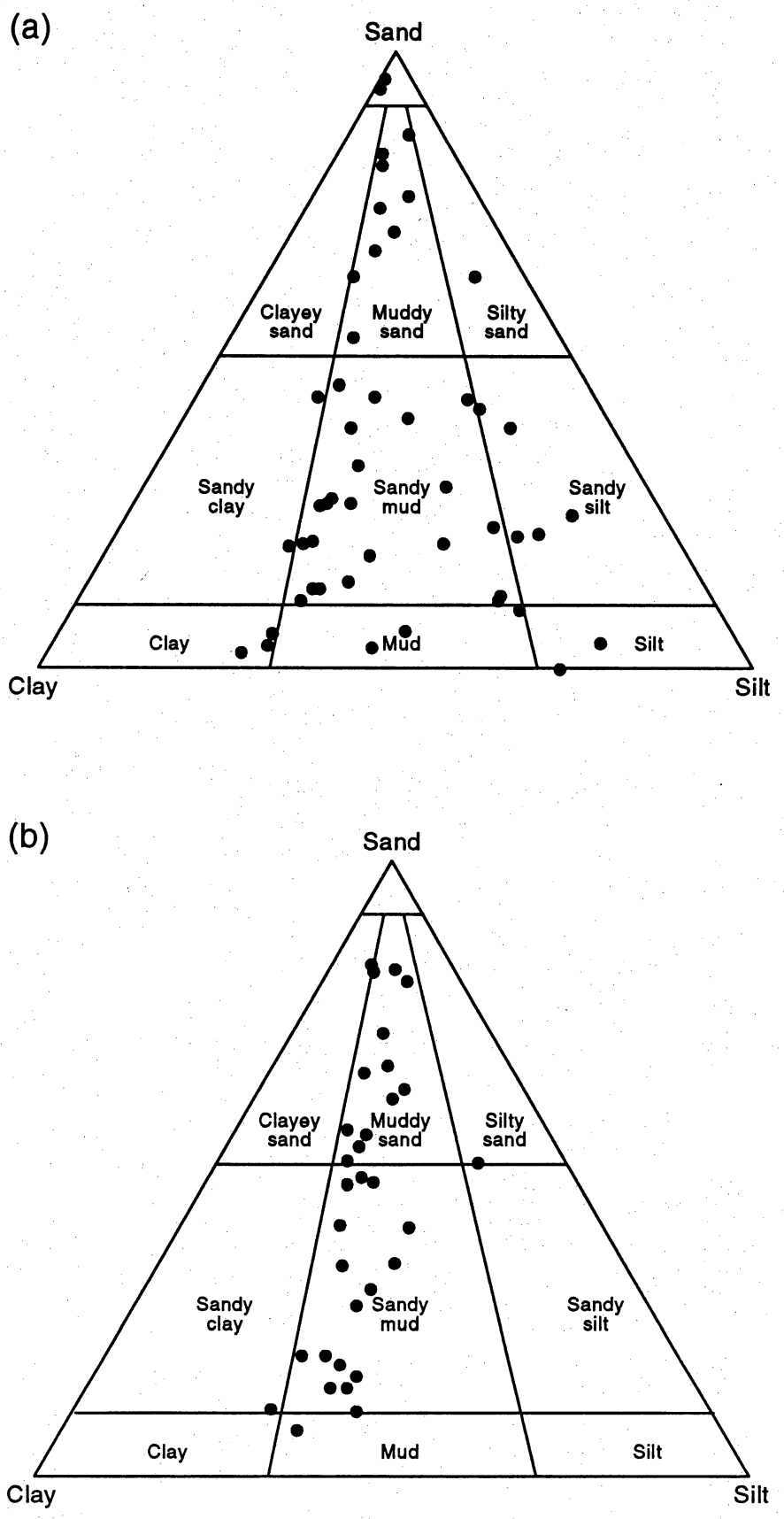

Figure 6. Textural classification of sediments from (a) cores and (b) trenches on Faskin Ranch. Dominant grain size is sandy mud and muddy sand. See app. B for sample depths. Gravel content in samples shown is <2 percent. Sand is 2 to 0.0625 mm, silt is 0.0625 to 0.0039 mm, and clay is <0.0039 mm. Classification adapted from Folk (1968).

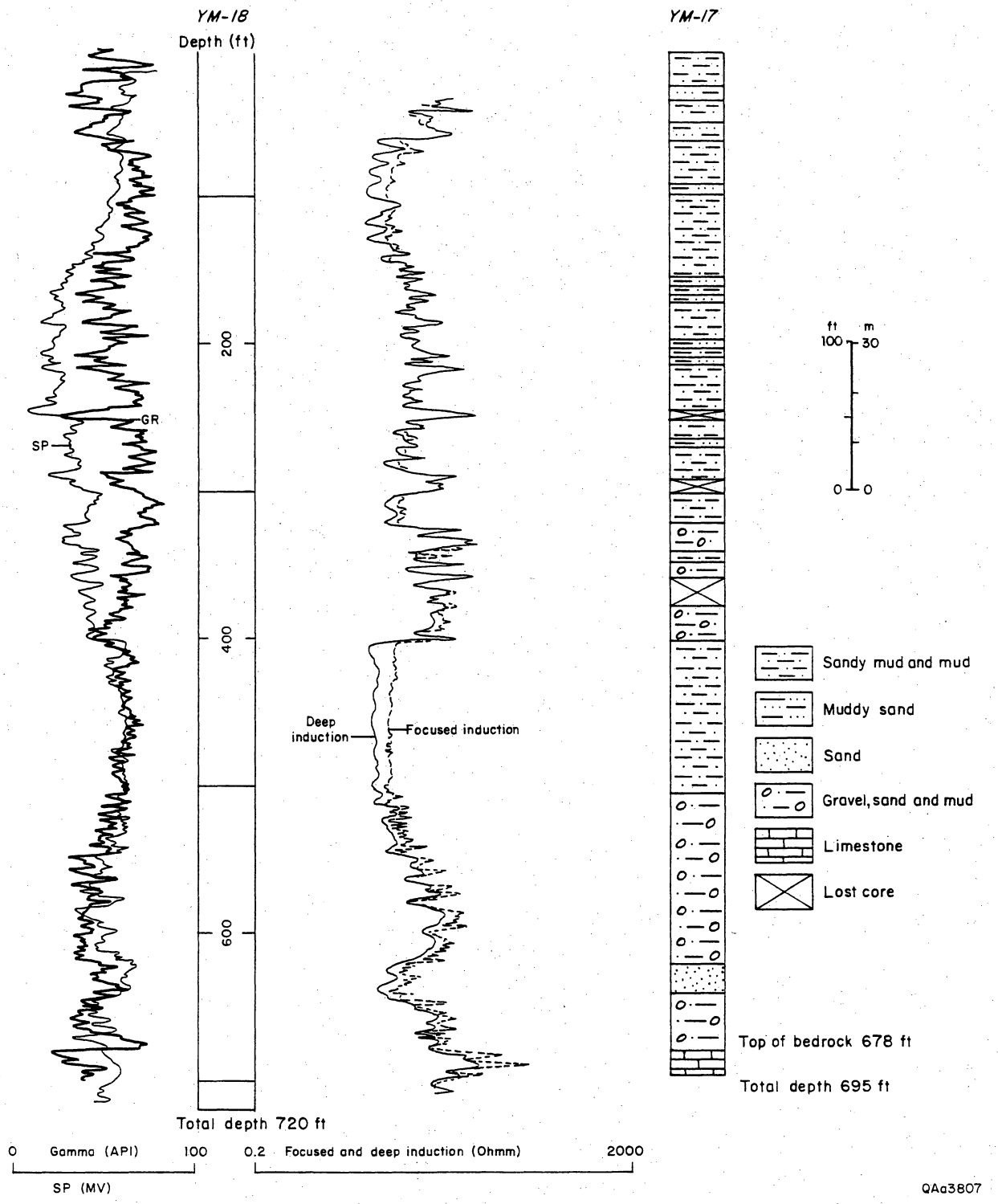

Figure 7. Example core log from borehole YM-17 and companion geophysical log from borehole YM-18, located 10 ft (3 m) away. Boreholes located on plate 1.

proposed repository site, sand and gravel are also locally present in the upper 50 ft (15 m) of basin fill. Gravel units present at the base of the basin fill appear to be thickest where the fill is thickest, attaining 200 ft (61 m) in borehole YM-17 on the north side of Faskin Ranch (fig. 7).

Sediments in the cores and trenches have been affected considerably by soil-forming processes, so that original sedimentary structures are not commonly preserved. Only in rare occurrences can crossbedding, upward-coarsening, or upward-fining sequences be discerned in the core. Thus, specific interpretations of depositional environments related to particular core sections, such as dune, braided channel-fill, splay, or floodplain/alluvial flat, have not been made. However, general interpretations of depositional processes may be made based on gross grain size and texture distribution.

Fluvial deposits are represented by fine gravels and coarse sand deposits that grade upward into fine sands and muds. Fine and very fine sand is preserved in beds from a few inches (cm) to a few feet (m) thick. In a few cores, upward-coarsening deposits exhibit horizontally laminated silts a few inches (cm) thick overlain by fine and very fine sands up to 2 ft (0.6 m) thick. These deposits are also interpreted as fluvial.

Well-sorted very fine sand deposits from 0.5 to 1 ft (0.1 to 0.3 m) thick that occur at several stratigraphic horizons in the cores are interpreted to be eolian in origin. Several active eolian deposits are evident today to the east of Grayton Lake, and the surface deposits on the northern side of the ranch, which are from 0 to 4 ft (1.2 m) thick, are also interpreted to be eolian (Langford, 1993).

Horizons composed of 40 to 50 percent clay are present throughout the section. The clay layers are from 6 inches (15 cm) to approximately 3 ft (1 m) thick and typically contain abundant root traces. The clays may have accumulated in low areas and represent interchannel environments where sediment accumulated in standing water, or they may have been deposited in a distal alluvial fan environment. The clay-rich strata may also represent the formation of illuvial, "B" soil horizons, which may have formed at shallow depths, 1.5 ft (0.5 m) below the land surface, and are now buried paleosols hundreds of feet below the surface.

Modern sediments in the draws are silt dominated, in contrast to sandier and clayier basin-fill deposits beneath (see Langford, 1993). The silts are a product of the processes that are occurring in the basin today, as explained in the "Quaternary History" section.

The upper section of alternating units of sandy mud and mud in the general basin-fill sequence are interpreted to represent distal alluvial fan, alluvial flat, ephemeral stream, and eolian deposits. Deeper in the core, muddy sands and sands are interpreted as alluvial fan, ephemeral stream, and eolian units laid down when the basin was younger and narrower. At the base of the basin-fill deposits, silty gravel and gravel units are interpreted as proximal alluvial fan and colluvial deposits deposited early in the basin history. Individual upward-coarsening and upward-fining sequences may be the result of fluvial deposition by ephemeral streams and alluvial fan distributary channels. Stream deposits were preserved in axial positions in the basin, and alluvial fan deposits were contributed from bedrock hillsides on the periphery of the basin. As the basin filled, the alluvial fans were buried by the more rapidly aggrading basin floor. In any core, alluvial fan gravels are succeeded by basin-floor muds and muddy sand, recording the burial of the alluvium fans (fig. 8).

The sand mineralogy of the basin-fill sediments is dominated by quartz, with smaller amounts of potassium feldspar, plagioclase, calcite, and a trace of amphibole (app. C). Silts are composed of quartz, potassium feldspar, plagioclase, kaolinite, montmorillonite, and illite. Clays are composed of montmorillonite, illite, and kaolinite (app. C).

Because much of the basin fill is composed of sediments high in silt and clay content, Vertisols have formed, and Vertisol characteristics such as mud- and sand-filled cracks and slickensides on ped faces are locally abundant in core. Calcic nodules, which are characteristic of many soils formed in subhumid and arid climates, occur throughout the basin fill, in some cores occurring continuously over hundreds of feet (meters) of thickness (see app. A).

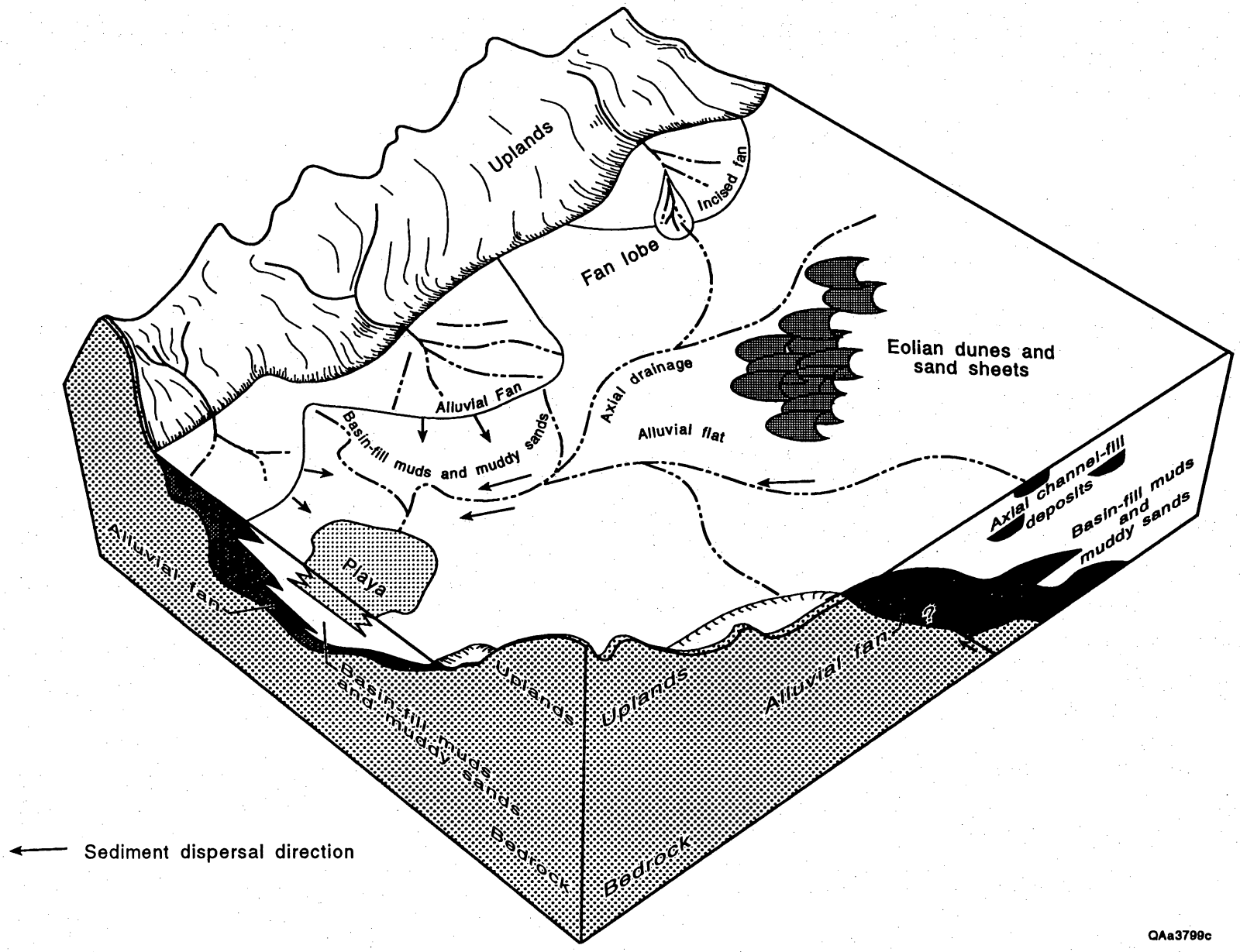

Figure 8. Schematic depositional and physiographic setting of Eagle Flat Basin during deposition of basin-fill sediments (prior to formation of Arispe surface).

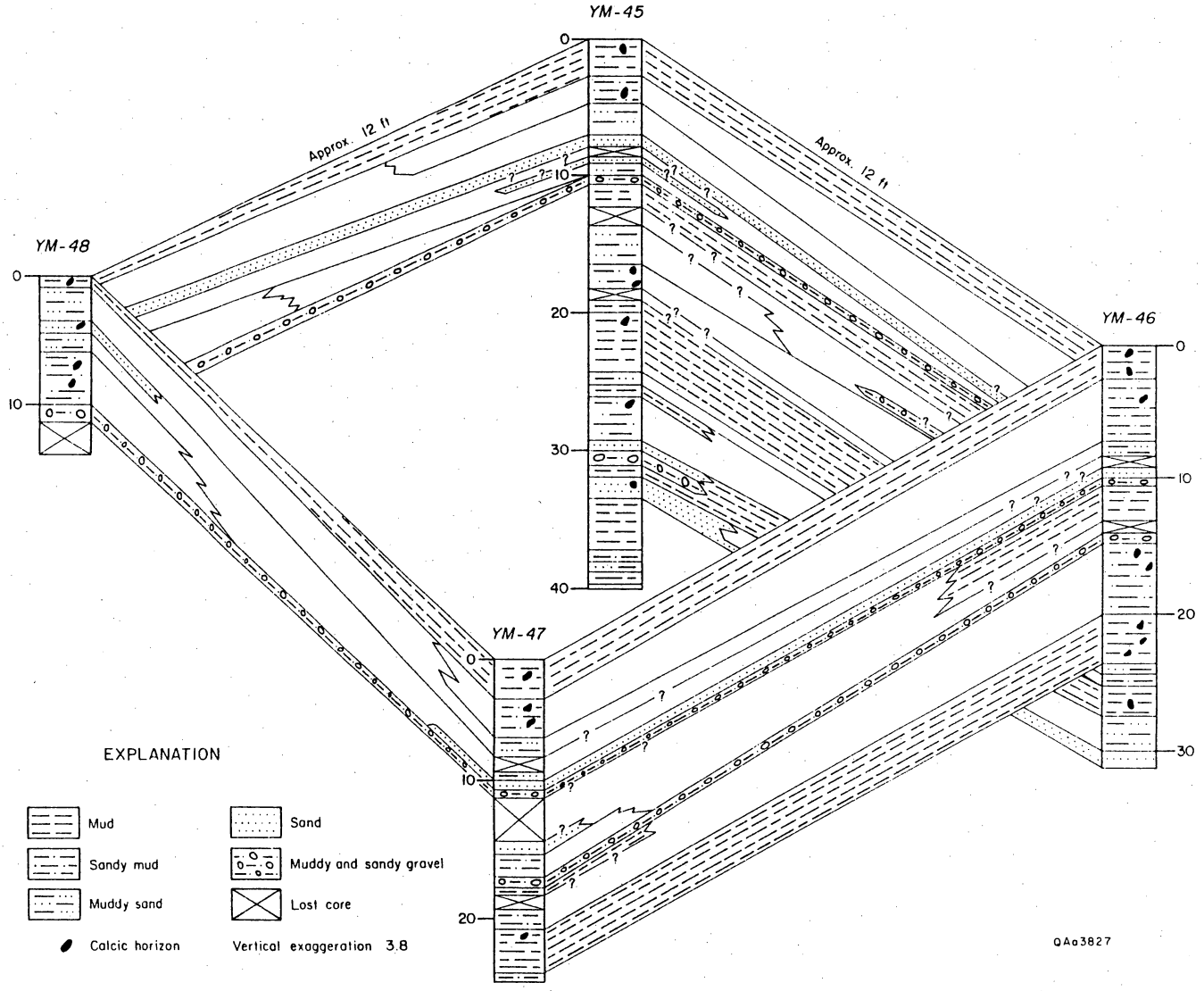

Figure 9. Fence diagram of boreholes located near the northwest corner of the proposed site. Mud strata are correlated between boreholes in this diagram because the mud strata may represent soil horizons or periods of landscape stability. Sand and gravel units show the degree of connectedness of these textural types. For reasons of clarity, the other textural patterns are not drawn between boreholes. See figure 5 for borehole locations.

Stratigraphy of the Proposed Repository Site

A closely spaced group of cores was located on the northern part of Faskin Ranch to allow detailed correlation and description of the sandy and gravelly near-surface units in that area. Eolian units in the upper few feet (m) are described in Langford (1993). This section deals with the distribution of strata in the upper 40 ft (12 m).

A wide range of grain sizes is present on the northern part of the ranch. Sediment texture changes abruptly, and correlation of individual textural units is difficult beyond a few thousand feet (m), a characteristic to be expected in fluvial sediments (fig. 9, plate 5, and trench 17 on plate 6). Channel complexes are from 1 to > 20 ft (0.3 to 6 m) in thickness (plate 7) and may contain pebble and a few cobble lenses interbedded with fine to medium sands. Eolian units below the near-surface eolian sand sheets are less abundant and relatively thin, less than 5 ft (1.5 m), but can be traced up to 1,500 ft (457 m) laterally. As mentioned for the regional area, eolian and fluvial units may have dual origins; each may be derived or reworked from the other.

Calcic horizons and some clay and silty clay units can be traced over longer distances than the other sedimentary strata, more than 5,000 ft (1,524 m) (plate 7). Calcic horizons vary in stage of development (see Gile and others, 1981). They form at a shallow depth below the ground surface, commonly 1.5 to 3.0 ft (0.5 to 1.0 m) in semiarid climates, and represent a relatively stable geomorphic period when little erosion or deposition occurred. The clay-rich units, possibly B horizons, and dense accumulations of root traces and other strongly developed paleosol characteristics may also represent periods of relative landscape stability.

PALEOMAGNETICS

Introduction

The purpose of this part of the study was to use magnetostratigraphic techniques to more precisely define the age of the basin-fill sediments and to provide a method for correlation

between cores. A series of oriented samples (inclination only) were collected from each of nine cores drilled through the Tertiary/Quaternary fill. These samples were demagnetized using standard alternating field (AF) and thermal demagnetization techniques in order to determine the magnetic polarity stratigraphy of each core. Following statistical analysis of the resultant magnetic polarity data, the magnetostratigraphy of each core was chronologically calibrated by a best-fit comparison to the geomagnetic polarity timescale (GMPTS).

This study was carried out in two phases. The first phase consisted of collection and analysis of cores YM-1 to YM-7. These cores produced very high fidelity paleomagnetic records that allowed detailed magnetostratigraphies and excellent correlation between cores to be developed. Correlation of the two deepest cores in this group (YM-4 and YM-6) to the GMPTS indicated that deposition was initiated in these parts of the basin by at least 5.0–5.5 Ma. These age determinations are somewhat uncertain because they are dependent on a one-to-one correlation between the core magnetostratigraphies and the GMPTS. This correlation is questionable for the upper parts of each core due to locally poor recovery in the top 20 ft (6.6 m).

The second phase of the paleomagnetic analyses was designed to meet two objectives. The first objective was to improve the resolution of the Brunhes Chron by detailed sampling of a short core (YM-53) that had 100 percent recovery and by sampling of exposed sediments in trench 17. Second, it was designed to develop a very detailed magnetostratigraphy for the basin. This was done by fine-scale sampling of a deep (672 ft [205 m]) core (YM-17) to basement in order to take full advantage of the high-fidelity paleomagnetic record preserved in the Eagle Flat Basin sediments. Cores YM-17 and YM-53 were drilled 33 ft (10 m) apart. Their magnetostratigraphies are combined and treated as a single entity (YM-17/53) in this report.

Methods

Sample Collection

Oriented samples (inclination only) were collected from nine cores drilled on the Faskin Ranch. The cores are stored at the Bureau of Economic Geology Core Research Center in Austin, Texas, and are designated YM-1 through YM-7, and YM-17/53 (a combination of YM-17 and YM-53). An attempt was made to collect one oriented paleomagnetic sample for every 3 ft (1 m) of core in cores YM-1 through YM-7. While that average was maintained, the spacing of samples was controlled, to a certain extent, by core quality, lithology and recovery. Preference was given to undisturbed sections where orientation was undoubted. Disturbed core and gravel lenses were avoided if orientation was uncertain. For core YM-17/53 the sample spacing was reduced to an average of one sample per ft (0.3 m) for clay, silt and sand lithologies. Conglomerates in YM-17 were sampled at 3 to 5 ft (0.9 to 1.5 m) intervals and restricted to the fine-grained matrix between clasts.

Samples were collected as 1- to 2-inch- (2.5- to 6-cm-) thick quarter to whole core sections. Orientation was maintained by scribing an arrowed up direction on the side of each sample. The depth of each sample was measured to the top and bottom of each sampled space within its core box. Sample identification was maintained by using the top sample depth measurement as an identification number.

Sample Preparation

All samples were prepared for analysis at The University of Texas at El Paso. Preparation involved trimming the samples to standard 1-inch (2.5-cm) cubes. At all times care was taken to preserve the original orientation of the sample. Preference was given to using the innermost section of core samples to avoid spurious magnetic directions caused by (a) distortion of soft sediments and their magnetic fabric during coring or (b) magnetizations induced by the core bit.

Magnetic Susceptibility Measurements

Magnetic susceptibility (MS) is a function of the concentration, distribution, and type of magnetic minerals present. Magnetic susceptibility is two to three orders of magnitude more sensitive to the presence of magnetite than any other mineral and largely reflects changes in this mineral's concentration (Butler, 1991). As basinwide depositional or erosional events often affect the magnetite depositional flux in similar ways, it is often possible to correlate between cores based on the preserved magnetite concentrations, using MS as a proxy.

Magnetic susceptibility measurements were made prior to any demagnetization studies to avoid spurious MS measurements that may occur through alteration of the original magnetic mineralogy during thermal demagnetization treatments. Susceptibility measurements were made on all samples using a Sapphire Instruments computer interfaced induction coil system housed in the Rock Magnetism and Paleomagnetics Laboratory at the University of New Mexico, Albuquerque (four full volume measurements with individual measurements being rejected if drift was $> 2 \times 10^{-6}$ SI units). The MS values reported in this study are given in SI units, which are dimensionless (app. D).

Magnetic Polarity Determination (Demagnetization) Studies

All paleomagnetic studies were also carried out at the Paleomagnetics and Rock Magnetism Laboratory. This facility is equipped with a 2G Enterprises horizontal access, three measurement axis (SQUID) Superconducting rock magnetometer (Goree and Fuller, 1976). This machine is interfaced with a fully automated specimen-handling system with an on-line alternating field (AF) demagnetizer capable of reaching peak inductions of 190 mT. Thermal demagnetizations were carried out using a Schonstedt TSD-1 oven. The entire system is housed in a large-volume magnetically shielded room (see Scott and Frohlich, 1985, for similar design details).

Determination of the magnetic polarity of samples collected from azimuthally unoriented core is solely dependent on the magnetic inclination direction. Inclination directions are considered to be successfully isolated when a linear decay to the origin is observed on a demagnetization vector decay diagram after a series of incrementally increasing sample demagnetization steps.

Stepwise sample demagnetization was carried out using either AF (0–140 mT in up to 15 steps) and/or thermal (0 to 710°C [32 to 1,310°F] in up to 20 steps) treatments. For cores YM-1 through YM-7 approximately one-third of the samples were chosen for initial AF demagnetization and one-third were treated thermally. In nearly all cases both methods worked equally well and gave comparable results. Since the AF method is the least destructive, it was used on the remaining samples. On the basis of the successful AF demagnetization results for cores YM-1 through YM-7, the thermal to AF sample demagnetization ratio was changed to 1:5 for cores YM-17/53.

Typical sample magnetic vector direction decays are presented as Zijderveld diagrams in figure 10. Many samples exhibited linear decays to the origin over the whole range of demagnetization steps, suggesting that the characteristic remanent magnetization (ChRM) has not been overprinted. Some samples do carry secondary magnetic overprints. These are represented by segments of the demagnetization vector that follow a curved path or fail to decay toward the origin. These overprints are usually of normal polarity and are easily removed early in the demagnetization process. They are probably caused by a viscous remanent magnetization (VRM) as a result of exposure to the Earth's current magnetic field. Some reverse polarity overprints were observed in the deeper sections of core YM-17. These reverse polarity overprints appear to be the result of VRMs acquired during periods of the Earth's history characterized by reverse magnetic polarity.

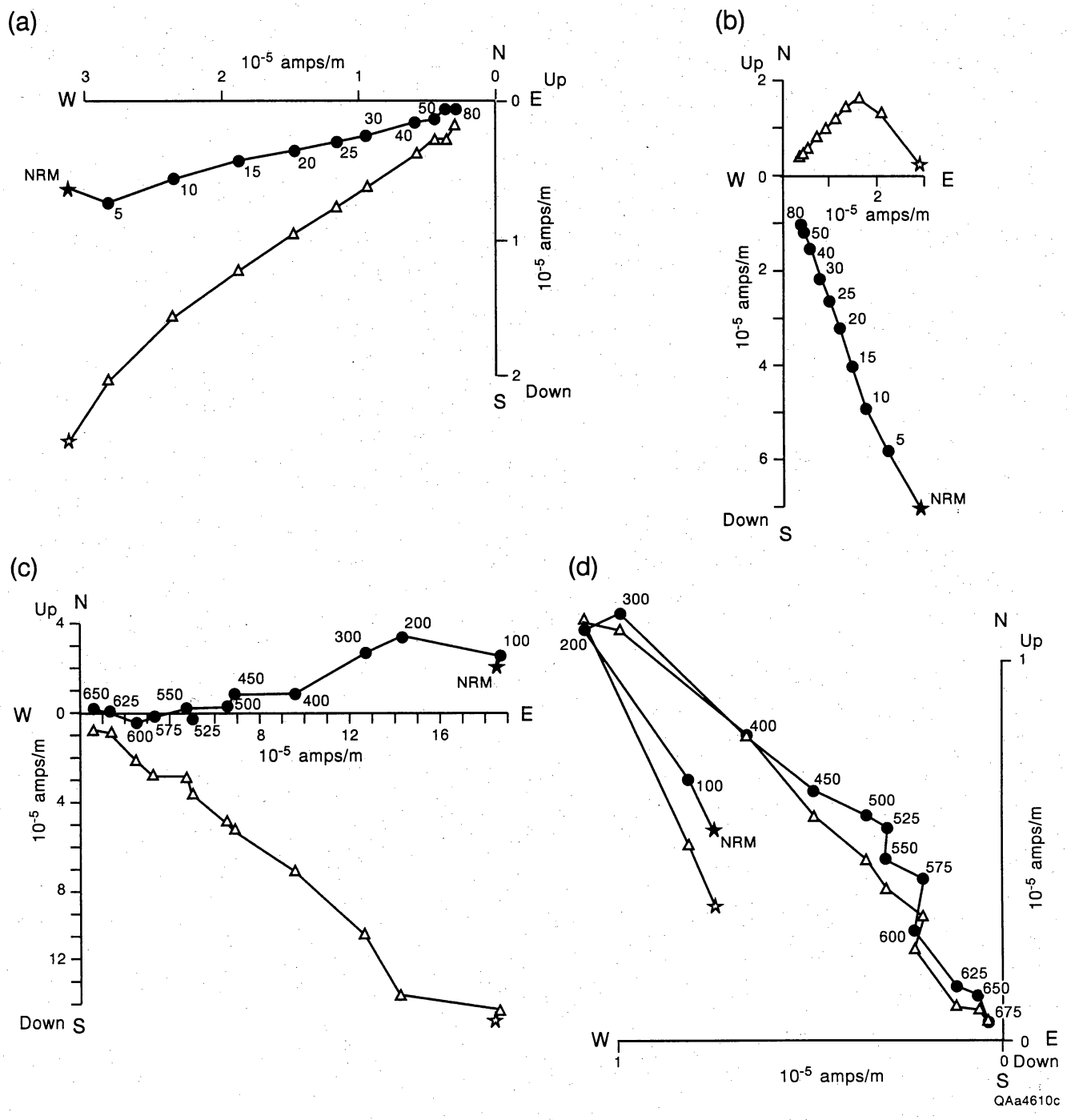

Figure 10. Magnetic vector decay (Zijderveld) diagrams. Part (a), sample number 90.2/YM#7, shows AF demagnetization of a normal polarity sample; part (b), sample number 112.9/YM#5, shows AF demagnetization of a reverse polarity sample; part (c), sample 70.1/YM#3, shows thermal demagnetization of a normal polarity sample; and part (d), sample 46.7/YM#4, shows thermal demagnetization of a reverse polarity sample. Black dots are projections of the field onto a vertical plane. Open are projections of the field onto a horizontal plane.

Statistical Analysis of Demagnetization Data

Using the algorithm of McFadden and Reid (1982) for statistical analysis of inclination-only data, an average inclination value has been calculated for the ChRM direction along with a precision parameter (k) and an estimate of accuracy (a_{95}) (app. D). For this study, values of $k > 15$ and $a_{95} < 15°$ are considered statistically significant. Samples that did not conform to these criteria are marked by an "x" on the inclination data plots of figure 11a–j and are ignored in the magnetic polarity interpretation.

Results

Susceptibility

The range of magnetic susceptibility, measured from all nine cores, varies from an anomalously low 6×10^{-5} to 2.59×10^{-2} and averages a relatively high 1.39×10^{-3} (SI units) (fig. 11a–j; app. D). This high average value reflects the presence of magnetite in these samples. Down-core magnetic susceptibilities are characterized by relative stability and a slight trend toward increasing values. Visual comparison between cores does not reveal any unique magnetic susceptibility fluctuations or trends that would allow correlation between cores.

Natural Remanent Magnetization Intensities

Natural remanent magnetization (NRM) intensities for all nine cores range from 1×10^{-6} Amps/meter (A/m) to 2.8×10^{-4} A/m and average 3.8×10^{-5} A/m (fig. 11a–j; app. D). There appears to be little or no correlation between down-core NRM intensity trends and magnetic susceptibility. However, NRM intensity values do exhibit a general correlation with interpreted magnetic polarity, with higher NRM intensities tending to occur within normal polarity zones and lower NRM intensities within reverse polarity zones. This result is not unexpected as viscous remanent magnetization (VRM) normal polarity overprints from the present-day

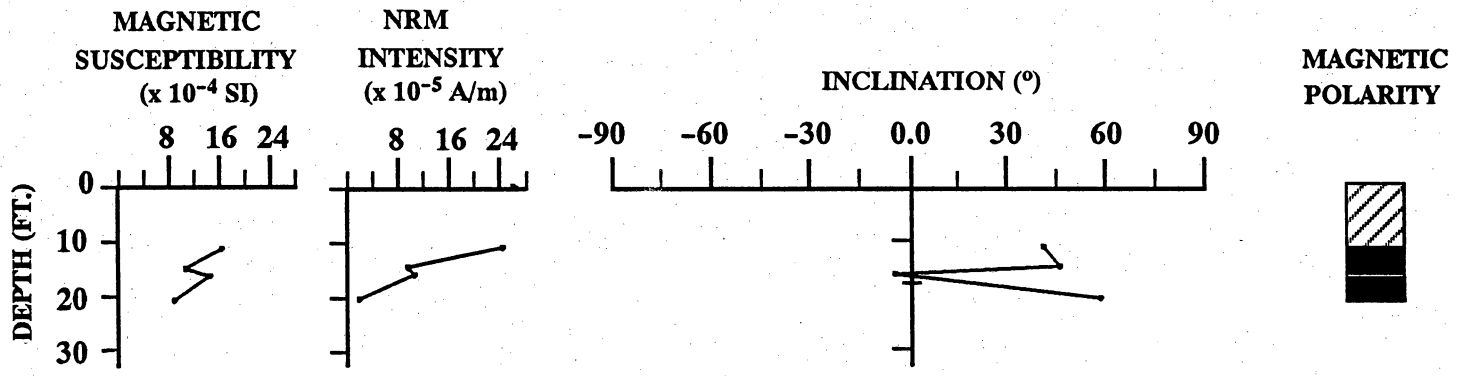

Figure 11a. Magnetic susceptibility, NRM intensity, calculated average inclination, and magnetic polarity interpretation for samples collected from borehole YM-1 (x = rejected sample; hatched shading = no core recovery).

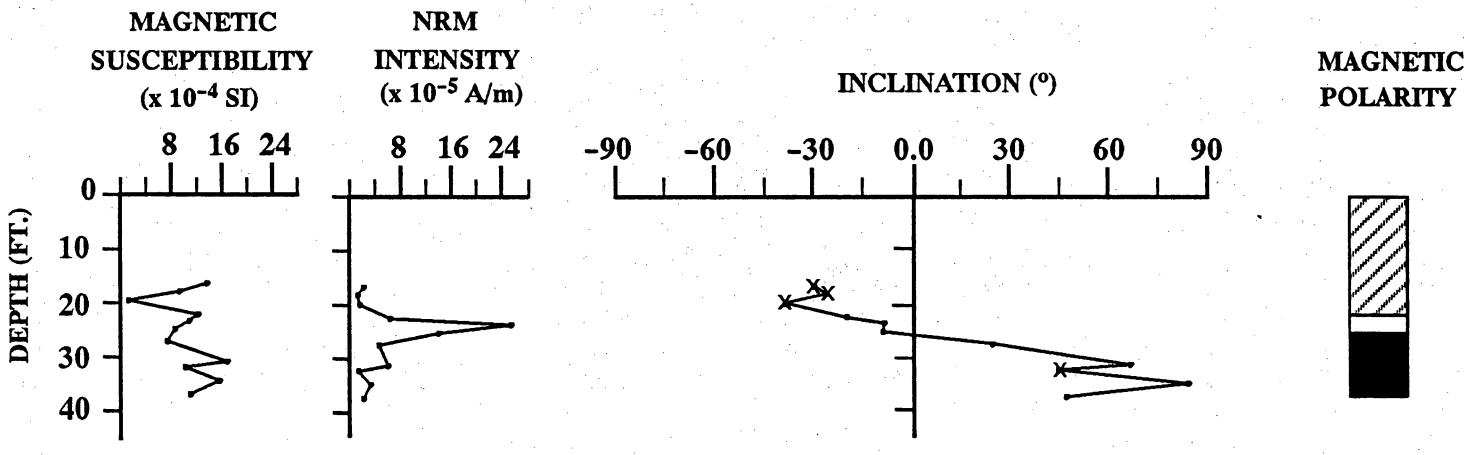

Figure 11b. Magnetic susceptibility, NRM intensity, calculated average inclination, and magnetic polarity interpretation for samples collected from borehole YM-2 (x = rejected sample; hatched shading = no core recovery).

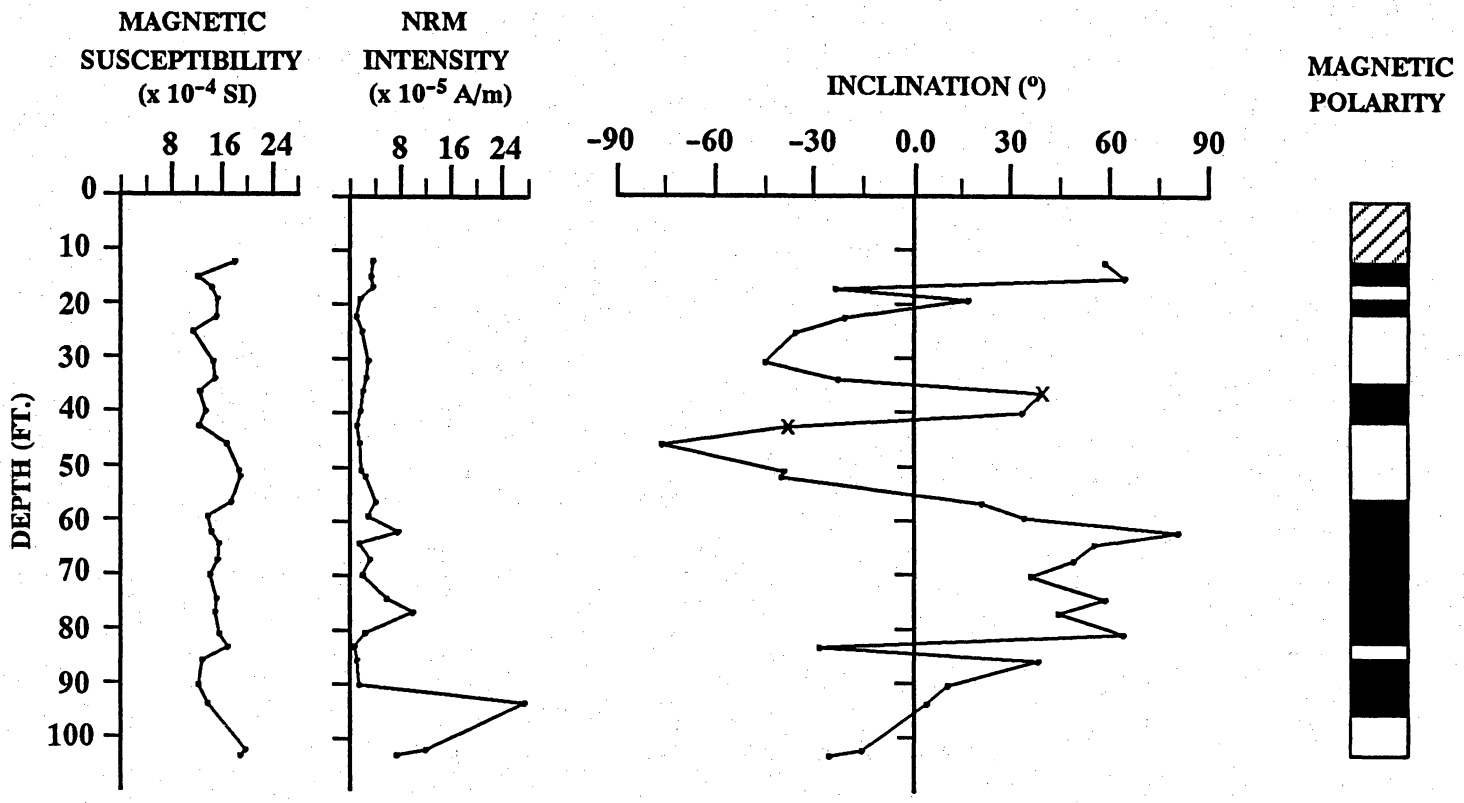

Figure 11c. Magnetic susceptibility, NRM intensity, calculated average inclination, and magnetic polarity interpretation for samples collected from borehole YM-3 (x = rejected sample; hatched shading = no core recovery).

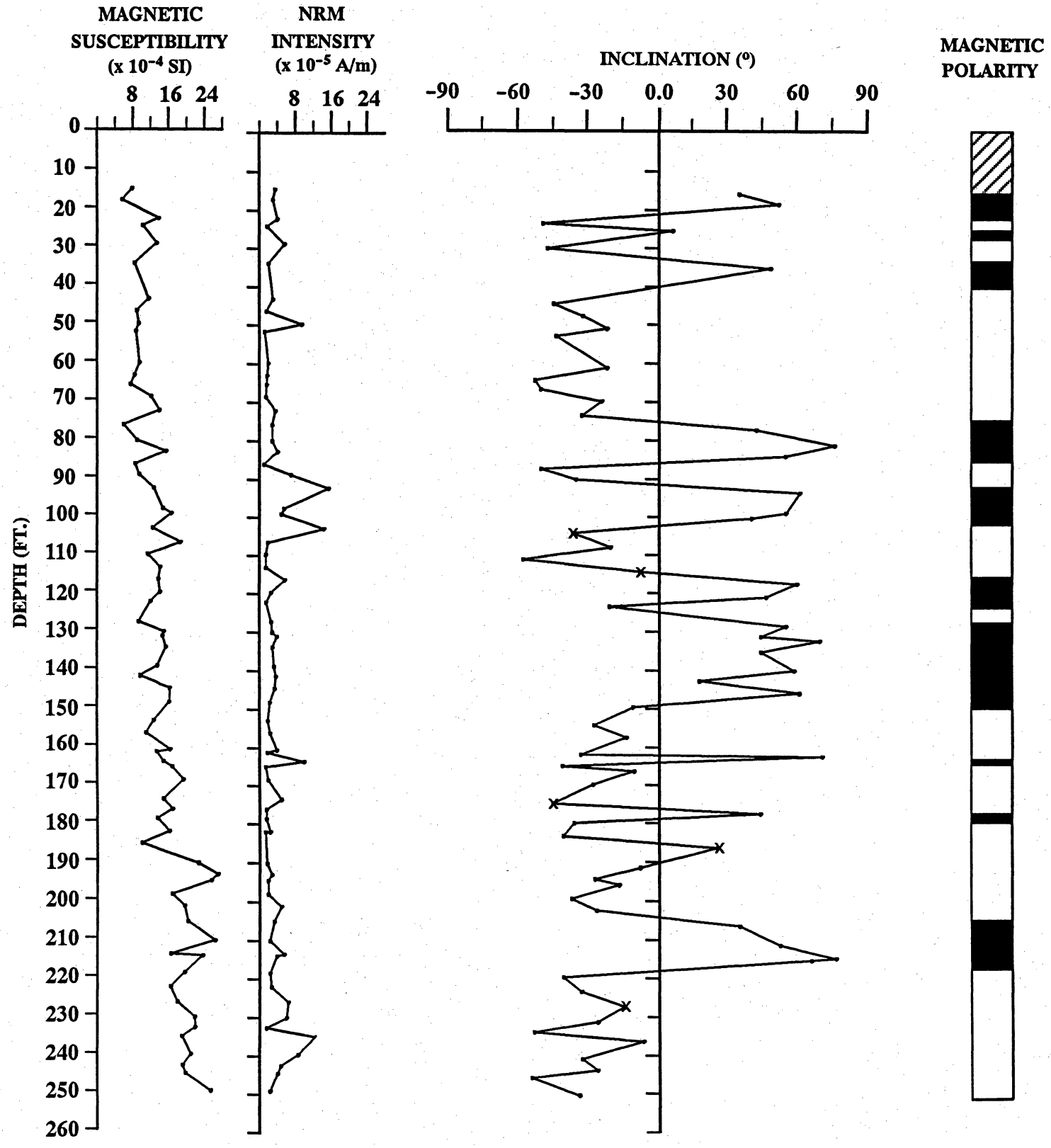

Figure 11d. Magnetic susceptibility, NRM intensity, calculated average inclination, and magnetic polarity interpretation for samples collected from borehole YM-4 (x = rejected sample; hatched shading = no core recovery).

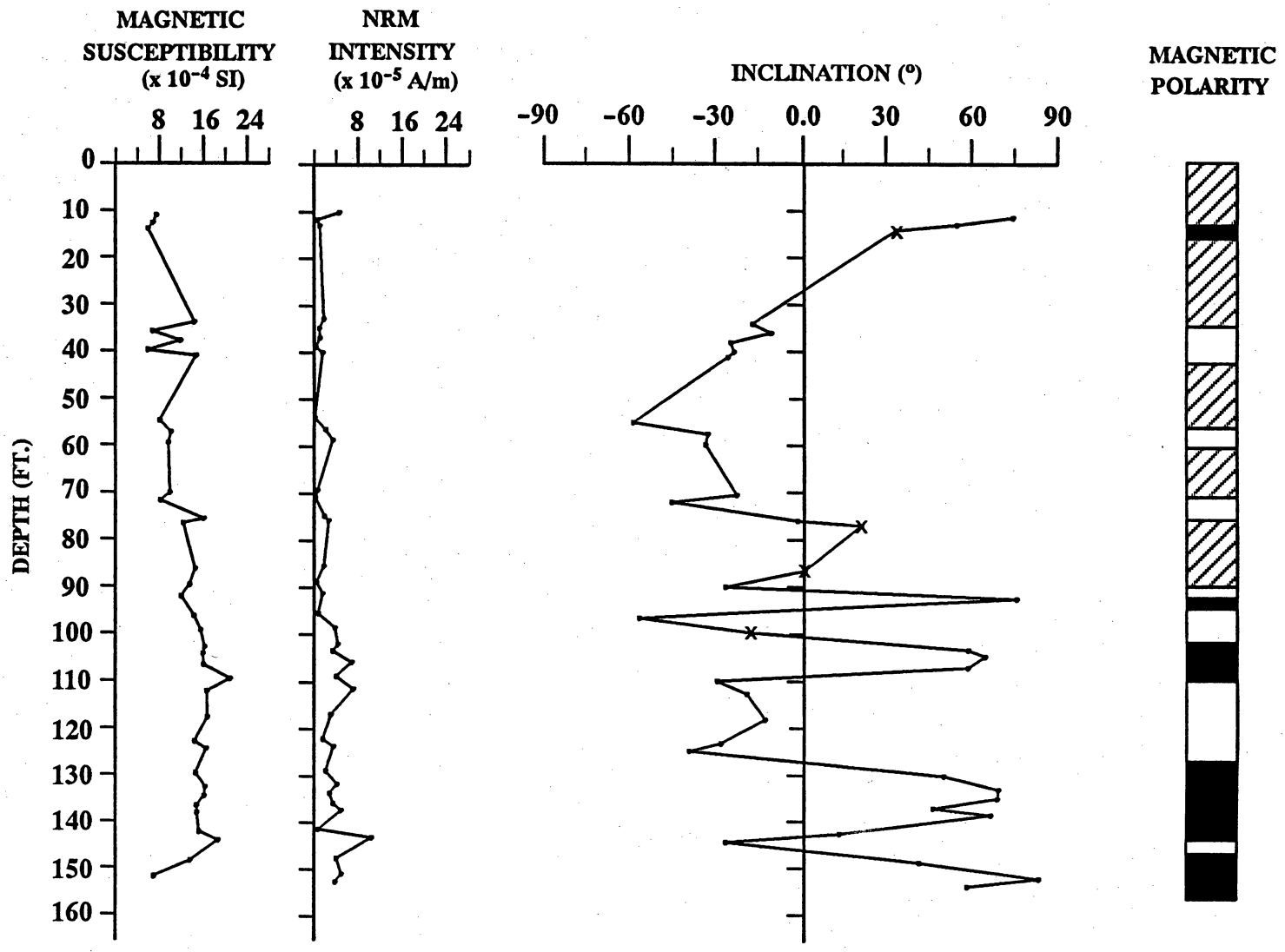

Figure 11e. Magnetic susceptibility, NRM intensity, calculated average inclination, and magnetic polarity interpretation for samples collected from borehole YM-5 (x = rejected sample; hatched shading = no core recovery).

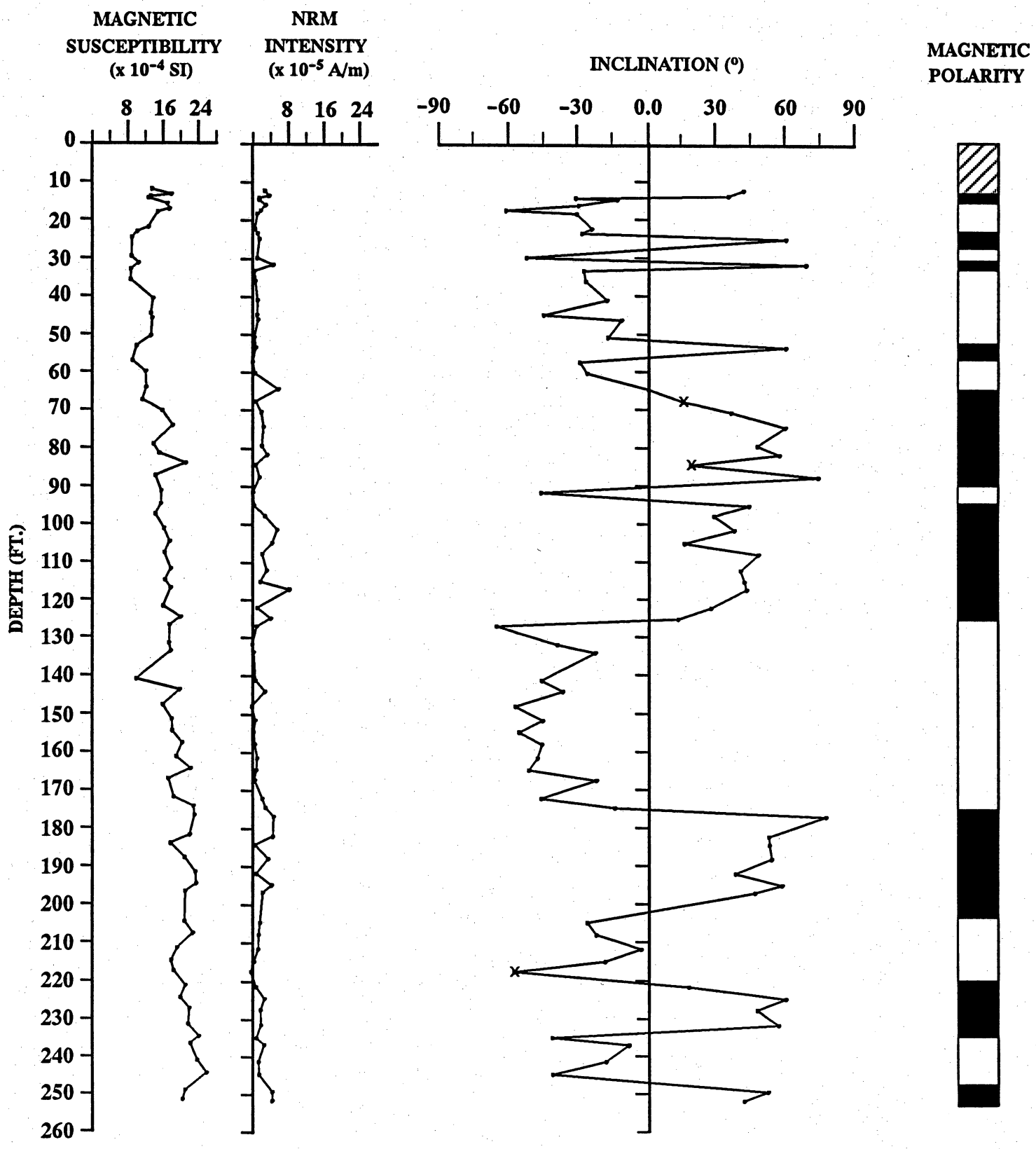

Figure 11f. Magnetic susceptibility, NRM intensity, calculated average inclination, and magnetic polarity interpretation for samples collected from borehole YM-6 (x = rejected sample; hatched shading = no core recovery).

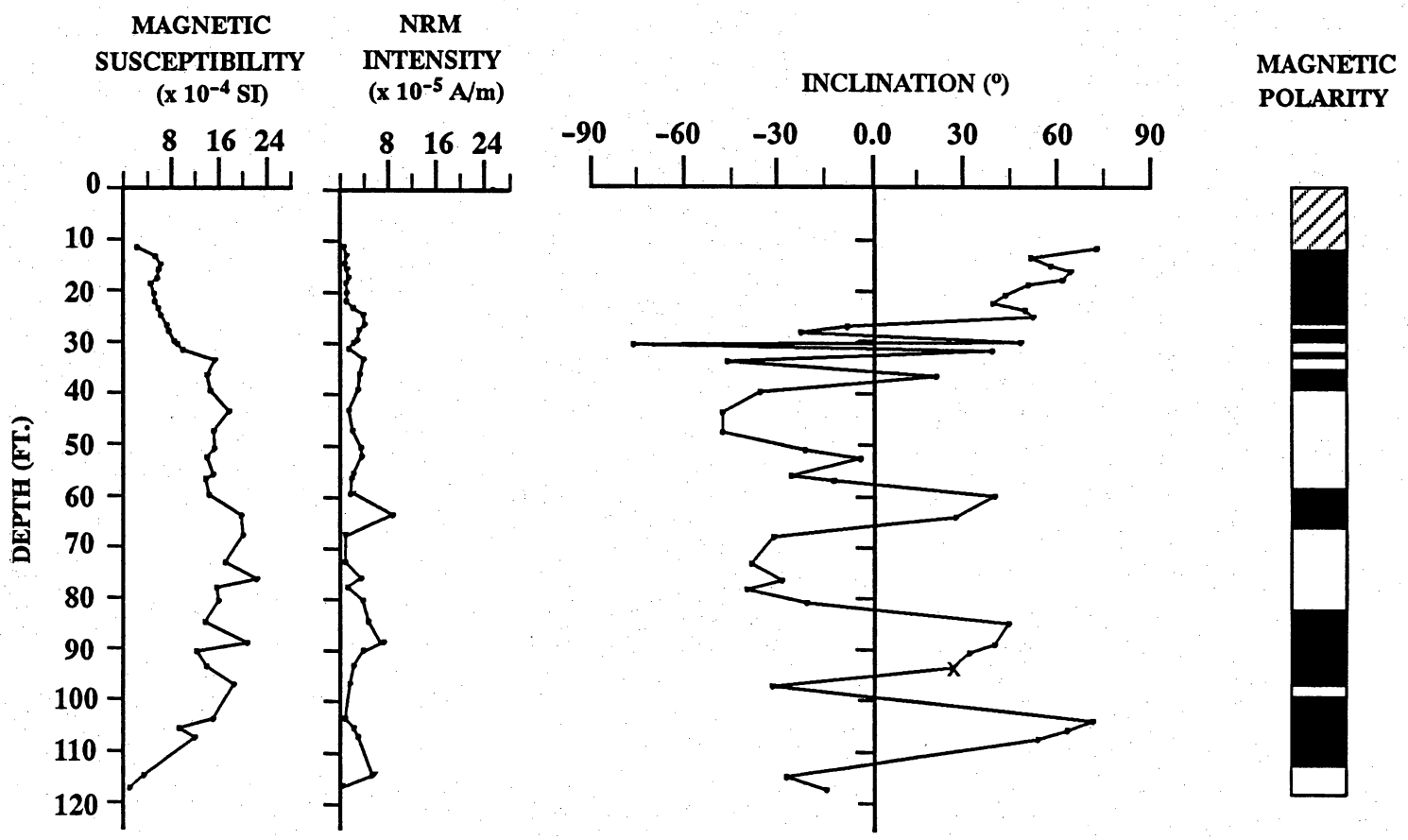

Figure 11g. Magnetic susceptibility, NRM intensity, calculated average inclination, and magnetic polarity interpretation for samples collected from borehole YM-7 (x = rejected sample; hatched shading = no core recovery).

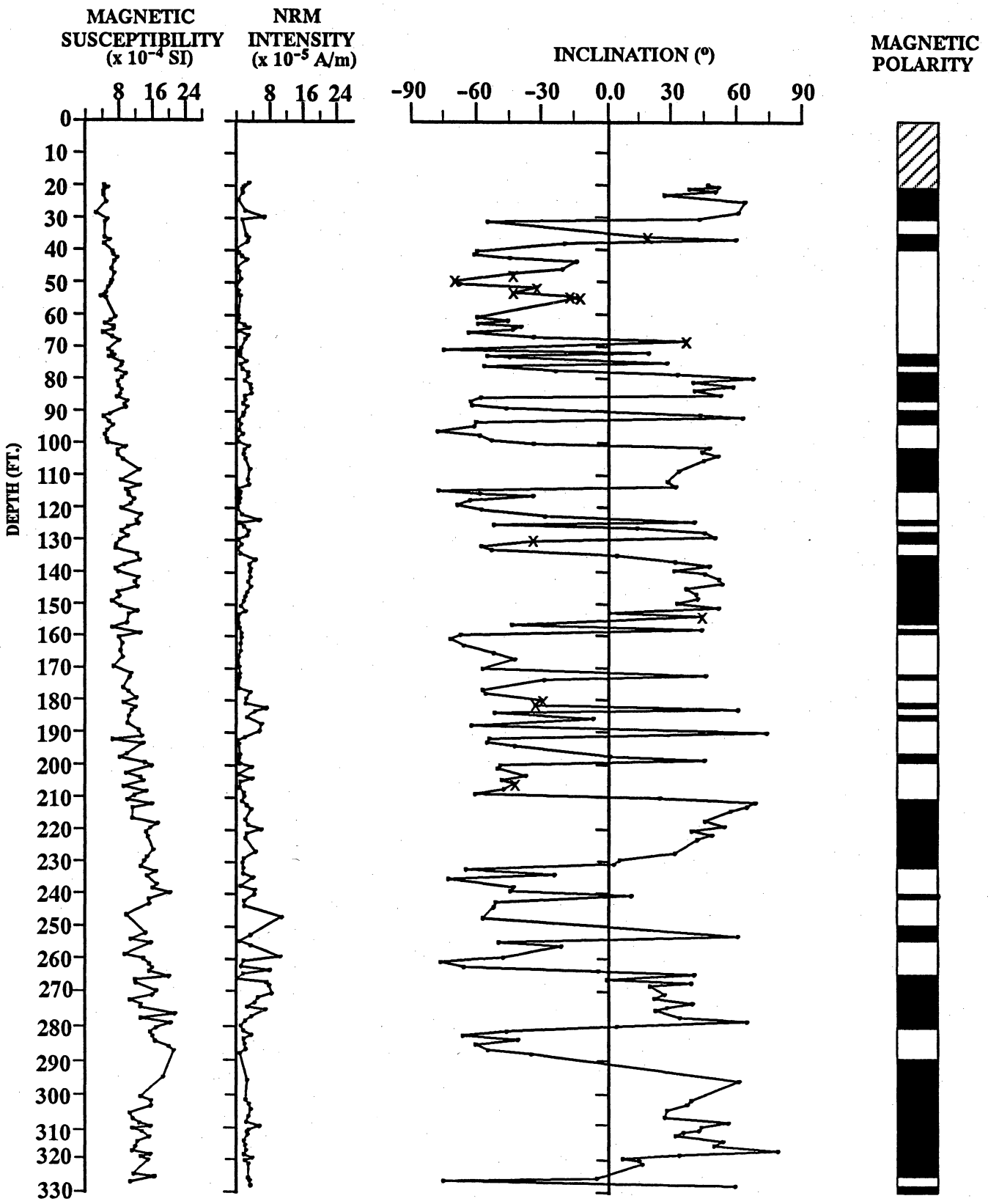

Figure 11h. Magnetic susceptibility, NRM intensity, calculated average inclination, and magnetic polarity interpretation for samples collected from borehole YM-17 (x = rejected sample; hatched shading = no core recovery).

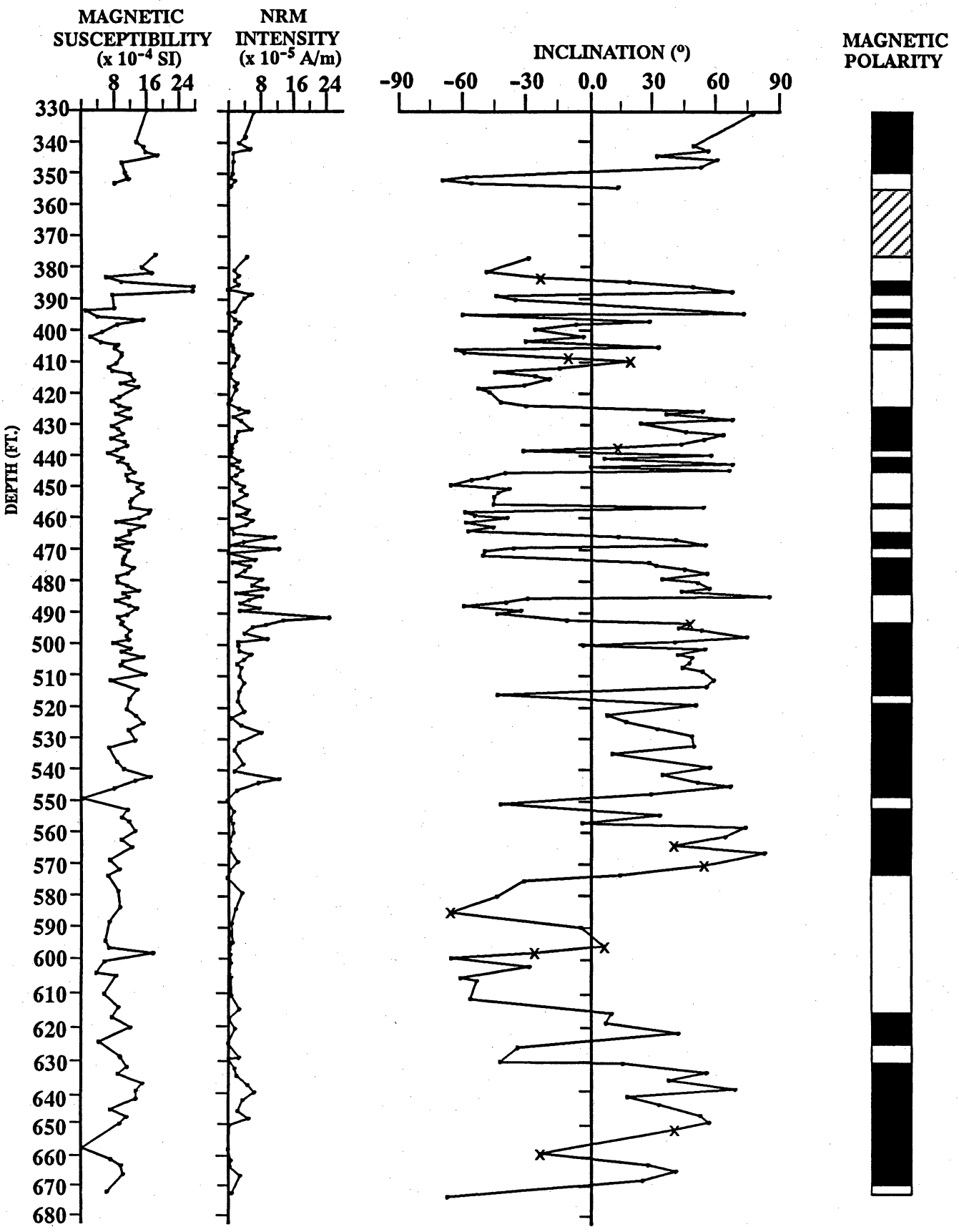

Figure 11h (cont.). Magnetic susceptibility, NRM intensity, calculated average inclination, and magnetic polarity interpretation for samples collected from borehole YM-17 (x = rejected sample; hatched shading = no core recovery).

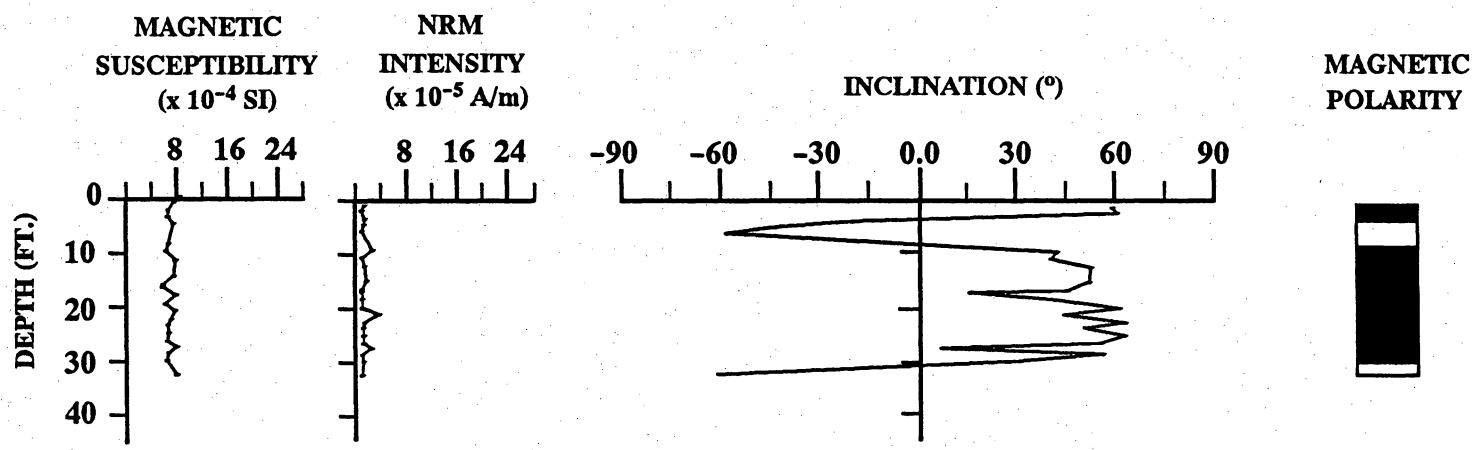

Figure 11i. Magnetic susceptibility, NRM intensity, calculated average inclination, and magnetic polarity interpretation for samples collected from borehole YM-53.

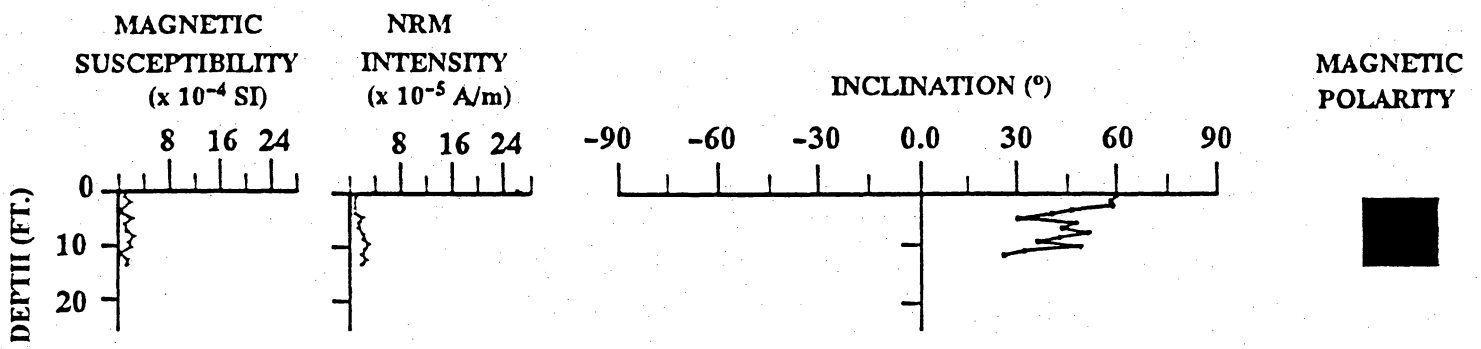

Figure 11j. Magnetic susceptibility, NRM intensity, calculated average inclination, and magnetic polarity interpretation for samples collected from trench 17 (x = rejected sample).

magnetic field tend to add to the NRM intensities of normal polarity samples and subtract from those of reverse polarity samples. Notable NRM spikes, representing episodes of dramatically increased magnetic mineral deposition, occur in core YM-17. These spikes may preserve volcanic ash fall deposits.

Demagnetization

The AF and thermal demagnetization regimes used in this study were based on results of a pilot demagnetization study conducted on selected samples from YM-6. Demagnetization trends produced by either method tended to be similar and relatively simple, consisting of removal of a normal polarity VRM by 20 millitesla (mT)/300°C (572°F) followed by a linear decay to the origin (fig. 10).

AF demagnetized samples were considered to be successfully treated if (a) magnetic intensities were reduced to below 15 percent of the NRM value and (b) a linear decay to the origin of the ChRM direction was observed by a peak field of 140 mT. For normal polarity samples, linear trends to the origin were frequently established over the complete range of demagnetization steps from 5 to 140 mT. Reverse polarity samples often exhibited the removal of a normal polarity overprint, in peak induction fields of up to 25 mT, before a linear decay to the origin was established by demagnetization fields of 25-140 mT (fig. 10). Both normal and occasional reverse polarity overprints were observed in the lower half of core YM-17, the greater age of these sediments allowing ample time for acquisition of VRM's and alteration overprints of either polarity. The general success of the AF demagnetization method implies that a low-coercivity mineral, probably magnetite, is the main carrier of the NRM in these samples.

Samples that failed the criteria for successful AF demagnetization were further treated by a thermal demagnetization regime. In most cases where additional thermal treatments were necessary, the AF treatment had failed to reduce sample magnetic intensities to below

15 percent of the NRM. The inability of the 140 mT peak induction field to fully demagnetize some samples indicates the presence of a high-coercivity magnetic mineral, in addition to the magnetite, in these samples.

All thermally treated samples were successfully demagnetized, with linear decays to the origin established between 300°C (572°F) and end-point temperatures of 500–710°C (932–1,278°F) (fig. 10). Samples demagnetized by lower end-point temperatures may be characterized as probably having magnetite as the main carrier of the NRM. Samples whose demagnetization regimes exceeded the Curie point of magnetite (583°C [1,081°F]) must contain at least one additional magnetic mineral as a partial carrier of the NRM. The high thermal stability, together with the high coercivity implied by unsuccessful or incomplete AF demagnetization treatments, suggests that hematite is present as an additional carrier of the NRM in these samples.

No changes in magnetic vector directions were observed in thermally demagnetized samples where peak demagnetization temperatures exceeded the Curie point of magnetite (fig. 10). This implies that samples having NRM contributions from both magnetite and hematite acquired them synchronously. This may only occur as a result of detrital deposition of both carriers of the NRM.

Polarity Interpretation

Magnetic polarity interpretation for individual samples was based on average inclination values and the results of the statistical analysis. Samples with $k < 15$ and/or $a_{95} > 15°$ were rejected from the magnetic polarity interpretation. Based on these criteria, 44 of the total of 648 samples collected from all 9 cores were rejected from the analysis.

For magnetostratigraphic interpretation, polarity zones are usually defined as the occurrence of a minimum of three superposed samples of the same polarity. However, the relatively compressed sections identified in this study magnify the impact of information loss

due to unrecovered core, rejected samples, and sample spacing. Therefore, to avoid the loss of additional detail in the magnetostratigraphy, magnetozones represented by single samples with statistically significant k and a_{95} values are recognized. The interpreted magnetic polarity stratigraphy for each core is presented in figure 11a–j.

Correlation between Cores

If allowance is made for variable sedimentation rates, it is possible to make visual correlations between the nine Faskin Ranch cores on the basis of their magnetostratigraphies. However, only cores YM-3, -4, -6, -7 and -17/53 allow detailed correlations. YM-1 and YM-2 are of minor value because their short lengths preclude the possibility of significant magnetostratigraphic records. Furthermore, YM-2 appears to entirely lack the expected Brunhes normal polarity zone. YM-5 is problematical because of poor recovery of oriented material (66 percent) and the occurrence of several samples rejected on the basis of the statistical analysis.

Proposed correlations are presented in figure 12. These correlations are based on matching magnetozones dominated by one polarity or the other. Based on this method, the top section of YM-17/53 (0–210 ft, 0–64 m) and the entire lengths of YM-6 (250.5 ft, 76 m) and YM-4 (249.5 ft, 76 m) may be easily correlated to each other. YM-4 is characterized by a more expanded sequence than YM-6, which in turn contains a more expanded sequence than YM-17/53. These differences are related to the siting of each core within the basin and to the fact that each core preserves its own individual record of local and variable depositional rates within the basin. The next longest polarity record is preserved by YM-3 (103.3 ft, 31 m). It appears to be a significantly compressed record, that is, a smaller amount of sedimentation in a given amount of time, compared to YM-4, YM-6, YM-7, or YM-17/53. It is followed in length of polarity record preserved by YM-7 (116.8 ft, 36 m), which has an expanded sedimentation record per unit time relative to cores YM-3, YM-4, YM-6, and YM-17/53.

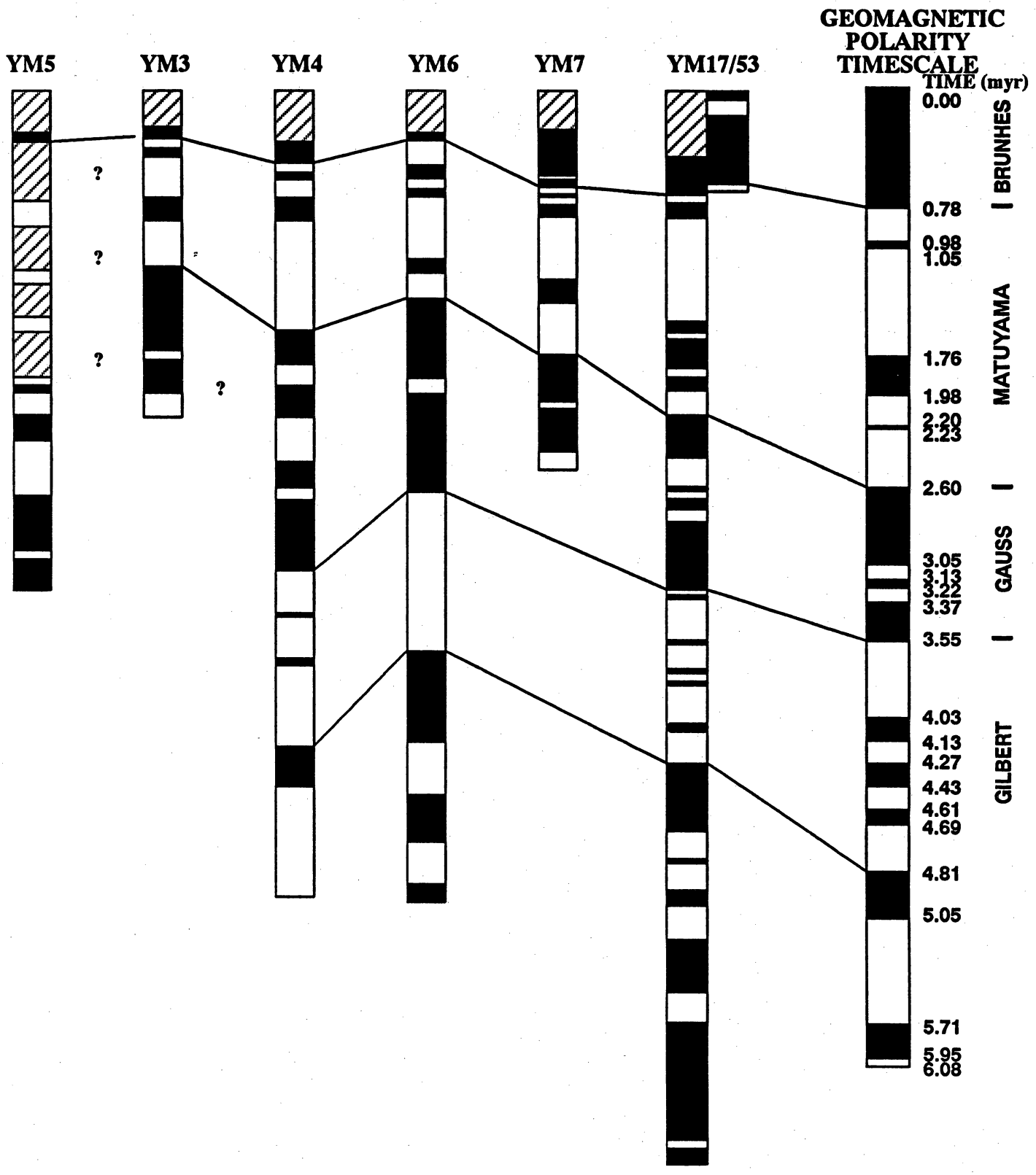

Figure 12. Proposed correlations between cores YM-3 through 7 and YM-17/53 and to the Geomagnetic Polarity Timescale. Depth scales vary. See individual logs for correct depths.

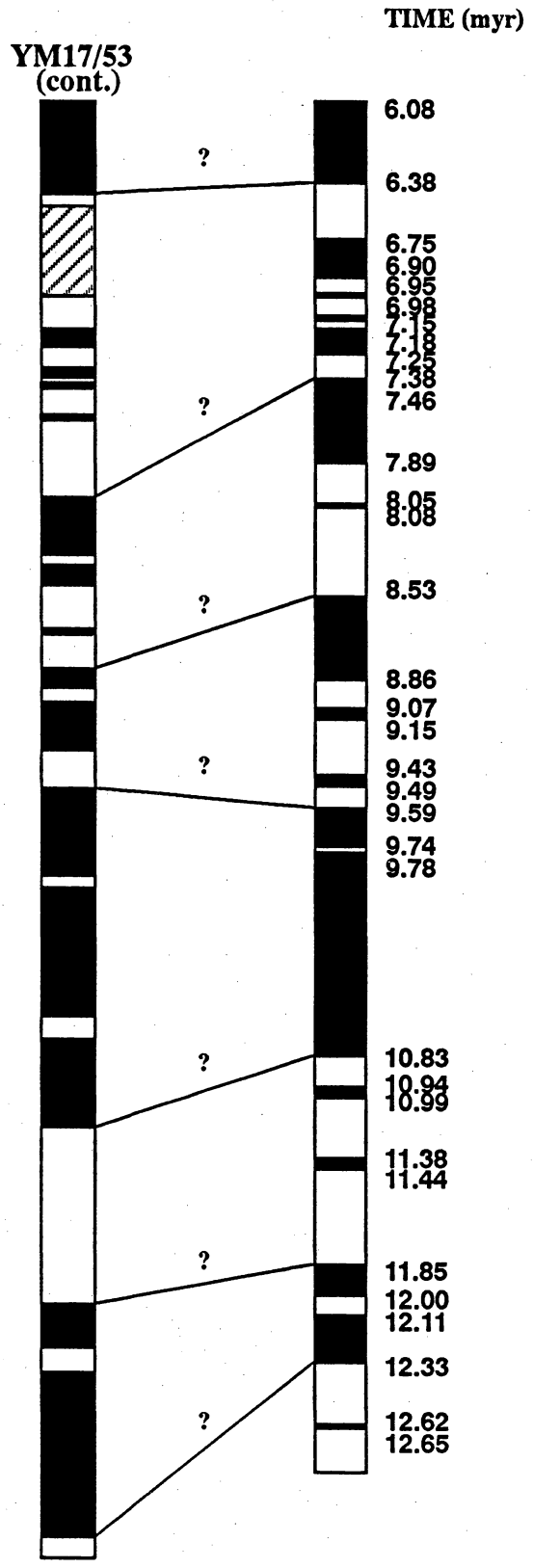

Figure 12 (cont.). Proposed correlations between cores YM-3 through 7 and YM-17/53 and to the Geomagnetic Polarity Timescale.

Correlation to the Geomagnetic Polarity Timescale

This study makes use of the Cande and Kent (1992) geomagnetic polarity timescale (GMPTS), the most recently published GMPTS. It should be noted that many paleomagneticists use the Harland and others (1990) or Berggren and others (1985) GMPTSs. The differences between the three timescales are minimal with respect to correlation of cores YM-1-7 to any of the timescales. The longer YM-17/53 sequence encounters significant revision in the lower parts where use of the Cande and Kent (1992) GMPTS requires an increase in age of approximately 0.4 m.y. with respect to equivalent chron sequences of the Harland and others (1990) and Berggren and others (1985) time sequences.

Initial correlation of the YM-1 through 7 and YM-17/53 magnetostratigraphies to the GMPTS is provided by recognition of the Brunhes Normal Polarity Chron as the normal polarity magnetozone that occurs at the top of cores YM-1, YM-3, YM-4, YM-6, and YM-7, and YM-17/53. Correlation of the remainder of the core magnetostratigraphies to the GMPTS is not unique for several reasons. A lack of other down-core tie points, variable depositional rates, unrecognized depositional hiatuses, and/or erosional events, incomplete core recovery, and sample quality and distribution all affect record completeness. There are two ways of dealing with this problem. The first is a pragmatic approach that correlates each core magnetozone to a timescale magnetochron in consecutive order, irrespective of magnetozone thickness. Such correlations tend to infer a higher degree of accuracy than is warranted by this data set. The second and more conservative approach is a best fit, by visual comparison, of the general core magnetozone pattern to the GMPTS. Although this method ignores some of the details of the magnetozone record, it still gives reasonable indications of core ages without inferring unique correlations between the GMPTS and a less than perfect data set.

The conservative best-fit method was used to apply age constraints to YM-4, YM-6, and YM-17/53 as these cores have the longest and most complete magnetostratigraphic records. On this basis, the Brunhes, Matuyama, Gauss, and Gilbert Chrons are represented in all three cores

(fig. 12). Assuming these correlations are valid, basal ages of between 4.5 and 5.0 Ma are indicated for both YM-4 and YM-6. Visual comparison of the YM-4 and YM-6 magnetostratigraphies reveals that the former is characterized by slightly higher sedimentation rates for all Chrons and therefore has a more expanded sequence. Since the cores are essentially of the same length, the base of YM-4 should be younger than that of YM-6. The longer YM-17/53 preserves a much older sequence than YM-4 or YM-6, but correlation of its magnetostratigraphy to the GMPTS becomes less certain with depth. This is particularly true for the lower half of the core where the presence of two thick conglomerate sequences clearly indicates significant variation in sedimentation rates. However, a long normal polarity interval does occur within the basal conglomerates, at a depth range of 490–570 ft (149–174 m). This is best correlated to the GMPTS if it is recognized as the relatively long duration upper zone of Chron 5n (9.59–10.99 Ma). If this provisional correlation is correct, an age of 12.3 Ma can be interpolated for the base of core YM17/53.

The interpretation of the ages of basal sediments of cores YM-3, -5, and -7 is also problematical. The shorter lengths and variable apparent compression of the magnetozone records are a function of the position of each core within the paleo-basin and the variability of depositional rates as the basin was filled. By visual correlation to the YM-4 and YM-6 cores, and to the GMPTS, it is apparent that the Brunhes, Matuyama, and upper Gauss Chrons are represented in cores YM-3, YM-5, and YM-7. Therefore, basal ages of greater than 2.45 Ma seem reasonable for these cores (fig. 12). The Brunhes and upper Matuyama Chrons are represented in core YM-2, suggesting a minimum basal age of 0.91 Ma. Core YM-1 contains only a short sequence of normal magnetic polarity and therefore may only preserve a Brunhes Chron sequence of less than 0.78 Ma (fig. 12).

Core YM-53 and trench 17 were both studied with the sole purpose of confirming the presence of the Brunhes Chron in the shallowest basin sediments. A sequence of totally normal magnetic polarity was expected to be preserved by samples collected from both YM-53 and trench 17. This proved to be the case for trench 17, but a sequence of 3 of the 22 samples

collected from YM-53 (2.9–5.2 ft, 0.9–1.6 m) were found, somewhat surprisingly, to be of reverse magnetic polarity. Although not shown in the figure 10 GMPTS, there are now up to eight very short duration reverse polarity "events" recognized within the Brunhes Chron. It would appear that the YM-53 sediments have fortuitously preserved one of these events.

Discussion

Magnetic susceptibility measurements of samples collected from cores YM-1 through 7 gave generally high values indicative of the presence of magnetite. This was later confirmed by AF and thermal sample demagnetization characteristics. Although MS may commonly be used as a correlation tool in its own right, it was not useful in this study. Apart from a slight trend for MS values to increase down core, there were no correlatable trends observed between cores. Much of this lack of success may be attributed to variable depositional and postdepositional histories and to the sampling spread within each core. This problem may be resolved by use of continuous downcore MS measurements, but this seems unwarranted given the general success of correlations based on core magnetostratigraphies.

Both AF and thermal demagnetization techniques were successful in isolating ChRM directions. Demagnetization curves were generally simple, the only detectable overprints being those developed in paleosols and soft normal or reverse polarity VRMs (fig. 10). Magnetite appears to be the dominant carrier of the NRM, but hematite was also present in many samples. No changes in magnetic vector decay directions were observed during thermal demagnetization of samples that contained both magnetite and hematite once the Curie point of magnetite was exceeded. This implies that the NRM contributions from each mineral were acquired synchronously as a primary detrital remanent magnetization (DRM). With the exception of paleosol horizons, no later magnetic components have been added to samples as a result of diagenesis and/or chemical or physical alteration. The average normal polarity inclination value for samples collected from all nine cores is 43.1° and that for reverse polarity

samples is –34.6°. The average normal polarity inclination is slightly lower than the theoretically expected value of 50.4° for the YM-1 through YM-7 site latitude. The negative polarity inclination is considerably lower than that expected. These discrepancies may probably be attributed to inclination shallowing effects caused by sediment compaction and, in the case of reverse polarity samples, by the presence of a normal polarity VRM overprint. The presence of the normal polarity VRM overprint is further evidenced by the consistently lower NRM intensities observed for reverse polarity samples.

The magnetic polarity stratigraphies established for cores YM-3, -4, -6, -7 and YM-17/53 allow reasonable correlations between them and the GMPTS. The suggested basal age of core YM-17/53 (672 ft, 205 m) sediments implies that deposition had been initiated in northwest Eagle Flat Basin by the middle Miocene (ca. 12.3 Ma). Evidence of the Brunhes, Matuyama, Gauss, and Gilbert Chrons is preserved in the shallower YM-4 (249.5 ft, 76 m) and YM-6 (250.5 ft, 76 m) cores and imply initiation of sedimentation at these depths in the basin by Miocene–Pliocene time (5.0–5.5 Ma). Evidences of the Brunhes, Matuyama, and Gauss Chrons are preserved in cores YM-3, YM-7, and probably YM-5.

Correlations between major chron boundaries do not occur at the same depths in each core. Visual examination of figure 12 clearly indicates that variable sedimentation rates between and within each core are responsible. Based on correlations to the GMPTS established in this study, average sedimentation rates for YM-4, YM-6, and YM-17/53 are about 0.6 inches/10^3yr (13.0 mm/10^3yr). These average sedimentation rates require a Brunhes-age stratigraphic thickness of approximately 38 ft (11 m) in these cores. Core YM-17/53 preserves 32 ft (10 m) of Brunhes-age material and YM-4 preserves 20 ft (6 m) and YM-6 13 ft (4 m) of Brunhes-age material. If the difference in elevation of these three cores is taken into account, however, the base of the Brunhes is at a similar elevation in all three cores.

Averaging the thicknesses of all nine cores suggests that sediment accumulation rates averaged 26 to 29 ft per m.y. (8 to 9 m per m.y.) during the Brunhes and Matuyama Chrons. The three wells that contain a complete Gauss interval averaged 79 ft per m.y. (24 m/m.y.) of

sediment accumulation. Sediment accumulation in the YM-17 well averaged 43 ft per m.y. (13 m/m.y.) during the Gilbert Chron.

QUATERNARY HISTORY

Within northwest Eagle Flat Basin, because only the upper 15 to 30 ft (5 to 10 m) of Cenozoic basin-fill strata is exposed in borrow pits and gullies, the borings drilled on the Faskin Ranch are the main sources of information about the deeper Tertiary and Quaternary filling of the basin. Before deposition of the basin-filling deposits, the Cretaceous strata in the north part of Faskin Ranch were eroded into an irregular northeast-sloping hillside (fig. 4). The basin-filling strata that accumulated on top of the hillside filled the depression in the manner of a bowl being filled with liquid (fig. 13). At any given time, there was a fairly low-relief basin floor abutting the hillside. As the basin filled, the earlier deposits and progressively more of the hillside was buried. The tops of the hills extend southeast from Sand Mountain to the hills near Grayton Lake, and the upper part of the hillside is preserved south of Blanca Draw. This section describes the basin-fill deposits on north Faskin Ranch in chronological order, from oldest to youngest. The wells that provided the stratigraphic data are shown the maps on plates 1A and 1B and on the cross sections on plates 2 through 7.

The oldest Tertiary sediments were cored in boreholes YM-17 and YM-63 at the north end of Faskin Ranch (figs. 11 and 12; app. A). Deposition began approximately 12 mya in YM-17 boring, judging from paleomagnetic reversal correlation (see earlier section). The YM-63 boring cored a slightly deeper part of the basin and recovered basin fill at an elevation approximately 50 ft (~15 m) lower than that of YM-17. The basal strata in YM-63 are probably somewhat older than 12 m.y.

Gravels and sands predominate in the lower 150 ft (50 m) of the YM-17 and YM-63 cores above the bedrock contact. Paleomagnetic reversal dating dates the top of this interval at approximately 10 m.y. These thick gravel deposits in the north part of the ranch probably

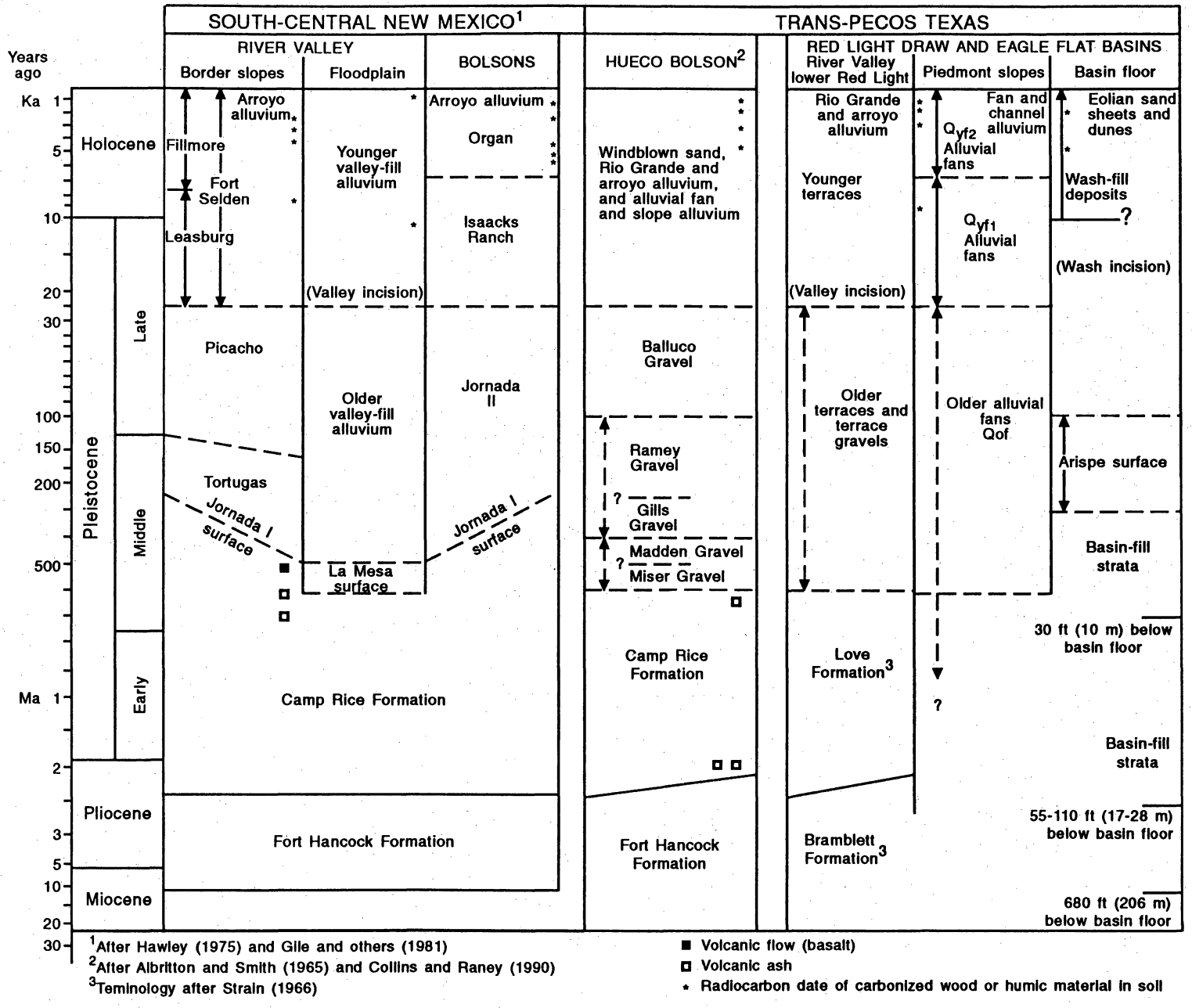

Figure 13. Neogene and Quaternary stratigraphy of south-central New Mexico and Trans-Pecos Texas.

formed along a steep slope that must exist between boreholes YM-5, YM-62, and YM-65 on the top of the slope and YM-17 and YM-63 lower on the slope (fig. 4). The gravel clasts are Cretaceous limestones and sandstones as are the underlying bedrock strata' but the clasts are generally well rounded and dissimilar to the underlying bedrock indicating that they were transported. They probably formed in alluvial fans, down which gravel was transported from the southwest.

The slope lies along the trend of an inferred north side down normal fault (Raney and Collins, 1923). No evidence, either from seismic data or cores, indicates whether the fault was active during deposition of the basin-fill strata (Raney and Collins, 1993). The fault may have been active during gravel accumulation 12 to approximately 5 to 6 mya. Alternatively, the fault having predated deposition entirely, the gravels may have accumulated along a fault-line scarp or an erosion hillslope.

Deposition near the YM-17 and YM-63 borings continued from 12 to approximately 4.5 to 5 mya, early in the Gilbert Chron, but sandy muds predominated. Because pebbles are present in many of the muds, the sediments are assumed to represent deposition on the basin floor and adjacent distal alluvial fans. Equivalent age gravels probably extend to the southeast of YM-17 and YM-63 and onlap bedrock in the northeast part of the proposed repository site. The YM-4 and YM-6 boring did not reach bedrock, and may overlie some of these alluvial fan gravels. No sediment accumulated on the rest of Faskin Ranch during this 6 million-yr period that marks the progressive burial of the steep hillside in the north part of the proposed repository site.

Boreholes YM-4 and YM-6 were cored to depths of 250 ft (~64 to 70 m) (figs. 11 and 12; app. A), but did not reach bedrock. They sampled deposits aged approximately 4.5 and 5 m.y. (see section above; fig. 12). Deposition began at the bedrock contact beneath borings YM-19 and YM-62 at approximately the same elevation (4,115 ft [1,253 m]) and probably represents coeval deposition. Initial deposition in borings YM-4 and YM-6 was basin-floor muddy sand and sandy mud, whereas in YM-19 and YM 62, 30 ft (10 m) of gravel was deposited on top of the Cretaceous bedrock. By 4.5 mya (in the Gilbert Chron of the early Pliocene) deposition had

filled Eagle Flat Basin to an elevation of 4,000 to 4,100 ft (1.218 to 1,249 m). Most of the proposed repository site formed a low-relief basin floor, bounded to the south, along the present trend of the Southern Pacific Railroad tracks, by a series of alluvial fans, inset into a hilly, gently sloping bedrock terrain.

During the 1.05 million-yr period of the Gauss Chron (2.62 to 3.55 mya), more Cretaceous bedrock was buried and deposition began in borings YM-5 and YM-7. By the end of the Gauss Chron (2.62 mya) the basin fill had aggraded to elevations ranging from 4,170 in YM-7, beneath the present-day floor of Grayton Lake, to 4,300 in YM-03 along the northeast flank of Devil Ridge in the west part of Faskin Ranch (plate 2). By this time, the depositional features of the basin had neared their present locations. Basin-floor sediments had been deposited all the way to the south of the Southern Pacific Railroad tracks. The present-day site of Grayton Lake was an alluvial fan as is indicated by alluvial fan gravels in the YM-7 core drilled in the center of the lake (plate 1b and plate 4). This alluvial fan was part of a series of fans that extended westward along the present-day course of Blanca Draw.

The sediments in the core are significantly different from the sediments exposed in the Hueco Basin and lower Red Light Draw. Sediments equivalent to the Gauss Chron in age are partly exposed in the Fort Hancock Formation in the Hueco Basin (Strain, 1966) and the Bramblett Formation in Red Light Draw (Akersten, 1970; Strain, 1980). During deposition of the Fort Hancock, because Hueco Basin had no outlet, it served as the terminal drainage of the upper Rio Grande (Kottlowski, 1958). The Fort Hancock Formation contains alluvial fan, fluvial, and playa depositional facies deposited in a closed basin that had extensive alluvial plains and ephemeral lakes and smaller playas (Strain, 1966; Gustavson, 1991). The Bramblett Formation is similar in lithology and depositional facies to the Fort Hancock, except that the lateral extent of the depositional facies is more restricted because of the narrower geometry of Red Light Draw (Strain, 1980).

Progressive filling of the basins and incision of the surrounding uplands has gradually integrated the Basin and Range fault-block basins into larger drainage systems. Integration of

the Rio Grande system continued through the Pliocene, and the Rio Grande was incised through the southern Indio and Quitman Mountains approximately 2.25 mya, following deposition of the Fort Hancock Formation (Gustavson, 1991), integrating Red Light Draw with the Hueco Basin and the lower Rio Grande. Following integration of the Rio Grande, a shallow valley was eroded through the southern Quitman Mountains from the Hueco Basin and into southern Red Light Draw. Gustavson (1991) suggests that this valley was eroded approximately 158 ft (48 m) into the Fort Hancock Formation in the southern Hueco Basin, and 406 ft (123 m) into the Bramblett Formation in southern Red Light Draw. This interpretation does not take into account any tectonic effects.

Filling this eroded valley and covering the Fort Hancock Formation were a series of sediments deposited by the throughflowing Rio Grande and its tributaries flowing from the margins of the Hueco and Red Light Basins. These sediments, known as the Love Formation in Red Light Draw and the Camp Rice Formation in the Hueco Basin (Strain, 1980), contain alluvial fan gravels and sands derived from the tributary drainages, along with sands and mudstones derived from the throughflowing Rio Grande (Gustavson, 1991) (fig. 11) In the Hueco Basin, the Camp Rice Formation rests everywhere on an unconformity (Albritton and Smith, 1965). In lower Red Light Basin, Strain (1966, 1971) reports that at least at some locations, the Bramblett and Love Formations are conformable. However, Gustavson (1991) estimates 406 ft (123 m) of incision in this location in the "Fort Hancock" (Bramblett Formation), prior to deposition of the "Camp Rice" (Love Formation). The earliest Camp Rice sediments are believed to have been deposited prior to 2.1 mya, and deposition ceased between 700,000 and 600,000 yr ago (Albritton and Smith, 1965; Gile and others, 1981; Gustavson, 1991). The Camp Rice and Love Formation strata are sandier, lighter colored, and more laterally varied than the underlying Fort Hancock and Bramblett strata.

Eagle Flat basin-filling strata do not exhibit the changes in lithology and appearance that characterize the onset of deposition of the Camp Rice and Love Formations, which overlie the Fort Hancock and Bramblett Formations, respectively. The cored strata from Faskin Ranch

exhibit little of the color or textural variation expressed in the Fort Hancock and Bramblett Formations and do not contain the extensive playa deposits described in the Fort Hancock Formation by Gustavson (1991).

In contrast, the bedrock knobs in the axis of the basin east of Grayton Lake and the alluvial fans that fill the valley at this location suggest that northwest Eagle Flat Basin has been a closed basin during most of its history. Today, converging alluvial fans topographically enclose northwest Eagle Flat Basin southeast of Grayton Lake. Either way, the deposits maintained a remarkable homogeneity throughout the Pliocene and Pleistocene.

Little change is recorded in Faskin Ranch cores during the succeeding Matuyama Chron (2.6 mya to 780,000 mya). The most significant change was the appearance of Grayton Lake, which was probably established about 780,000 yr ago, at the end of the Matuyama Chron, according to the influx of muds recorded at this time in YM-7 (figs. YM-11 and app. A). By this time the landscape near the proposed repository site had assumed its present character.

No evidence exists in Faskin Ranch cores of the late Pliocene–early Pleistocene unconformity found in Hueco and Red Light Basins that reflects the integration of the Rio Grande drainage. At a time of profound change in lithology from Fort Hancock to Camp Rice deposition, Faskin Ranch sediments retain a remarkable uniformity. They also maintain a consistent sediment accumulation rate during the time that the erosional valley was cut by the Rio Grande in these basins. Furthermore, the northwest Eagle Flat Basin sediments are a uniform brown, in contrast to the more variegated colors of the Hueco Basin and Red Light Draw sediments. Eagle Flat basin-fill mudstones are much more silt and sand rich than the Fort Hancock mudstones (compare Gustavson, 1991), and they contain much less sand and gravel than does the Camp Rice Formation (Strain, 1966; Gustavson, 1991).

During the Brunhes normal-polarity Chron, 780,000 yr ago to the present and including the middle and late Pleistocene, approximately 20 to 30 ft (~7 to 10 m) of basin-fill sediments accumulated in north Faskin Ranch (fig. 11, app. A). By this time, the northwest Eagle Flat Basin floor covered the entire proposed repository site, and drainage was generally from north

to south and northwest to southeast, toward the present course of Blanca Draw. At the beginning of the Brunhes Chron, one axis of braided-stream channel deposition extended from north to south along the east margin of the repository site (as is indicated by gravels and coarse-grained sands in the bases of cores YM-72, YM-73, YM-74, and YM-75) (plates 5 and 7). The orientation and extent of this channel have been inferred from a grid of resistivity soundings, which indicated a trend of slightly higher resistivities extending north and south at the approximate depths of the gravels in the cores (data collected under the direction of Dames and Moore, 1993).

Sedimentation continued gradually to aggrade the basin floor at the proposed repository site. A second set of braided-stream channels deposited a complex of channel-fill sediments about 15 ft (~5 m) thick along a trend running north-northwest to south-southeast through the center of the proposed repository site. This set of channel-fill deposits lies approximately 10 to 20 ft (~3 to 6 m) below the surface (see YM-4 through YM-15 in plate 7). Extrapolation of sediment accumulation rates based on paleomagnetic reversal dating indicates that these channels were deposited between 230,000 and 500,000 yr ago.

Well-defined channel fills 3 to 6 ft thick (1 to 2 m) and as much as 150 ft wide (50 m) are exposed in the borrow pits along the interstate. In texture, the sediments in these channels resemble the gravels and sands cored in YM-15 and YM-4. Deposition on the proposed repository site was generally sandier in the upper 15 to 20 ft (5 to 7 m), largely as the result of the presence of these braided channel fills and associated deposits.

This period of slow sediment accumulation probably terminated about 100,000 to 300,000 yr ago, when the landscape stabilized and soil began to form (Langford, 1993). The end of sediment accumulation was marked by the formation of a calcic soil extending across most of northwest Eagle Flat Basin, including northern Faskin Ranch (Langford, 1993)—the Arispe Surface. This surface can be dated by comparing the accumulated calcium carbonate in the soil with similar accumulations in southern New Mexico. Because the New Mexico soils are not precisely dated, we can only approximate the age of the Arispe Surface as early late Pleistocene

(Langford, 1993): it is only the most recent in a series of hiatuses recorded by calcic soils in the cores (app. A).

One part of Eagle Flat that may be younger than the Arispe Surface is a tongue of land approximately 1 mi (~2.6 km) wide paralleling Blanca Draw and extending southeast from near the town of Sierra Blanca to the confluence of the branch of Blanca Wash extending from Sand Mountain. Borings in this tongue, 1 mi (~2.6 km) east of Sand Mountain, contain approximately three-fourths as much soil calcium carbonate as does the soil under the Arispe Surface. This lesser amount of soil carbonate suggests a soil age of approximately 70,000 yr.

After the Arispe Surface was established, including the possibly younger tongue, it was incised by the dendritic drainage system of the modern Blanca Draw to a depth of 15 to 25 ft (4.6 to 7.6 m) below the level of the Arispe Surface. After incision, the washes were refilled by a combination of slopewash down the flanks of the draw and braided streams flowing down Blanca Draw. Blanca Draw contains successively finer deposits, the uppermost 3 ft (1 m) containing the finest sediments of any on Faskin Ranch (see Langford, 1993). Radiocarbon dates from wash-fill sediments within the draws indicate that the refilling of the washes had probably begun earlier than 16,000 yr ago and they were largely filled, to within 5 ft (1.5 m) of the present-day wash floor, earlier than 2,350 yr ago. Currently the wash floors lie 7 to 10 ft (2.3 to 3 m) below the Arispe Surface. The washes are largely aggrading by sediment, mostly silts, washing in from their flanks. Some of the tributaries of Blanca Draw have been filled by eolian sediment and no longer form continuous drainages.

The most recent sediments in the basin floor of Eagle Flat Basin are eolian sands that form a sand sheet across the repository site and much of the rest of the basin floor to the north and east. They are inferred to have remained episodically active into historical times. Active dune migration is recorded by buried plants and exposed roots at several places in Eagle Flat Basin. The surficial sediments of the Eagle Flat study area, including the proposed Faskin Ranch site, are discussed in more detail in Langford (1993).

PSEUDO-FISSURES AND FISSURES

Introduction

Surface collapse features on Faskin Ranch characterized by linear patterns of holes, pipes, and elongate depressions at the surface are believed to be pseudo-fissures, similar to those described by Shlemon and LaChapelle (1992). The pseudo-fissures occur entirely within wash, or draw, areas (fig. 14). A linear group of surface depressions that is much longer and wider than the pseudo-fissures also exists on an upland area of the ranch. This feature is an earth fissure, consisting of a closely spaced series of depressions marked by a distinct vegetation line.

Pseudo-fissures

Pseudo-fissures are typically expressed at Faskin Ranch as shallow, elongate, trough-shaped features or as alignments of subcircular holes or depressions in the wash areas. They have been identified in Blanca Draw, related tributaries, and in a low area parallel to Blanca Draw near Grayton Lake (fig. 14). Pseudo-fissures have not been found on interfluvial, piedmont, or upland areas. The highest concentration of pseudo-fissures is located in a tributary to Blanca Draw south of the Southern Pacific Railroad tracks and north of Cross Tracks tank (fig. 15). No pseudo-fissures have been identified on the proposed repository site. Pseudo-fissures occur elsewhere in the region outside Faskin Ranch, on the flanks of Eagle Flat Draw east of Faskin Ranch and in Blanca Draw on the Hoover property to the west.

Surface Character and Distribution

Pseudo-fissures on Faskin Ranch range in size from single holes, 4 inches (10 cm) or smaller in diameter and as much as 14 inches (35 cm) deep, to elongated depressions, up to 24 ft (8 m) long and as much as 2 ft (70 cm) deep. Most pseudo-fissures occur as linear arrays of open holes and shallow depressions. Typical single depressions range from 8 to 16 inches (20 to 40 cm)

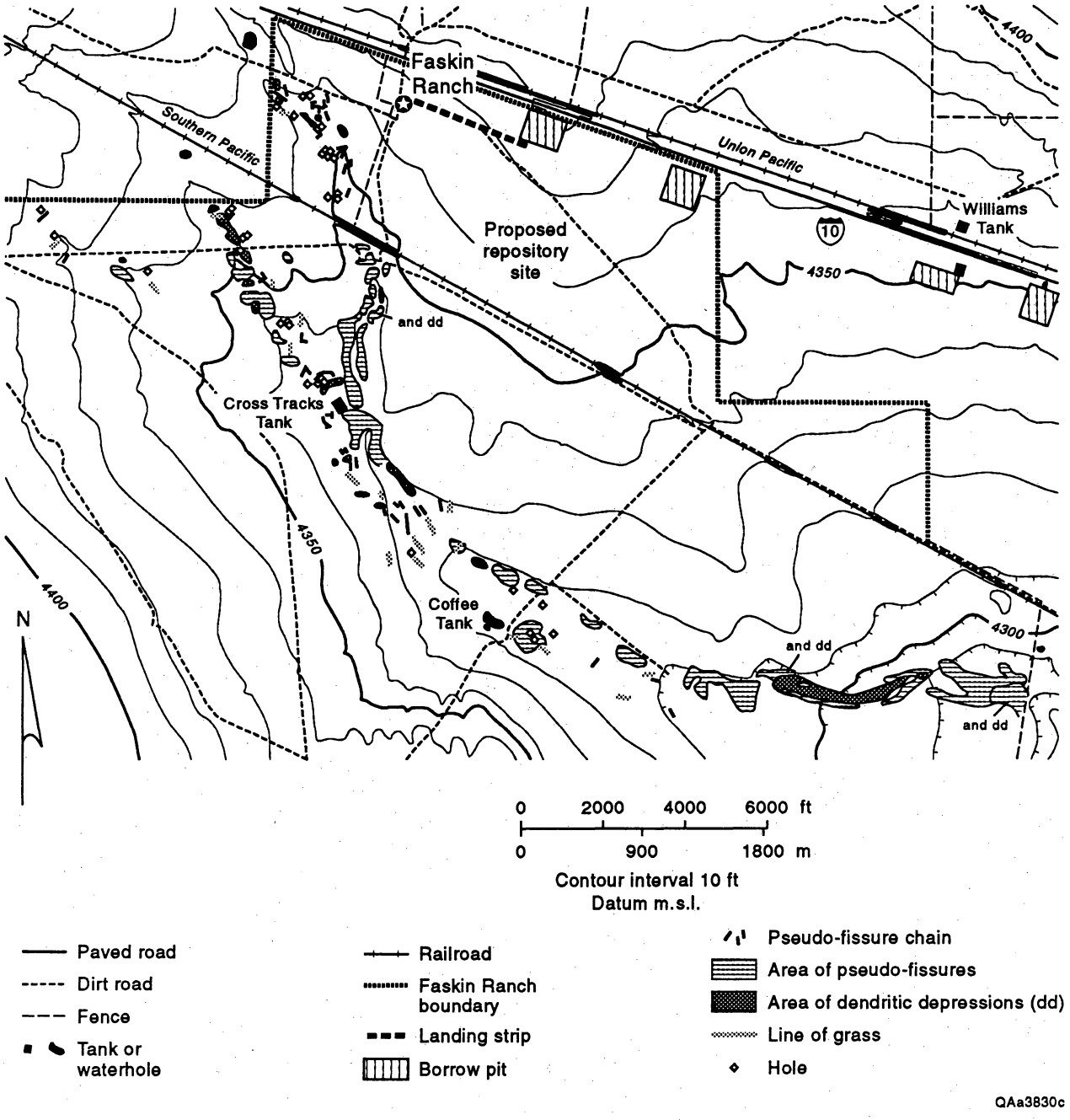

Figure 14. Pseudo-fissures and related features mapped in Blanca Draw and the tributary draw that joins it at Cross Tracks tank. Mapping was done inside the boundaries of Faskin Ranch.

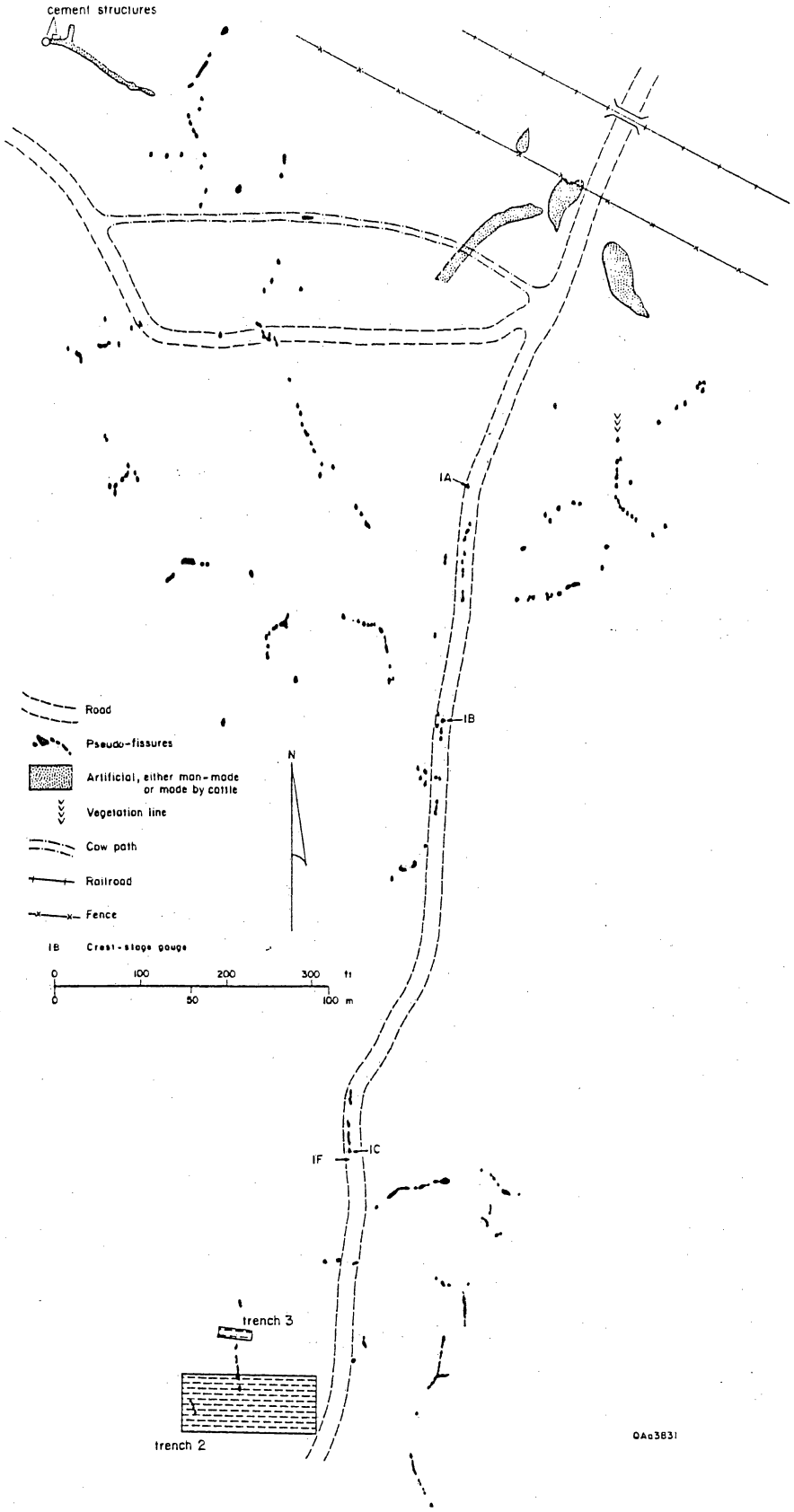

Figure 15. Map of pseudo-fissures in the main tributary to Blanca Draw, south of the Southern Pacific Railroad and north of Cross Tracks tank. Trenches 2 and 3 were excavated at the south end of the map area.

deep and are 1 to 6.6 ft (0.4 to 2 m) long. Larger features are present immediately south of the Southern Pacific tracks at the railroad bridges. Trench 4, at the eastern railroad bridge (fig. 3), contained cow manure and railroad slag as deep as 3 ft (1 m), supporting the interpretation that these large features result from the activities of man or cattle.

The pseudo-fissures in the wash deposits are commonly associated with animal burrows or holes that may have originated as burrows. Animal burrows may be present because the wash deposits are relatively easy for the animals to excavate or because of the proximity to tanks or the presence of vegetation. Some burrowlike features, possibly natural pipes, exit from the bottom of the pseudo-fissure walls, parallel with the floor, or they may enter from the middle of a pseudo-fissure wall. Burrows may, in some cases, contribute significantly to the shapes and orientation of the pseudo-fissures because they may focus water flow and initiate piping.

Mapping of Pseudo-Fissures in Wash Bottoms

Because pseudo-fissures are concentrated in the wash bottoms on Faskin Ranch, the wash bottoms were walked in a series of parallel traverses in order to map the distribution of pseudo-fissures and similar features. Prior to walking the washes, an area known to contain pseudo-fissures was traversed at different spacings. Most pseudo-fissures were encountered and mapped when traverses were spaced 33 and 66 ft (10 and 20 m) apart; therefore, we used a 66-ft (20-m) spacing between traverses.

Typical, well-expressed pseudo-fissures consist of curvilinear strings of holes and cracks in the ground (fig. 15). Between or extending past the holes and cracks may be a shallow depression or a curvilinear stripe of thicker grass. There is a gradation from well-developed pseudo-fissures to lines of grass with no visible holes. Likewise, there is a gradation from curvilinear strings of holes to isolated round holes with vertical sides. Conversely, some holes in the ground occur as pairs or as isolated single holes, are oval, and have one sloping side. These

holes are considered to be burrows and were not mapped. The following list describes the features mapped in the washes.

1. **Pseudo-fissure**—a curvilinear group or chain of holes and cracks in the ground, commonly linked by a shallow depression. Where several pseudo-fissures occur close together, the area including them was mapped as an area of pseudo-fissures. Well-defined pseudo-fissures consist of chains of depressions. About 120 individual depressions were measured during mapping of the pseudo-fissures. These have log-normal size distributions, with a mean length of 1.8 ft (0.56 m), a mean width of 1.3 inches (0.4 m), and a mean depth of 13.4 inches (0.34 m). The depressions tend to be elongate along the line of holes (fig. 15). Depressions have a log-normal distribution of length-to-width ratios, with a mean along pseudo-fissure dimension 1.4 times the across-pseudo-fissure dimension.

Chains of holes are closely spaced. Figure 16 is a histogram of the distances between nearest-adjacent holes. Most holes are within 3 ft (1 m) of the nearest adjacent depression. Beyond 22 ft (7 m), there is a random distribution of the distances between depressions. Therefore, when depressions are separated farther than 22 ft (7 m), there is little confidence that they are part of the same pseudo-fissure, and a separation of more than 22 ft (7 m) is inferred to indicate that depressions may be part of unrelated pseudo-fissures.

Pseudo-fissures are relatively short, when compared to known fissures in the Trans-Pecos area. The mapped pseudo-fissures average 43 ft (13 m) long, the longest being 125 ft (38 m). Most of the pseudo-fissures mapped in the Blanca Draw tributary north of Cross Tracks tank are oriented north-south, subparallel to the axis of the wash (fig. 17). The angles between adjacent individual depressions are generally less than 10° (fig. 18). This indicates that most depressions are in relatively straight chains. This is confirmed by dividing the sinuous length of the chain pseudo-fissure by a straight-line cord along its length. The sinuosity (L_s/L_c) of the pseudo-fissures is 1.04, indicating very little sinuosity within individual pseudo-fissure chains. In contrast, pseudo-fissures that connect to each other generally do so at high angles. The mean angle of 21 mapped pseudo-fissure chain connections is 58° (fig. 19).

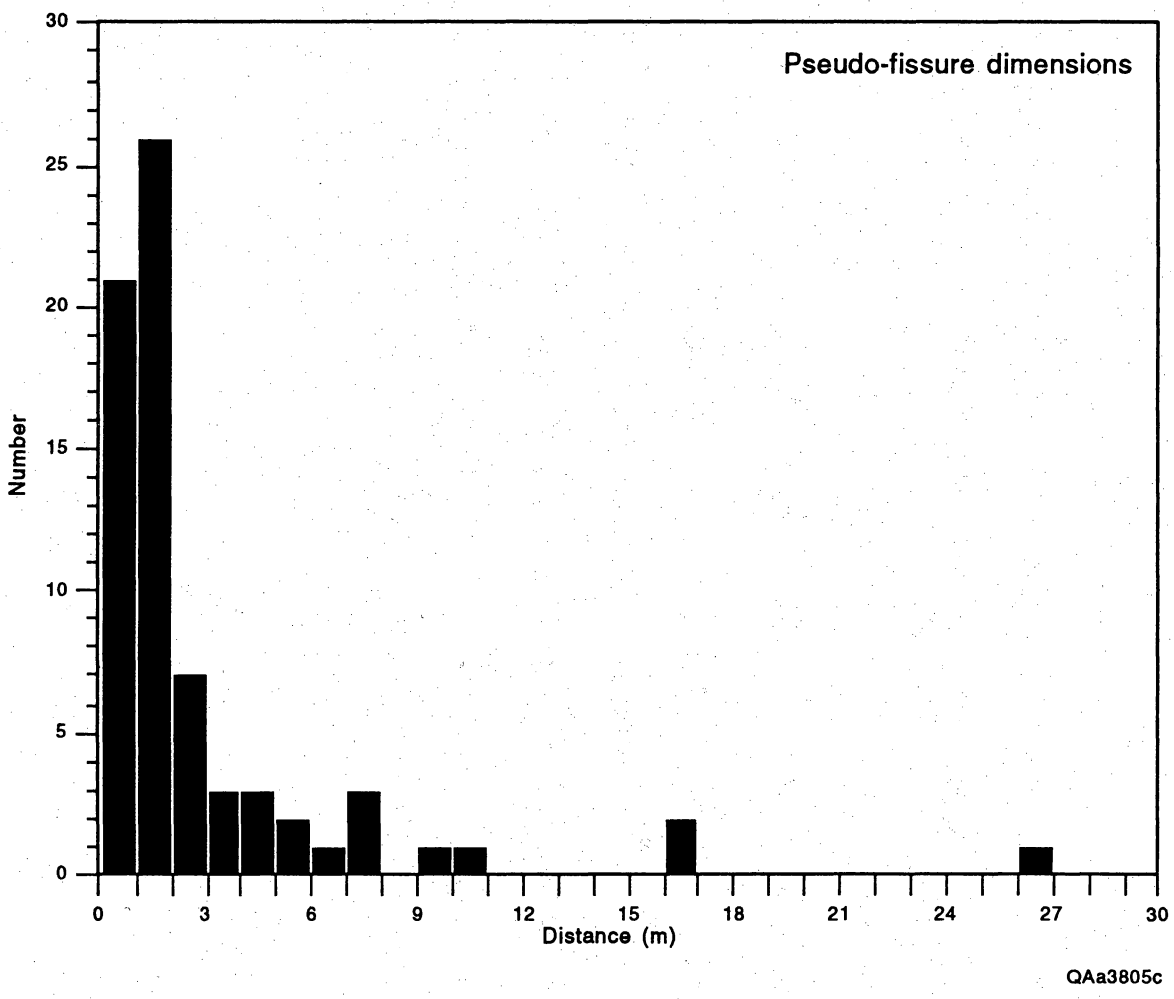

Figure 16. Histogram of the distances between nearest-adjacent single depressions and holes along pseudo-fissure chains. Data taken from the fenceline to 900 ft (300 m) south of the fenceline shown in figure 15.

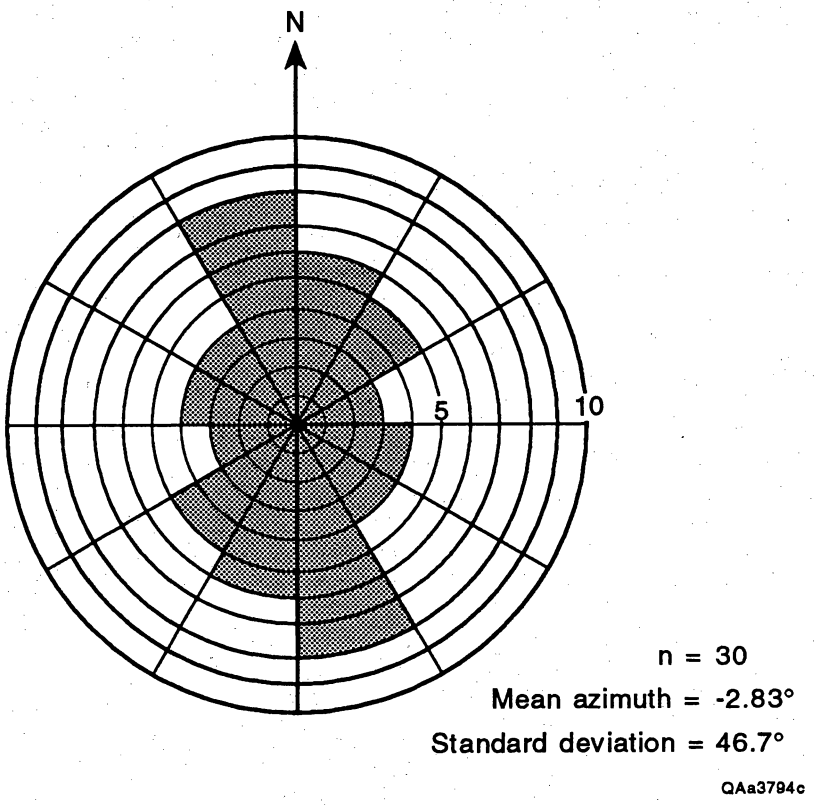

Figure 17. Rose diagram of pseudo-fissure chain azimuths within the mapped area north of Cross Tracks Tank (area from the fenceline to 900 ft [300 m] south of the fenceline shown in figure 15).

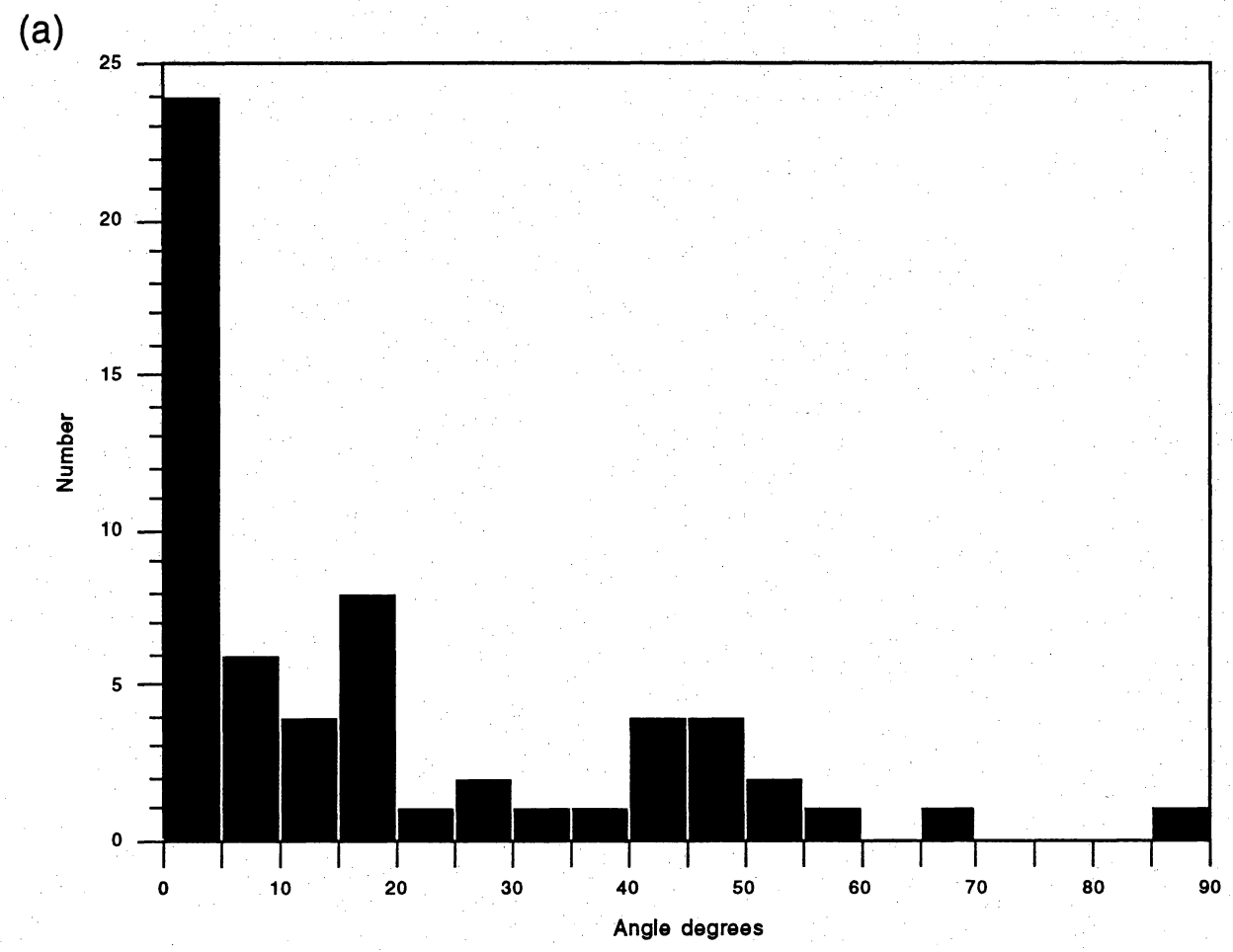

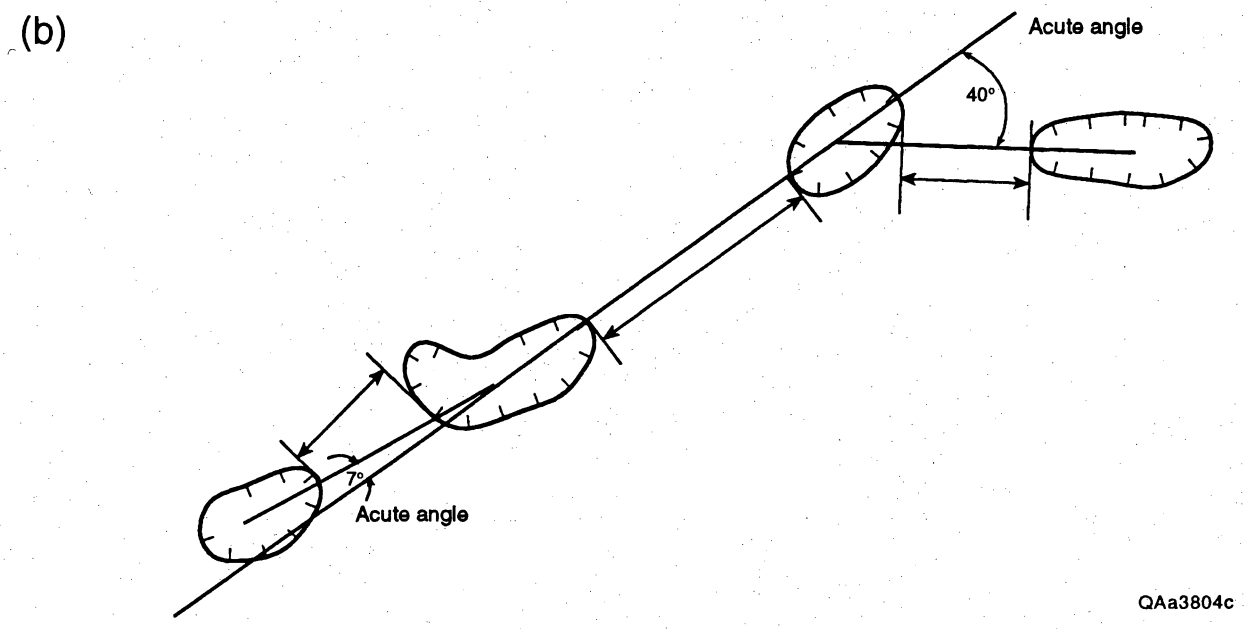

Figure 18. (a) Histogram of the deviation in degrees from a straight line connecting depressions separated by less than 22 ft (7 m). This includes both single and multiple pseudo-fissure chains. Data taken from the fenceline to 900 ft (300 m) south of the fenceline shown on figure 15. (b) Method used to measure distances between individual pseudo-fissure depressions and acute angles both between and within pseudo-fissure chains for figures 16 and 18a.

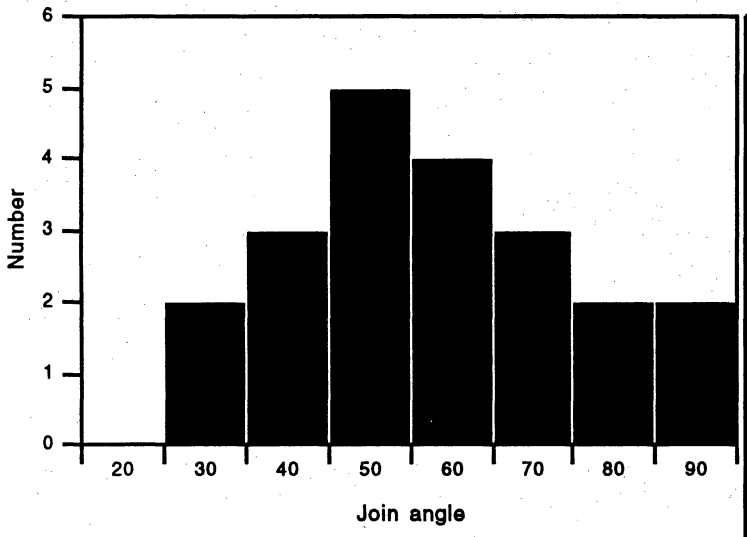

	Join Angle
Minimum	30
Maximum	90
Sum	1230
Number of samples (points)	21
Mean	58.571429
Median	60
Root mean square	61.19835
Standard deviation	18.175729
Variance	330.35714
Standard error	3.9662693
Skewness	0.19734165
Kurtosis	-0.95436728

QAa3792c

Figure 19. Histogram of the join angle between connecting pseudo-fissure chains. Data taken from the fenceline to 900 ft (300 m) south of the fenceline shown in figure 15.

The chains of depressions also seem to join in a reticulate or netlike pattern (fig. 15). However, few pseudo-fissures terminate within 22 ft (7 m) of an adjacent pseudo-fissure. Most pseudo-fissures connect to either 0 or 1 other pseudo-fissure. They average 0.8 connections per pseudo-fissure.

2. **Grass Lines**—Curvilinear lines of thicker grass that rarely occur along a linear depression. Grasses in the study area commonly grow in lines and circles as part of their normal growth habit, and most lines of grass are not related to pseudo-fissures. However, longer, straighter grass lines, or those containing holes, may be related to the formation of pseudo-fissures, and these were mapped separately.

3. **Holes**—Many holes have sloping entrances and continue to angle below the surface. These are probably burrows. Other holes have vertical walls on all sides and do not continue as a tunnel beneath the surface. These were mapped because they may be related to pseudo-fissures or may be poorly expressed pseudo-fissures.

4. **Dendritic Depressions**—Dendritic depressions are irregularly shaped depressions, no more than 12 inches (30 cm) deep and usually shallower than 8 inches (20 cm) deep, commonly linked into dendritic networks converging on larger central depressions. Dendritic depressions were mapped, even though they are not pseudo-fissures, because they may be related to the same process (discussed below). Dendritic depressions are readily differentiable from pseudo-fissures due to (1) their rough, generally nonlinear, irregular shapes, with abrupt changes in direction, and (2) their shallow bowl shape, with few or no deep cracklike depressions. There is no gradation from pseudo-fissures to dendritic depressions. Each type is distinct. Therefore, we do not believe that dendritic depressions represent either incipient or senescent pseudo-fissures. Dendritic depressions are restricted to Tobosa grass flats in the wash bottoms, and are generally much shallower than pseudo-fissures. They rarely exhibit mud cracks or small vertical holes in the larger depressions.

Subsurface Study

Trenches were dug to determine the subsurface morphology of the pseudo-fissures (table 2). A trench through the end of a pseudo-fissure in the main tributary to Blanca Draw (trench 2, figs. 3 and 20) revealed no open or filled crack beneath the surface depression. A distinct change in sediment color is present beneath the pseudo-fissure, characterized by an apparent accumulation of calcic material on one side and a medium-gray organic-rich zone on the other side. Calcic concentrations from a series of samples taken across the color transition zone (fig. 20) show that the darker gray zone has less calcic material than the apparent calcic-rich area, but that the apparently calcic-rich area is not significantly different in calcic concentration from sediment at the same level horizontally (fig. 20). At trench 5, which intersects a pseudo-fissure located in a narrow depression that acts as a tributary to Blanca Draw (fig. 3), a similar apparent accumulation of calcic material is located beneath the pseudo-fissure, but no organic-rich zone or crack is apparent.

Stage-Gauge Measurements

A series of stage-gauge measurements were made in three selected pseudo-fissure locations (fig. 3) to determine the degree to which the depressions collected water. Group 1, gauges 1A–1F, were placed in the region of densest pseudo-fissures south of the Southern Pacific tracks. Gauges A, B, and C in this group were located in the bottom of pseudo-fissures in the road near the center of the wash, and they each collected water, 0.4 inches (1 cm) or more, twice during the 10-month monitoring period (table 3). The two gauges on the hillslope above this wash area (D and E) each recorded water only once, less than 0.4 inches (1 cm) in depth. The stage gauge on the road surface in the wash bottom collected no surface runoff, even when gauge 1C, about 10 ft (3 m) away, collected 1 and 1.3 inches (2.7 and 3.2 cm) of water. Based on these data, the pseudo-fissures collect water more than the hillslopes or the wash bottom.

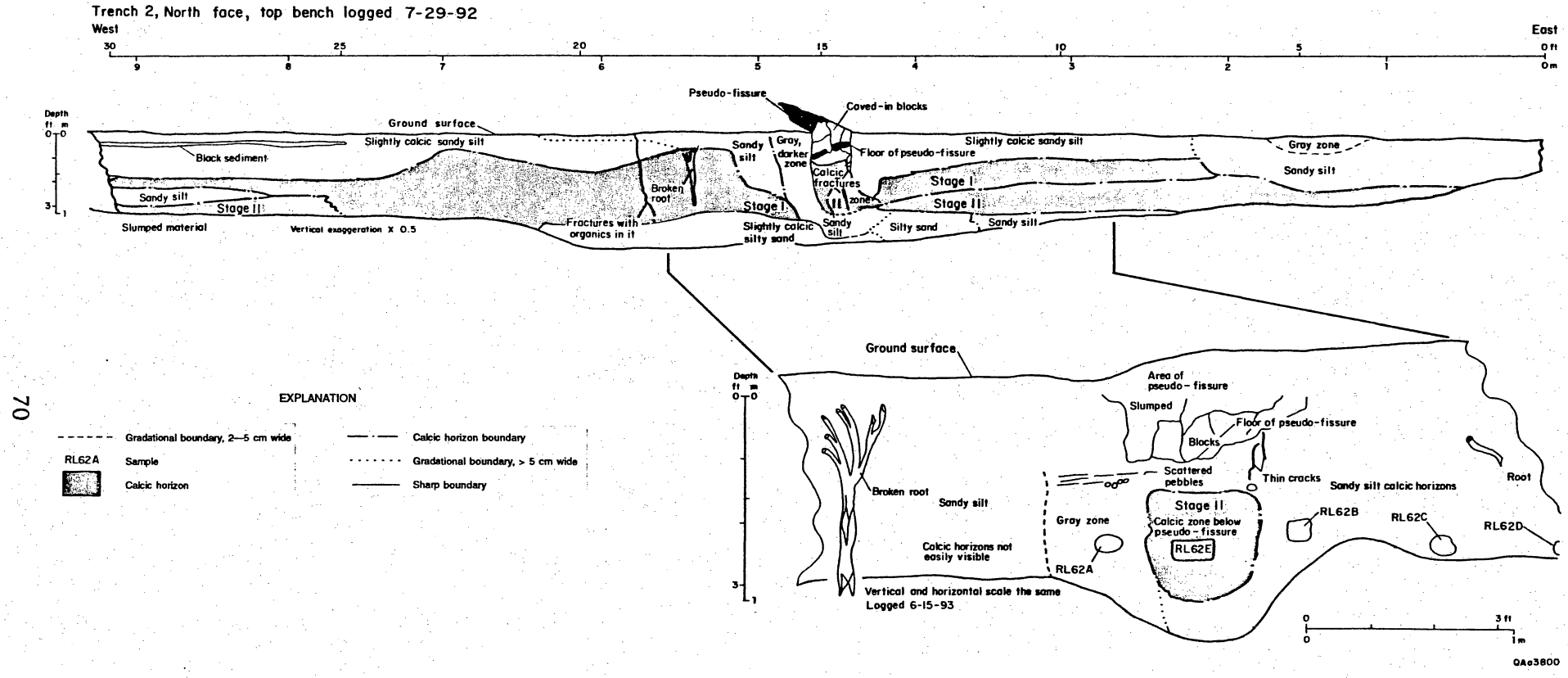

Figure 20. Lithologic description of trench 2. Calcium carbonate content of the soil is 9 percent for sample RL62A, 16.1 percent for sample RL62B, 18.4% for sample RL62C, and 18.0 percent for sample RL62D. Not shown in this figure are samples SDFR8 (17.4 percent soil carbonate) and SDFR9 (17.8 percent soil carbonate), taken just below the calcic horizons and at 12 ft (4m) deep, respectively. See figure 3 for trench location.

Table 2. Trenches dug on Faskin Ranch.

Trench no.	Purpose of investigation	Size[1]
1	Vegetation linear on aerial photographs	large
2	Pseudo-fissure	large
3	Pseudo-fissure	small
4	Large depression	small
5	Pseudo-fissure	small
6	Dendritic depressions	small
7	Linear on aerial photographs	small
8	Channel area (large depression)	small
9	Hoover fissure	small
10	Channel area (large depression)	small
11	Calcic horizon morphology	small
12	Pseudo-fissure	small
13	Pseudo-fissure	small
14	Vegetation linear on aerial photographs	small
15	Vegetation linear	small
16	Vegetation linear	small
17	Stratigraphy and paleomagnetic sampling	large
18	Hoover fissure	large

[1]Small = ≤10 ft deep or ≤ 25 ft long. Large = ≥ 10 ft deep or ≥ 25 ft long.

Table 3. Crest-stage gauge measurements (in centimeters), highlighted where greater than zero. Locations of gauges shown in figure 3.

Gauge	p[1]	Total times wet	10/26/92	11/16/92	12/14/92	1/5/93	1/21/93	2/8/93	3/30/93	4/22/93	5/4/93	7/6/93
1A	P	2	0	0	0	0	3.3	0	0	0	0	3.1
1B	P	2	1.5	0	0	0	2	0	0	0	0	0
1C	P	2	0	0	0	0	0	0	0	0	2.7	3.2
1D		1	0.5	0	0	0	0	0	0	0	0	0
1E		1	0	0	0.8	0	0	0	0	0	0	0
1F		0	0	0	0	0	0	0	0	0	0	0
2A		1	0	0	0	0	0	0	0	0	2.2	0
2B	P	1	0	0	0	0	0	0	0	0	0	1.3
2C		6	0.2	0	1.6	0	0	1.7	0	0.7	2.7	2.8
3A		3	0.8	0	0	0	4	0.8	0	0	0	0
3B	P	3	3.6	0	0	0	4.6	0	0	0	0	7.8
3C		6	1.9	1.4	1.9	2.2	2.4	0	0	0	0.4	0

[1]Crest-stage gauge located in a pseudo-fissure.

The observation that pseudo-fissures collect water more frequently than the hillslopes or the wash bottom is confirmed by eyewitness accounts on two occasions, when a small, shallow stream of water was observed flowing down the road and into the pseudo-fissures. When one pseudo-fissure filled with water from a flow down the road, then the adjacent few down the wash would also contain water, although there would be no flow over the surface into them, since it had all been captured by the farthest upstream pseudo-fissure. Damp soil and water could be observed in the pseudo-fissures the day following a rain, although the remainder of the wash bottom was dry.

Group 2, gauges 2A–2C (fig. 3), was located in a small interfluvial drainage between Blanca Draw and the tributary wash to the east. Gauge 2C received the most water of the group, more than gauge 2B located in the pseudo-fissure. However, gauge 2B could not be placed in the very bottom of the pseudo-fissure due to its depth of >1.5 ft (>0.5 m), and water accumulation may have occurred but been unrecorded.

Group 3, gauges 3A–3C (fig. 3), was located at a pseudo-fissure in a distinct vegetation linear, one of two parallel linears in an area immediately west of Grayton Lake that are interpreted to be either an abandoned channel of Blanca Draw or vegetation linears developed from cattle trails. The topographic expression of this low area is clearly expressed as a "u" shape on the 5-ft (1.5 m) contour map of northern Faskin Ranch prepared for this project by Cooper Aerial of Phoenix, Inc. The two vegetation linears mark each side of the abandoned channel, much like the two lines of mesquite that occur on each side of Blanca Draw as it crosses from the Hoover property onto Faskin Ranch near trench 8. The linears lead directly between Coffee Tank and the tank in Grayton Lake and are composed predominantly of yucca plants and bushes. No cracks were present in two trenches dug through the linears. Dry sandy mud and muddy sand basin-fill deposits were encountered.

Comparisons of rainfall and stage heights from February to July (table 4) show that rainfall from single storm events of 0.09 in (2.2 mm) or less did not result in an accumulation of water at the adjacent stage gauges. Rainfall amounts of 0.3 in (8 mm) or more from single storm events,

Table 4. Rainfall in millimeters at three tipping bucket rain gauges from February through June 1993. Gauges located on figure 4. Gauge FR1 located at crest stage-gauge group 1 and gauge FR3 located at crest stage-gauge group 3. No rainfall gauge located at crest-stage gauge group 2. S - steady rain, sh = showers.

Gauge	2/28/93	4/13/93	4/29/93	5/19/93	5/28/93	6/(17/18)	6/(18/19)	6/23/93	6/26/93	6/30/93
FR1	2.8	0.8	malfunction	2.8	4.6	2.8	2.6	4.0	1.4	1.4
FR2	6.0 s	2.4	1.4	8.0 s	3.2	2.6	12.4 s	0.0	0.0	1.4
FR3	5.6 sh	2.8	1.0	8.0 s	3.0	2.8	10.0 s	0.0	0.0	0.6

in late May and June at rain gauge stations FR1 and FR3, do coincide with relatively high water level readings in the pseudo-fissures (compare tables 3 and 4). More detailed hydrologic characteristics of the pseudo-fissures are described in Scanlon and Xiang (1993).

Possible Origins

The depressions and holes on Faskin Ranch have been named pseudo-fissures because they are similar in scale and probable origin to pseudo-fissures described in California by Shlemon and LaChappelle (1992). The pseudo-fissures studied by Shlemon and LaChapelle (1992) are described as local surface phenomena related to near-surface desiccation in clayey sediments. They are characterized by surface depressions less than 2 inches (5 cm) deep and 6 inches (20 cm) long, smaller, but similar in geometry to the pseudo-fissures on Faskin Ranch. Hairline cracks present below the California pseudo-fissures were shorter than 9 ft (3 m). No cracks were visible below the pseudo-fissures on Faskin Ranch. Surface crack morphology is evident in the pointed ends observed on pseudo-fissure depressions southeast of Cross Tracks tank; these features appear to have originated as surface cracks. Ground cracks (11 inches and 6 ft [30 cm and 2 m], respectively) were also observed in the vicinity of pseudo-fissures in the drainage directly east of Sand Mountain and adjacent to the road at trenches 12 and 13.

Surface or near-surface desiccation is a possible origin for the pseudo-fissures on Faskin Ranch. Cracking below the surface which then propagates upward and causes collapse provides a mechanism of formation for both the piping features and the surface depressions. This mechanism was suggested for similar features in South Dakota (White, 1970) (fig. 21). Rodent burrowing considerably enhances the connectivity and piping between many pseudo-fissures on Faskin Ranch.

Hydrocompaction of the soil may be responsible for the loss of soil volume necessary to explain the depressions and the piping features. We obtained soil density and dispersivity measurements of the soils at four locations (table 5). One was in the wash floor adjacent to

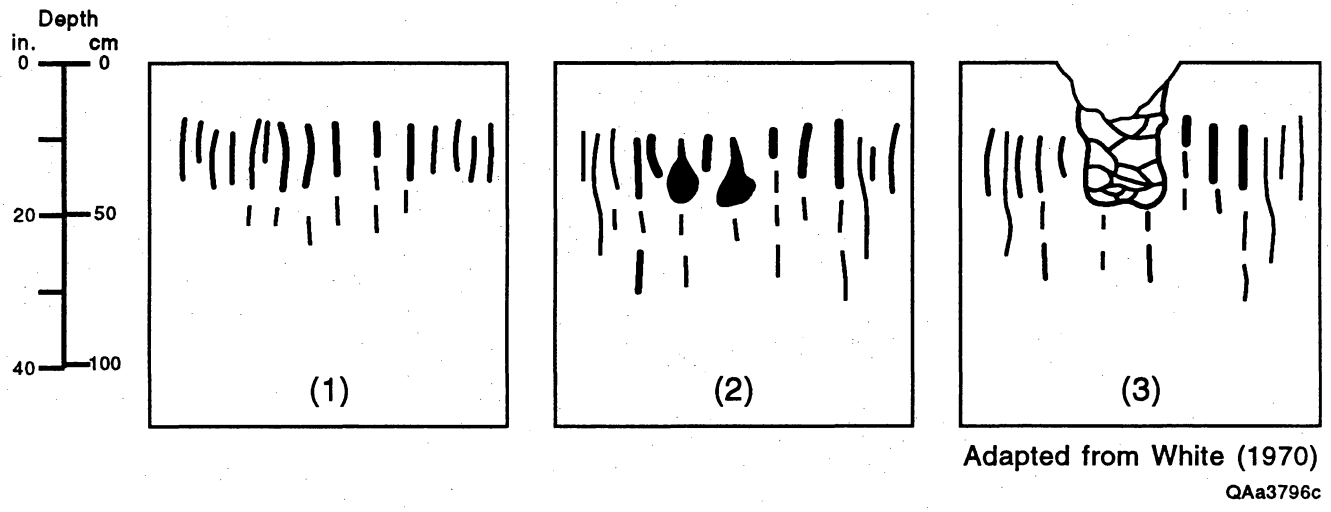

Figure 21. A proposed theory for formation of pseudo-fissures. In (1) cracks form in clayey soils, in (2) piping enlarges cracks beneath the surface, and in (3) piping features collapse at the surface forming depressions. Adapted from White (1970).

Table 5. Engineering test results from near-surface samples. Sample locations shown in figure 3. Samples with highest dispersivity values have the greatest potential for expansion and collapse.

Sample	Depth (ft)	Soil type (USCS)	Moisture (%)	Dry density (pci)	Saturation (%)	%<200 (%)	Swell/Collapse (+/-, %)	Dispersivity (%)	0.002 mm (%)
TW1,#1	0.25	CL	9.3	82	24	79	-1.4	55	23.9
TW1,#2	2.00	CL	11.5	75	25	93	-1.4	19	37.5
TW1,#3	3.00	CL	10.9	88	32	91	0.3	13	44.2
TW2,#1	0.25	CL	9.7	84	26	83	-0.8	27	25.4
TW2,#2	2.50	CL	9.1	84	24	85	-0.7	14	36.3
TW2,#3	3.00	CL	7.7	88	22	76	-1.4	16	35.9
BW1,#1	0.25	CL	10.3	92	33	73	2.2	13	26.1
BW1,#2	2.00	CL	10.3	97	36	82	1.3	2	41.1
HF1,#1	0.25	CL	7.1	79	17	67	-5.4	23	20.1
HF1,#2	2.50	CL	4.8	101	19	72	-0.2	18	30.9
HF1,#3	3.30	CL	3.3	99	12	45	-2.8	41	12.3

Sample locations
TW1 = Adacent to pseudo-fissures in wash floor
TW2 = In wash floor in areas having few pseudo-fissures
BW1 = In wash floor in areas having pedritic depressions
HF1 = Adjacent to Hoover fissure

several pseudo-fissures. Two others were in wash floors but not near pseudo-fissures, and the fourth was adjacent to Hoover fissure. Samples were collected from two or three depths at each location. The dry density of the wash fills averaged 86 pounds per inch^3 (pci) for all depths, whereas the Hoover fissure samples averaged 93 pci, which is a higher, but not statistically significant difference. Dispersivity, or erodibility, was similar for all samples except from the uppermost sample collected adjacent to the pseudo-fissures (TW1, #1 on table 5). This sample was highly dispersive. Although only a single measurement, it does indicate the possibility of hydrocompaction as a factor in the formation of pseudo-fissures. Sediment in the pseudo-fissures has low permeability, similar to that in the rest of the Draw (already compacted) (Guelph permeameter data, see Scanlon and Xiang, 1993). Compaction occurs by burrowing and livestock trampling as well as by thorough wetting of the sediment after it has been deposited (hydrocompaction). Hydrocompaction (Slaff, 1993) occurs in soils in which clay and silt grains form bridges between soil particles that collapse when the soil becomes saturated. A near-surface phenomenon, it occurs where surface waters accumulate and may contribute to the formation of some of the pseudo-fissures. Pseudo-fissures are most abundant in areas of the draws where the gradient is lowest and hence most conducive to (1) accumulation of standing water and resultant growth of vegetation that encourages livestock visitation, and (2) burrowing encouraged by the softness of damp ground. Wetting and drying cycles combined with soil type are probably most important to pseudo-fissure formation, and may explain why there are no pseudo-fissures outside of the wash areas.

Fissures

Earth fissures are linear surface features characterized by collapse and erosion that commonly exhibit extensional cracks in the subsurface. They have been described in the southwest United States and California by many authors and in the local Hueco Bolson, Red Light Draw, southeast Eagle Flat, Green River Valley, and Ryan Flat areas by Baker (1927),

Underwood and DeFord (1969), Albritton and Smith (1965), and eyewitness accounts. Both regional and local fissure occurrences are summarized in a compilation by Baumgardner and Scanlon (1992).

Surface Character

A true earth fissure that exhibits different morphology, extent, and hydrologic characteristics from the pseudo-fissures is present on the northwest side of Faskin Ranch (fig. 22). The fissure is a 0.75-mi- (1.2-km-) long linear feature marked clearly by vegetation on aerial photographs and on the ground by a linear series of depressions, averaging 66 ft (20.1 m) in length, 6.8 ft (2.09 m) in width, and 1 ft (0.3 m) in depth. The fissure is significantly longer and wider than the pseudo-fissures but the depth of the surface depression is about the same (compare fig. 23, table 6, fig. 24, and fig. 25), and it is nearly 0.5 mi (0.8 km) away from drainages where the pseudo-fissures occur. Although it appears as a drainage on the USGS topographic map, this interpretation was probably made based on the presence of the vegetation linear; no topographic expression of the linear is visible on the 5-ft (1.5-m) contour map prepared for this project by Cooper Aerial of Phoenix, Inc.

The hydrologic characteristics of the fissure are important to the criteria that set it apart from pseudo-fissures and from other vegetation linears on the ranch that are not fissures. Hydrologic data on this fissure are discussed in depth by Scanlon and Xiang (1993). To facilitate discussion of this fissure in comparison to other similar features, it is called the Hoover fissure, the name of the property where most of the fissure lies.

Subsurface Character

Hoover fissure was trenched in two locations (plate 6). No single well-defined extensional fracture was evident. However, discontinuous extensional cracks and vertically elongate sand-filled features extend to the base of trench 9 (plate 6). These funnel-shaped areas of sand 2 to

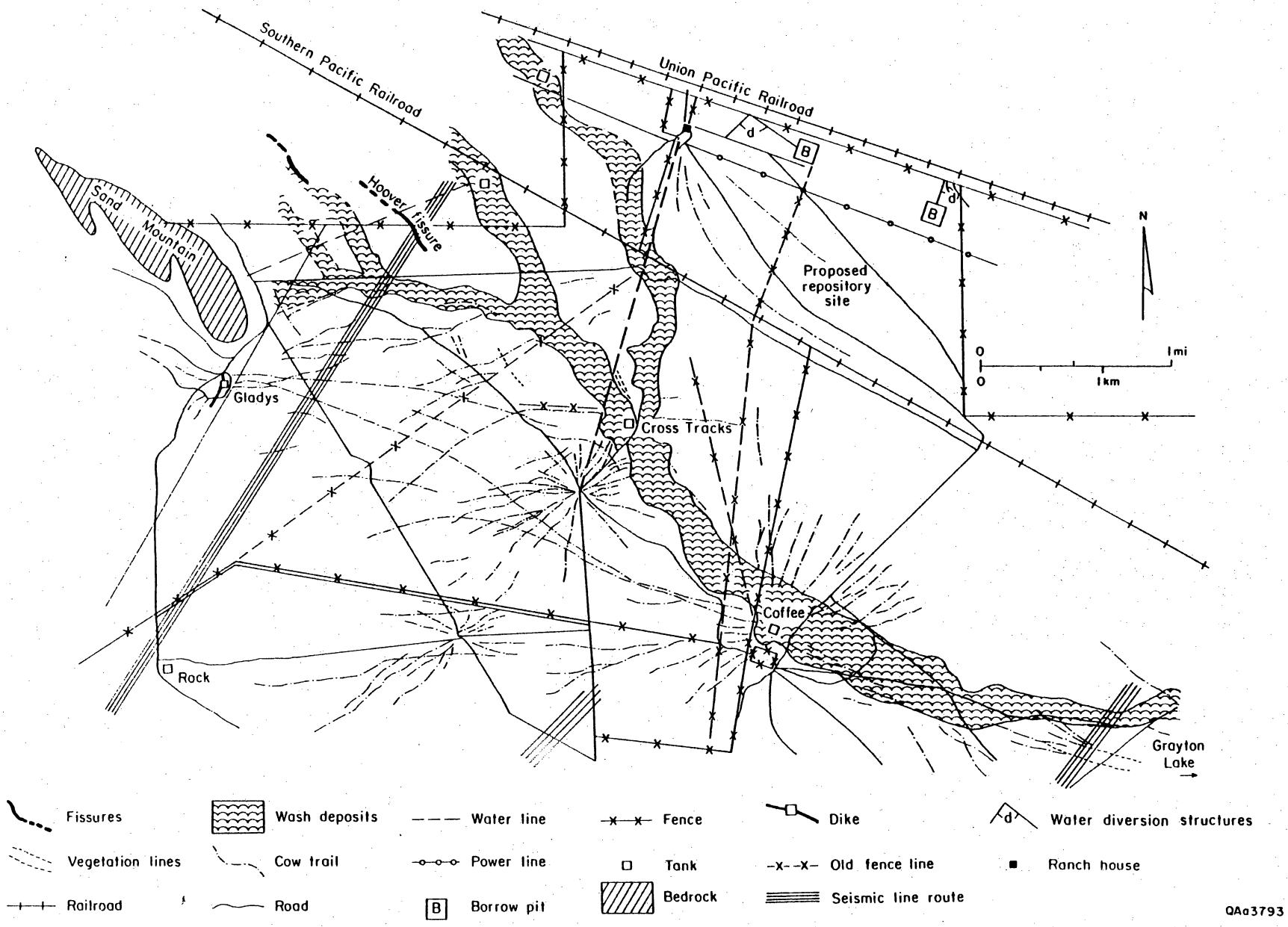

Figure 22. Hoover fissure and other linears on northern Faskin Ranch. Map drawn from 1980 1:24,000-scale color aerial photographs taken by Intrasearch and from 1991 1:20,000-scale black and white aerial photographs taken by the Texas Department of Highways and Public Transportation. Pseudo-fissures within mesquite-covered drainages are not visible on aerial photographs and are not shown on this map.

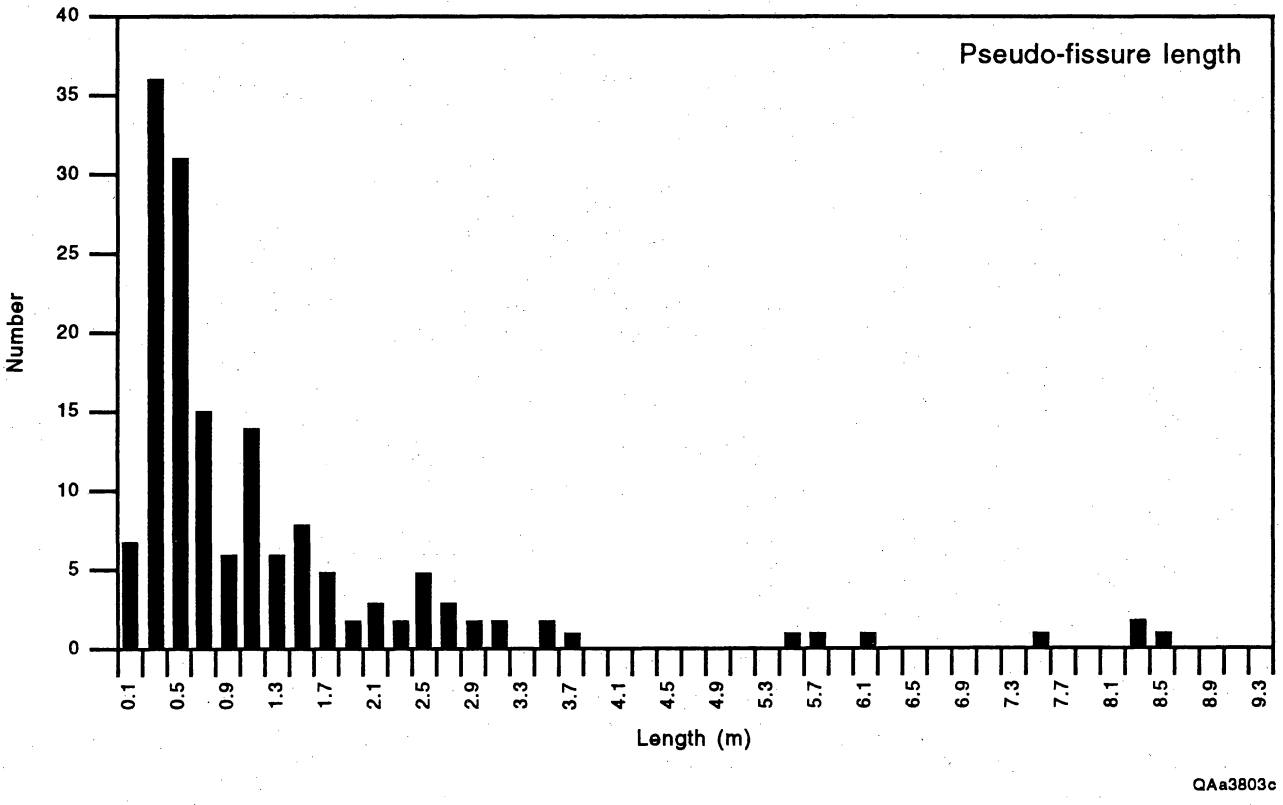

Figure 23. Histogram of individual pseudo-fissure depression lengths. Data taken from the fenceline to 900 ft (300 m) south of the fenceline shown in figure 15.

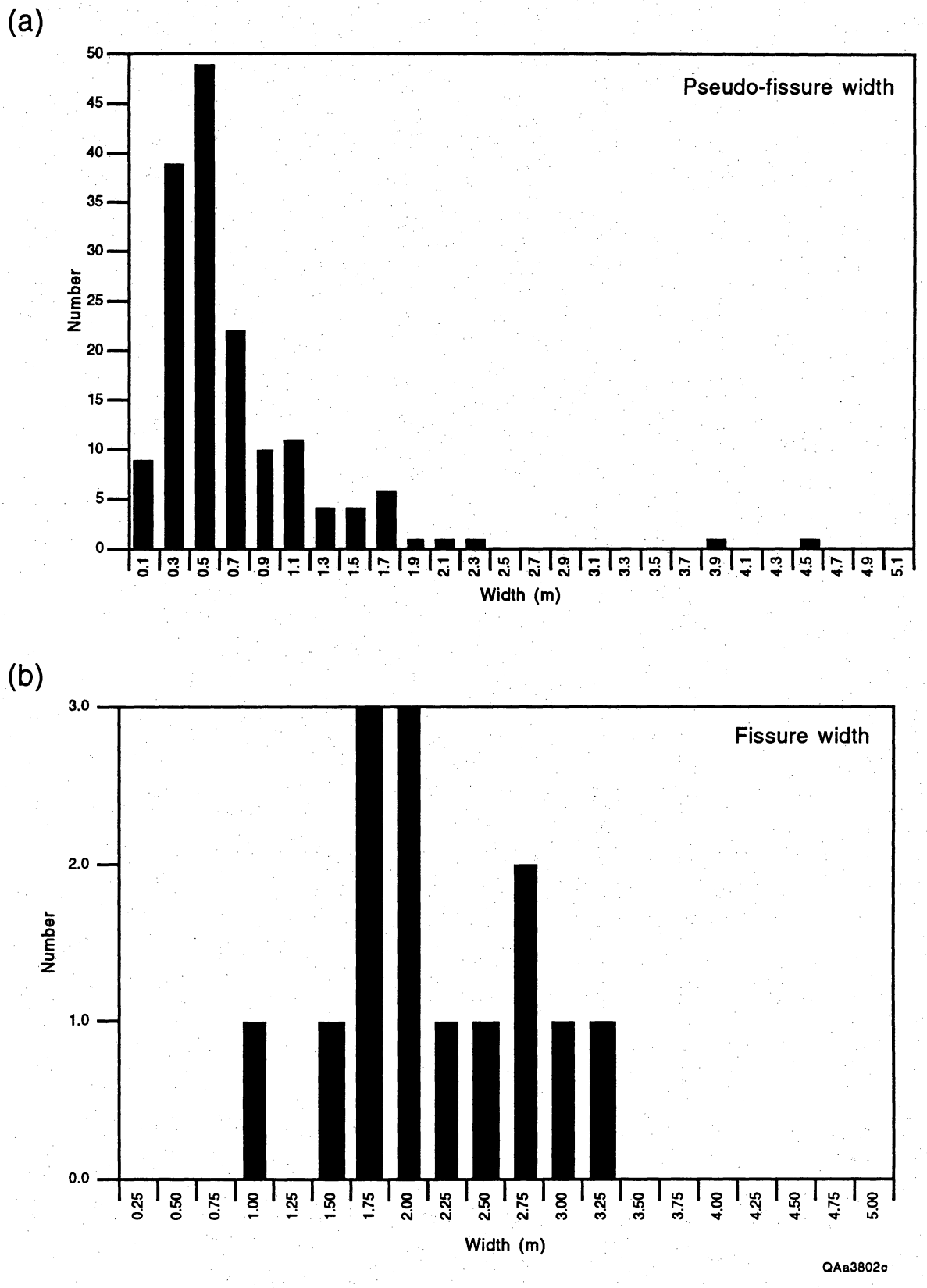

Figure 24. (a) Histogram of individual pseudo-fissure depression widths. Data taken from the fenceline to 900 ft (300 m) south of the fenceline shown in figure 15. (b) Widths measured along Hoover Fissure on northeast Faskin Ranch property.

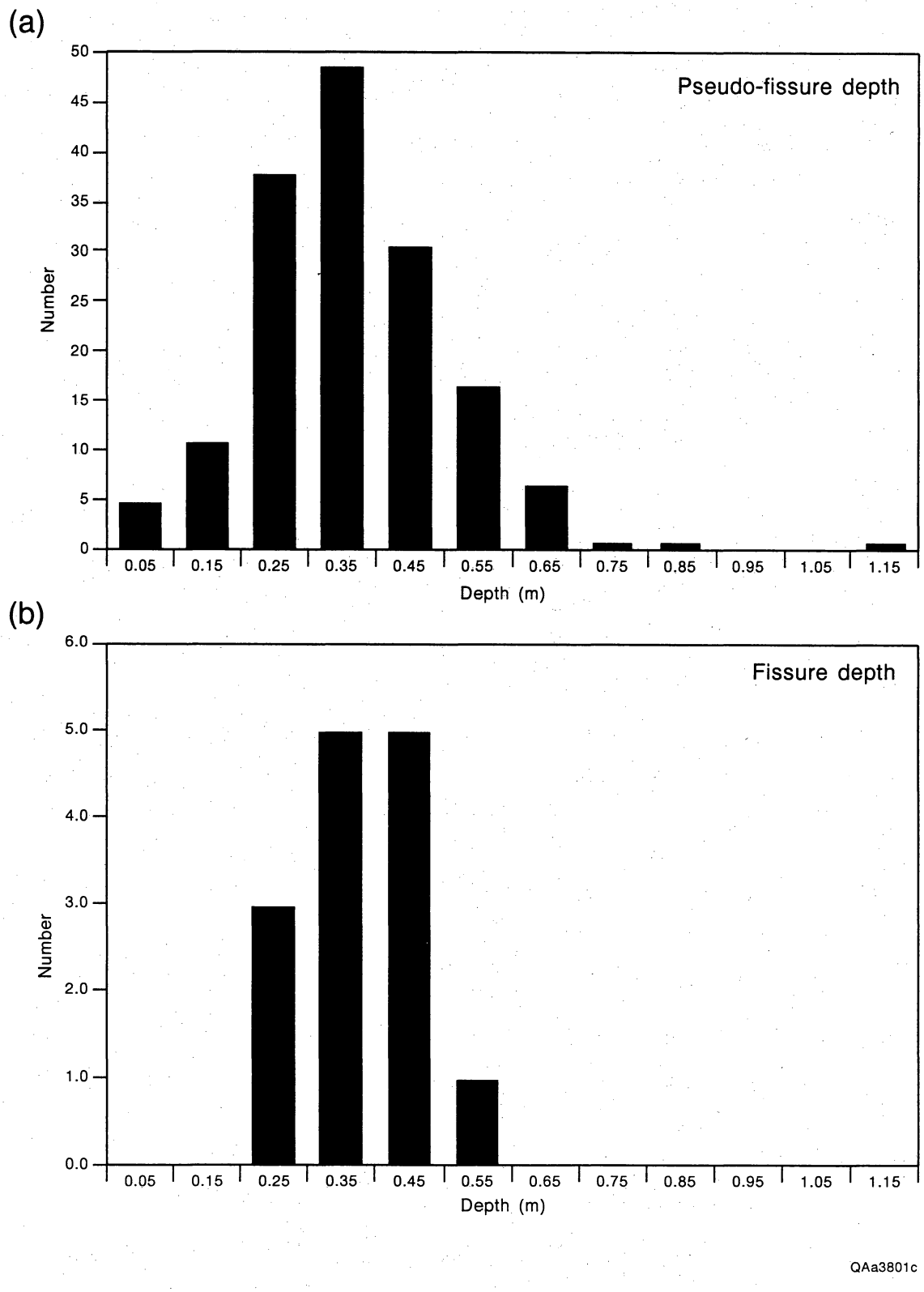

Figure 25. (a) Histogram of individual pseudo-fissure depression depths. Data taken from the fenceline to 900 ft (300 m) south of the fenceline shown in figure 15. (b) Depths measured along Hoover fissure on northeast Faskin Ranch property.

Table 6. Dimensions of Hoover fissure. Several width and depth measurements were taken across three linear groups of joined depressions. Width and depth data from this table are plotted in figures 24 and 25. NA=not available.

Length (m)	Width (m)	Depth (m)
32.2	2.40	NA
	3.10	0.40
	2.10	0.32
	2.80	0.47
	1.90	0.35
	1.00	0.36
	1.70	0.38
	1.60	0.20
	1.30	0.30
6.1	2.50	0.33
	1.85	0.21
19.1	3.10	0.30
	1.95	0.38
	1.60	0.25
	2.50	0.32

4 inches (5 to 10 cm) wide and several feet (decimeters) long are present within finer-grained sediment below the general area of the fissure but are not centrally located to the linear depressions. Two possible origins for the sand-filled features may be burrows or piping features. Two calcic horizons, A and B, that are continuous to the east on Faskin Ranch, are disrupted in a broad area (more than 39 ft [12 m] wide and 12 ft [3.6 m] deep) below the fissure depressions. The horizons typically have vertically oriented strings or groups of calcic nodules that are 1 to 1.5 ft (30 to 46 cm) long. A gap exists in the uppermost calcic soil horizon beneath the fissure. In trench 9 (plate 6) the blocks of calcic soil are in the middle of the fissure, displaced downward relative to the rest of the calcic horizon. These may be either blocks of calcic soil material that have fallen into the open fissure and subsequently buried or they may be patches of calcic soil dissolved along the fissure and reprecipitated.

The lower calcic horizon consists of discontinuous sharp-edged blocks of calcic soil that have as much as 73 percent calcium carbonate by weight (sample RL63D), whereas the adjacent material has a little as 17 percent calcium carbonate (sample RL63C). The embayed sharp margins of the block in the lower calcic horizon indicate that it has partly dissolved. Thin (0.8-inch- [2-cm-] wide) sand-filled cracks that form as a natural soil process in Vertisols are present in the walls of trench 18; similar sand- and mud-filled cracks are found throughout the cores (designation "v", app. A) and in trench 17 (plate 6).

Age

The wide, shallow character of the surface depressions could be indicative of a relatively old fissure. Thus, the absence of a defined open or sediment-filled crack below the center of the surface depressions of Hoover fissure could be because the fissure is relatively old.

Preliminary results indicate sediment samples from both a mud-filled crack about 2 ft (65 cm) below ground surface in the center of the fissure and a calcic zone slightly deeper near the edge of trench 18 are a minimum of 10,000 yr old (Langford, 1993; his samples RCFR5 and

RCFR6). Thus, the crack is not being filled with recent sediment, and is not part of a currently forming fissure system.

Possible Origins

Baumgardner and Scanlon (1992) discussed at length the possible origins of fissures in the desert climate and Basin and Range tectonic setting at the nearby Fort Hancock area. Possible origins include desiccation, differential subsidence over a bedrock escarpment, faulting, ground-water withdrawal caused by people, and ground-water withdrawal caused by nature. Desiccation has been described as a cause for polygonal vegetation linears and cracks at Wildhorse Basin to the east (Goetz, 1985). Although the Hoover fissure is linear and not polygonal, desiccation of clay at depth cannot be ruled out as a cause for the fissure. Neal and others (1968) described both polygonal and linear desiccation features at Indian Springs playa, Nevada. Lister and Secrest (1985) described both linear and polygonal patterns of fissures formed by desiccation at Red Lake Playa, Arizona. The presence of silt and clay and the absence of clean sand at depth is confirmed by core YM-35 (app. A), located in the center of the fissure; the extent of the fine-grained basin fill near Hoover fissure is shown in boreholes YM-3 and YM-19 (plate 2).

Aquifer subsidence in sediments that overlie a subsurface bedrock escarpment, documented for an origin for fissures in the Picacho Basin, Arizona (Jachens and Holtzer, 1979; Larson and Péwé, 1986), is another possible cause of Hoover fissure. The top of bedrock drops off steeply between boreholes YM-5 and YM-63 (plate 3); a similar bedrock irregularity could occur between Sand Mountain and the area northeast of Hoover fissure. A difference in compaction rates on the two sides of this postulated buried bedrock hill could have caused the fissure. This method of fissure formation is also proposed for the fissures near Camp Rice Arroyo (Baumgardner and Scanlon, 1992). The Arizona setting is associated with known ground-water withdrawal by people, and the Camp Rice Arroyo setting is associated with theorized ground-

water withdrawal caused after the integration of the Rio Grande drainage in Hueco Bolson approximately 2.25 mya (Gustavson, 1991).

Faulting has been described as an origin for some of the cracks at Wildhorse Basin north of Van Horn (Goetz, 1985). In northwest Eagle Flat Basin, no Quaternary faulting has been documented. It does not seem reasonable that Hoover fissure could have been caused by fault activity. A resistivity survey was run perpendicular to Hoover fissure. Moist zones were indicated, but no fault signature was evident in the survey (W. Price, written communication, 1993).

Ground-water withdrawal due to pumping has been documented as a cause for earth fissuring throughout the southwest (Holzer, 1984; Pewe and others, 1987; Pampeyan and others, 1988; Contaldo and Mueller, 1991). No wells in northwest Eagle Flat Basin produce water from an aquifer in the basin-fill sediments, and production of ground water from the aquifer in the bedrock has been minor in the few wells near Hoover fissure. Hoover fissure could not be caused by overpumping of aquifer zones in the region.

Natural lowering of the groundwater could have occurred when the Rio Grande entrenched the lower part of Red Light Draw in response to the lowering of base level coincident with the integration of flow from the Hueco Bolson to the Gulf of Mexico prior to 2.1 mya (Gustavson, 1991). However, judging from YM-19, basin-fill sediments beneath Hoover fissure are probably less than 250 ft (<75 m) thick, and judging from YM-19 and Faskin well, the current water table is probably more than 700 ft (>210 m) below surface. Any natural lowering of the water table over geologic time probably thus would not result in the current fissure features at the Hoover fissure.

Water ponding in a cattle trail over many years could have created surface depressions and dissolution of the calcic horizon beneath. A simple ponding explanation of the fissure does not require the formation of a tensional crack beneath the surface. Evidence of a preexisting cattle trail cannot be substantiated. The vegetation linear is clearly visible on Army Map Service 1:60,0000-scale aerial photographs taken in 1957; it is possible to project the trend of the

linear to another segment of a vegetation linear (crossed by trench 1) on the other side of a tributary draw. Cattle trails have become vegetation linears in several places on the ranch, the surface depression of the trail serving as a place where water is caught and plants grow larger.

The question of how sediment is moved to form the surface depressions is unexplained by any of the previously discussed theories of origin. The geometry of the depressions indicates that they formed by subsidence and compaction, and perhaps sediment could move downward along a crack or cracks in the subsurface, but the narrow cracks seen in many fissures would have to be tens of yards (meters) long to accommodate the sediment absent at the surface (Baumgardner and Scanlon, 1992). No continuous, central cracks are visible in the two trenches in Hoover fissure. The question of sediment movement, like that of the fissure origin, remains unanswered.

SUMMARY

The basin-fill stratigraphy, paleomagnetics, Quaternary history, and pseudo-fissures/fissures sections of this report describe parts of the geology of the Eagle Flat study area in southern Hudspeth County, Texas. Basin-fill sediments are composed predominantly of sandy mud and mud; sands are abundant at the surface in the vicinity of the proposed repository, and gravels are abundant at the base of the basin fill deposits adjacent to the bedrock. Relatively coarser surface deposits exhibit both fluvial and eolian characteristics. Fluvial deposits are represented by fine gravels and coarse sand deposits that fine upward into fine sands and muds. These may represent ephemeral stream deposits. Eolian deposits occur predominantly within 3 ft (1 m) of the surface and are well sorted fine and very fine sands.

Because much of the basin fill is composed of sediments high in silt and clay content, Vertisol characteristics such as mud- and sand-filled cracks and slickensides on ped faces are common. Calcic nodules, characteristic of semiarid soils, are distributed throughout the basin fill.

Sediment texture varies locally, and lateral continuity of individual units is limited to a few thousand feet (meters). Channel complexes are from 1 to over 20 ft (0.3 to 6 m) in thickness and contain pebble and a few cobble lenses interbedded with fine to medium sands.

Paleomagnetic studies conducted on 648 samples allow correlation between cores and provide an estimate of the age of the basin-fill sediments. Strong average MS measurements suggest that magnetite is an important magnetic mineral in these cores. There is good evidence for some variation in sedimentation rates both down and between cores. Core YM-17/53 preserves the longest sedimentary record and indicates that sedimentation was initiated in this part of the basin approximately 12 mya, during the middle Miocene. Cores YM-4 and YM-6 preserve relatively complete records of the Brunhes, Matuyama, Gauss, and Gilbert Chrons, indicating that sediments that lie 250 ft (76 m) beneath the present surface were deposited by 5.0 mya, and perhaps as early as 5.5 mya.

In contrast to the variable and episodic deposition in Hueco and Red Light Basins, Eagle Flat Basin was marked by accumulation of sediment gradually and uniformly. Sediments in the Faskin Ranch cores were deposited in alluvial-fan, basin-floor, and playa environments. Gradual expansion of the basin floor, over the 12-million-yr history recorded in the cores, progressively buried the Cretaceous hills that originally occupied the north Faskin Ranch area. The alluvial fans at the bases of the hillslopes were also buried. The present-day dimensions of the basin were established by about 780,000 yr ago, when the basin floor had aggraded to approximately 20 to 30 ft (7 to 10 m) below the present-day surface.

Approximately 150,000 to 300,000 yr ago, deposition ceased over much of Eagle Flat Basin, and the Arispe Surface was established. This surface was subsequently incised and partially refilled by slopewash and braided streams in Blanca Draw. The most recent deposition on the proposed repository site consists of eolian sheet sands, which remain active.

The surface collapse features on Faskin Ranch characterized by linear patterns of holes, pipes, and elongate depressions are believed to be pseudo-fissures, similar to those described by Shlemon and LaChapelle (1992). The pseudo-fissures are distributed entirely within wash, or

draw, areas. No pseudo-fissures have been identified on the proposed waste repository site. No cracks were visible below the pseudo-fissures on Faskin Ranch, but these pseudo-fissures may be older than those in California, and the cracks, if they existed, could have been obliterated by soil-forming processes such as the calcic horizon formation.

Surface or near-surface desiccation is a possible origin for the pseudo-fissures on Faskin Ranch. Cracking below the surface, which then propagates upward and causes collapse, provides a mechanism of formation for both the piping features and the surface depressions.

A linear group of surface depressions that is much longer and wider than the pseudo-fissures is present on the northwest part of Faskin Ranch, and is considered to be an earth fissure. This feature, called Hoover fissure, consists of a closely spaced series of depressions marked by a distinct vegetation line. The fissure has no measurable, near-surface, vertical displacement and may have formed initially by tensional forces in the earth.

Hoover fissure was trenched in two locations; no extensional crack was discovered below the surface. Two calcic horizons that are continuous to the east on Faskin Ranch are disrupted below the fissure depressions. The horizons appear to be dissolved and reprecipitated.

Possible origins of Hoover fissure include desiccation, differential subsidence over bedrock escarpment, faulting, ground-water withdrawal caused by people, and ground-water withdrawal caused by nature. Faulting and ground-water withdrawal by people probably did not cause Hoover fissure. However, the other three possible origins listed here cannot be ruled out as a cause of the fissure.

ACKNOWLEDGMENTS

This study was funded by the Texas Low-Level Radioactive Waste Authority under interagency contract no. IAC(92-93)-0910. The conclusions presented in this report are not necessarily endorsed or approved by the Authority.

The report benefited from reviews by Jay Raney and Thomas C. Gustavson. Discussions on fissures with Mark Sherrier are greatly appreciated. X-ray diffraction analyses were prepared under the supervision of Steve Tweedy. Sediment analyses and data were prepared by Randy Duffy, Steve Rooks, Ravi Nigudkar, Allan Standen, and Rodney Heathcott, under the supervision of George Bush and Ken Duncan. Radiocarbon analyses were performed by the Laboratory of Isotope Geochemistry at the University of Arizona. Paleomagnetic analyses were carried out at the Paleomagnetic and Rock Magnetism Laboratory, University of New Mexico, with the permission of Dr. John Geissman. Geologic data preparation assistance was provided by Scott Goode and Kristine Scherf. Figures were drafted by Abdunnur "Abdul" Suleiman and Randy Hitt, Michele Bailey, Kerza A. Prewitt, and Maria E. Saenz, under the direction of Richard L. Dillon. The text was assembled by Jamie H. Coggin. Word processing was by Susan Lloyd.

REFERENCES

Akersten, W. A., 1967, Red Light local fauna (Blancan) of the Love Formation, southeastern Hudspeth County, Texas: The University of Texas at Austin, Master's thesis, 168 p.

Albritton, C. C., Jr., and Smith, J. R., Jr., 1965, Geology of the Sierra Blanca area, Hudspeth County, Texas: U.S. Geological Survey Professional Paper 479, 131 p.

Antevs, E., 1948, Climatic changes and pre-white man, *in* The Great Basin, with emphasis on glacial and postglacial times: University of Utah Bulletin 38, p. 193–198.

Axelrod, D. I., and Bailey, H. D., 1976, Tertiary vegetation, climate and altitude of the Rio Grande depression, New Mexico–Colorado: Paleobiology, v. 2, p. 235–254.

Baker, C. L., 1927, Exploratory geology of a part of southwestern Trans-Pecos Texas: The University of Texas at Austin, Bureau of Economic Geology Bulletin 2745, 70 p.

Baumgardner, R.W., Jr., and Scanlon, B. R., 1992, Surface fissures in the Hueco Bolson and adjacent basins, West Texas: The University of Texas at Austin, Bureau of Economic Geology Geological Circular 92-2, 44 p.

Berggren, D. V., Kent, D. V., Flynn, J. J., and Van Couvering, J. A., 1985, Cenozoic geochronology: Geological Society of America Bulletin, v. 96, p. 1407–1418.

Bryant, V. M., and Holloway, R. G., 1985, A Late-Quaternary paleoenvironmental record of Texas: an overview of the pollen evidence, *in* Bryant, V. M., Jr., and Holloway, R. G., eds., Pollen records of Late-Quaternary North American sediments: Dallas, Texas, American Association of Stratigraphic Palynologists, p. 39–70.

Butler, R. F., 1991, Paleomagnetism: magnetic domains to geologic terranes: Boston, Blackwell Scientific Publications, 319 p.

Cande, S. C., and Kent, D. V., 1992, A new geomagnetic polarity timescale for the late Cretaceous and Cenozoic: Journal of Geophysical Research, v. 97, p. 13,917–13,951.

Collins, E. W., and Raney, J. A., 1993, Late Cenozoic faults of the region surrounding Eagle Flat study area, Trans-Pecos Texas: The University of Texas at Austin, Bureau of Economic Geology final contract report prepared for the Texas Low-Level Radioactive Waste Disposal Authority.

Contaldo, G. J., and Mueller, J. E., 1991, Earth fissures of the Mimbres Basin, southwest New Mexico: New Mexico Geology, v. 13, no. 4, p. 69–74.

Copeland, Peter, and Bowring, S. A., 1988, U-Pb zircon and 40-Ar/39-Ar ages from Proterozoic rocks, West Texas: Geological Society of America, South-Central Section, Abstracts with Programs, v. 20, no. 2, p. 95–96.

Denison, R. E., 1980, Pre-Bliss (pC) rocks in the Van Horn region, Trans-Pecos Texas, *in* Dickerson, P. W., and Hoffer, J. M., eds., Trans-Pecos region, southwestern New Mexico and West Texas: New Mexico Geological Society Guidebook, 31st Field Conference, p. 155–158.

Denison, R. E., and Hetherington, E. A., Jr., 1969, Basement rocks in far West Texas and south-central New Mexico, *in* Kottlowski, F. E., and LeMone, D. V., eds., Border stratigraphy

symposium: New Mexico Bureau of Mines and Mineral Resources Circular 104, p. 1–14.

Freeman, C. E., 1972, Pollen study of some Holocene alluvial deposits in Dona Ana County, southern New Mexico: Texas Journal of Science, v. 24, p. 203–220.

Folk, R. L., 1968, Petrology of sedimentary rocks: Austin, Texas, Hemphill's, 170 p.

Gile, L. H., Hawley, J. W., and Grossman, R. B., 1981, Soils and geomorphology in the Basin and Range area of Southern New Mexico—Guidebook to the Desert Project: New Mexico Bureau of Mines and Mineral Resources, Memoir 39, 222 p.

Goddard, E. N., Trask, P. D., DeFord, R. K., Rove, O. N., Singewald, J. T., Jr., and Overbeck, R. M., 1948, Rock-color chart: Boulder, Colorado, Geological Society of America, unpaginated.

Goetz, L. K., 1985, Giant polygonal dessication cracks in Wildhorse Flat, West Texas—revisited, *in* Dickerson, P. W., and Muehlberger, W. R., eds., Structure and tectonics of Trans-Pecos Texas: West Texas Geological Society, Publication 85-1, p. 235–238.

Goree, W. S., and Fuller, M., 1976, Magnetometers using RF-driven SQUIDS and their applications in rock magnetism and paleomagnetism: Review of Geophysics and Space Physics, v. 14, p. 591–608.

Gustavson, T. C., 1991, Arid basin depositional systems and paleosols Fort Hancock and Camp Rice Formations (Pliocene-Pleistocene), Hueco Bolson, West Texas and adjacent Mexico: The University of Texas at Austin, Bureau of Economic Geology, Report of Investigations No. 198, 49 p.

Hall, S. A., 1977, Late Quaternary sedimentation and paleoecological history of Chaco Canyon, New Mexico: Geological Society of America Bulletin, v. 88, p. 1593–1618.

Hall, S. A., 1985, Quaternary pollen analysis and vegetational history of the Southwest, *in* Bryant, V. M., Jr., and Holloway, R. G., eds., Pollen records of Late-Quaternary North America: Dallas, Texas, American Association of Stratigraphic Palynologists, p. 95–123.

Harland, W. B., Armstrong, R. L., Cox, A. V., Craig, L. E., Smith, A. G. and Smith, D. G., 1990, A geologic timescale, 1989: New York, Cambridge University Press, 263 p.

Hibbs, B.J., and Darling, B. K., 1993, Physical hydrology and ground-water modeling of the Eagle Flat study area and surrounding region, southern Hudspeth County, Texas: The University of Texas at Austin, Bureau of Economic Geology final contract report prepared for the Texas Low-Level Radioactive Waste Disposal Authority.

Holzer, T. L., 1984, Ground failure induced by ground-water withdrawal from unconsolidated sediment: Geological Society of America Reviews in Engineering Geology, v. 6, p. 67–81.

Horowitz, A., Gerald, R. E., and Chaiffetz, M. S., 1981, Preliminary paleoenvironmental implications of pollen analyzed from Archaic, Formative and Historic sites near El Paso, Texas: The Texas Journal of Science, v. 33, no. 1, p. 61–72.

Jachens, R. C., and Holzer, T. L., 1979 Geophysical investigations of ground failure related to ground-water withdrawal—Picacho Basin, Arizona: Ground Water, v. 17, no. 6, p. 574–585.

King, P. B., and Flawn, P. T., 1953, Geology and mineral deposits of the Precambrian rocks of the Van Horn area, Texas: University of Texas, Austin, Bureau of Economic Geology Publication 5301, 218 p.

Kottlowski, F. E., 1958, Geological history of the Rio Grande near El Paso: Franklin and Hueco Mountains, 1958 field trip guidebook of the West Texas Geological Society, p. 46–54.

Lambe, T. W., and Whitman, R. W., 1969, Soil mechanics: New York, John Wiley and Sons, 553 p.

Langford, R. P., 1993, Landscape evolution in the Eagle Flat and Red Light Basins, Chihuahua Desert, South Central Trans-Pecos, Texas: The University of Texas at Austin, Bureau of Economic Geology final contract report prepared for the Texas Low-Level Radioactive Waste Disposal Authority.

Larkin, T. J., and Bomar, G. W., 1983, Climatic atlas of Texas: Texas Department of Water Resources publication LP-192, 151 p.

Larson, M. K., and Pewe, T. L., 1986, Origin of land subsidence and earth fissuring, northeast Phoenix, Arizona: Bulletin Association of Engineering Geologists, v. 23, no. 2, p. 139–166.

Lister, L. A., and Secrest, C. D., 1985, Giant desiccation cracks and differential surface subsidence, Red Lake Playa, Mojave County, Arizona: Bulletin Association of Engineering Geologists, v. 22, no. 3, p. 299–314.

Markgraf, V. B., Forester, J. P., Singh, R. M., and Strenberg, R. S., 1984, San Agustin Plains, New Mexico: age and paleoenvironmental potential reassessed: Quaternary Research, v. 22, p. 336-343.

McFadden, P. L. and Reid, A. B., 1982, Analysis of paleomagnetic inclination data: Geophysics, Journal Royal Astronomical Society, v. 69, p. 307–319.

Muehlberger, W. R., 1980, Texas lineament revisited, *in* Dickerson, P. W., and Hoffer, J. M., eds., Trans-Pecos region, Southwestern New Mexico and West Texas: New Mexico Geological Society Guidebook, 31st Field Conference, p. 113–121.

Neal, J. T., Langer, A. M., and Kerr, P. F., 1968, Giant desiccation polygons of Great Basin playas: Geological Society of America Bulletin, v. 79, no. 1, p. 69–90.

Owenby, J. R., and Ezell, D. S., 1992, Monthly station normals of temperature, precipitation, and heating and cooling degree day, Texas: Climatography of the United States No. 81, U.S. Department of Commerce, National Climatic Data Center, Asheville, North Carolina, unpaginated.

Paine, J. G., Miller, K. C., and Hau, Fa, 1993, Seismic reflection, refraction, and surface wave studies at the proposed low level radioactive waste repository, Hudspeth County, Texas: The University of Texas at Austin, Bureau of Economic Geology final contract report prepared for the Texas Low-Level Radioactive Waste Disposal Authority.

Pampeyan, E. H., Holzer, T. L., and Clark, M. M., 1988, Modern ground failure in the Garlock fault zone, Fremont Valley, California: Geological Society of America Bulletin, v. 100, p. 677–691.

Pewe, T. L., Raymond, R. H., and Schumann, H. H., 1987, Land subsidence and earth-fissure formation in eastern Phoenix metropolitan area, Arizona, *in* Davis, G. H., and VandenDoler, E. M., eds., Geologic diversity of Arizona and its margins: excursions to choice areas: Arizona Bureau of Geology and Mineral Technology Geological Survey Branch Special Paper 5.

Raney, J. A., and Collins, E. W., 1993, Regional geologic setting of the Eagle Flat study area, Trans-Pecos Texas: The University of Texas at Austin, Bureau of Economic Geology final contract report prepared for the Texas Low-Level Radioactive Waste Disposal Authority.

Scanlon, B. R. and Xiang, J., 1993, Unsaturated zone hydrology in the Eagle Flat Basin, Chihuahuan Desert, southern Hudspeth County, Texas: The University of Texas at Austin, Bureau of Economic Geology final contract report prepared for the Texas Low-Level Radioactive Waste Disposal Authority.

Scott, G. F., and Frohlich, C., 1985, Large volume magnetically shielded room: A new design and material, *in* Kirschvink, J. L., Jones, D. S., and MacFadden, B. J., eds., Magnetite biomineralization and magnetoreception in organisms: a new biomagnetism: New York, Plenum Press, p. 197–220.

Shlemon, R. J., and LaChapelle, W. A., 1992, Pseudo earth fissures in the Lancaster area Antelope Valley, California: Proceedings, Association of Engineering Geologists 35th Annual Meeting, p. 165–169.

Slaff, S., 1933, Land subsidence and earth fissures in Arizona: Arizona Geological Survey, Down to Earth Series 3, 24 p.

Strain, W. S., 1966, Blancan mammalian fauna and Pleistocene formations, Hudspeth County Texas: Austin, Texas, Texas Memorial Museum Bulletin 10, p. 1–55.

_____ 1971, Late Cenozoic bolson integration in the Chihuahua tectonic belt, *in* Seewald, K., ed., The geologic framework of the Chihuahua tectonic belt: West Texas Geological Society Publication 71-59, p. 167–173.

Strain, W. S., 1980, Pleistocene rocks in El Paso and Hudspeth Counties, Texas adjacent to Interstate Highway 10: New Mexico Geological Society, 31st field conference, p. 179–181.

Underwood, J. P., Jr., 1963, Geology of Eagle Mountains and vicinity, Hudspeth County , Texas: The University of Texas at Austin, Bureau of Economic Geology Geologic Quadrangle Map No. 26.

Underwood, J. R., Jr., and DeFord, R. K., 1969, Large-scale desiccation fissures in alluvium, Trans-Pecos Texas and northern Chihuahua (abs.): Geological Society of America, Abstracts with Programs, v. 1, pt. 2, p. 31.

Van Devender, T. R., and Spaulding, W. G., 1979, Development of vegetation and climate in the southwestern United States: Science, v. 204, p. 701–710.

Wells, S. G., Bullard, T. F., and Smith, L. N., 1982, Origin and evolution of deserts in the Basin and Range and Colorado Plateau Provinces of western North America, *in* The geological story of the world's deserts: Stria, v. 17, p. 101–111.

White, E. M., 1970, Giant desiccation cracks in central South Dakota soils: Soil Science, v. 110, p. 71–73.

Appendix A. Descriptions of cores taken on Faskin Ranch. Cores located on plate 1. Unified soil classification textural equivalents shown in table B-1.

EXPLANATION


Mud (silt and clay)

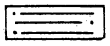
Sandy mud (20-49 percent sand)

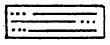
Muddy sand (50-80 percent sand)

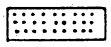
Sand (greater than 80 percent sand)

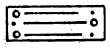
Muddy and sandy gravel (< 50 percent pebbles and cobbles)

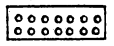
Gravel (≥ 50 percent pebbles and cobbles, sandy matrix)


Lost core

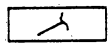
Root mold

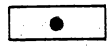
Calcic horizon Stage I, II, III of Gile and others (1981, page 67)


Pebble clasts

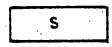
Slickensides

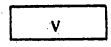
Sand or mud-filled cracks, 0.5-4 cm wide

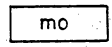
Nodular fabric

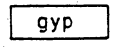
Gypsum crystals

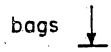
Core not taken, cuttings only

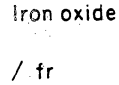
Iron oxide staining (orange-red color)

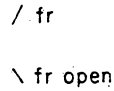
Fracture, filled, line shows plunge (angle from horizontal)

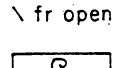
Open fracture, line shows plunge (angle from horizontal)

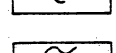
Fossils

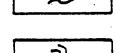
Ripple crossbedding

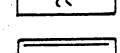
Contorted bedding

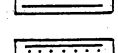
Claystone bedrock, orientation of bedding shown in vertical core

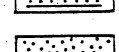
Sandstone and siltstone bedrock

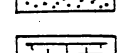
Sandstone bedrock

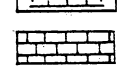
Marl bedrock

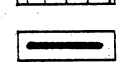
Limestone bedrock

Top of bedrock

QAa3790

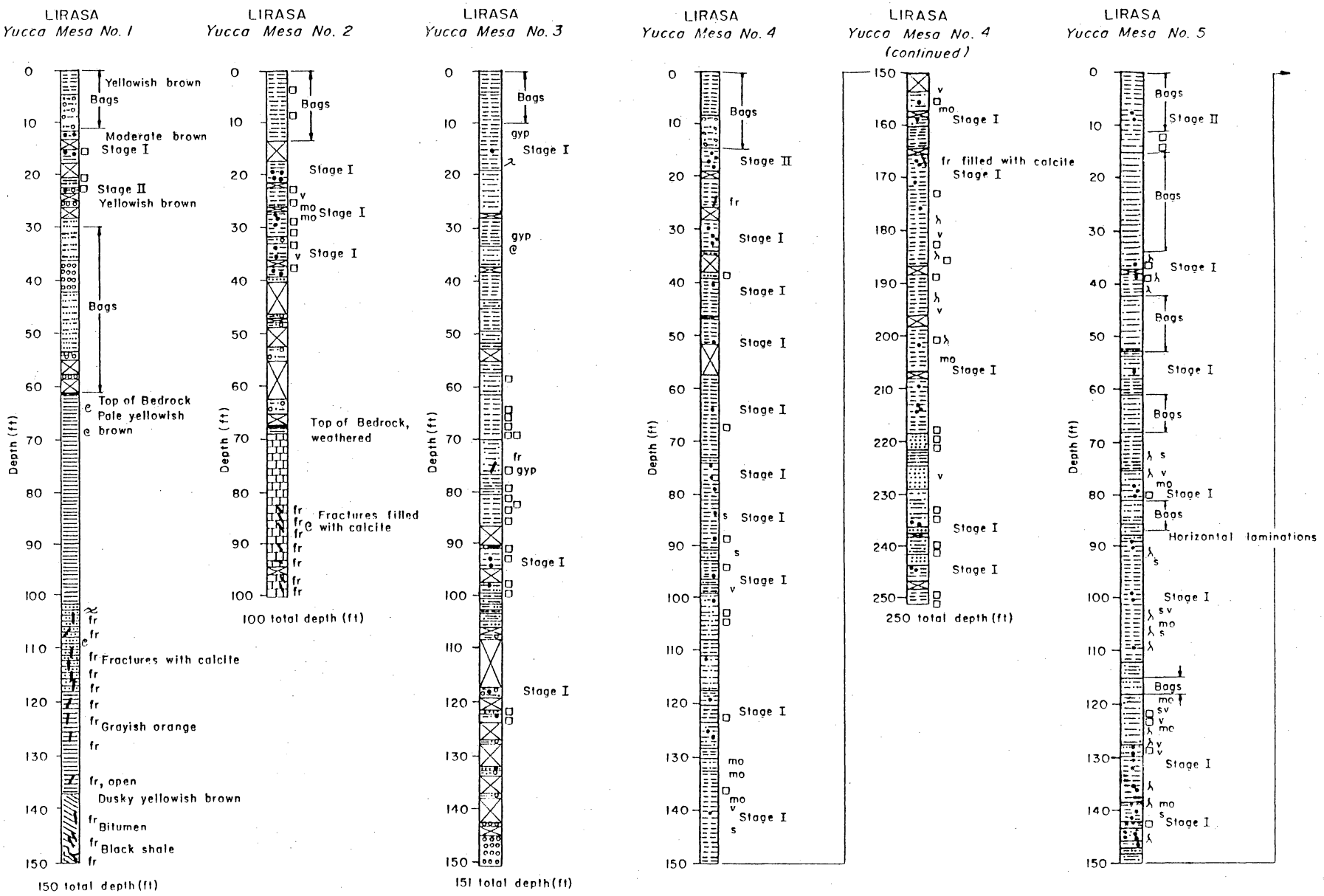
LIRASA
Yucca Mesa No. 1
Depth (ft)
Yellowish brown
Bags
Moderate brown
Stage I
Stage II
Yellowish brown
Bags
Top of Bedrock
Pale yellowish
brown
Fractures with calcite
Grayish orange
fr, open
Dusky yellowish brown
Bitumen
Black shale
150 total depth (ft)
LIRASA
Yucca Mesa No. 2
Depth (ft)
Bags
Stage I
Stage I
Top of Bedrock,
weathered
Fractures filled
with calcite
100 total depth (ft)
LIRASA
Yucca Mesa No. 3
Depth (ft)
Bags
gyp
Stage I
gyp
fr
gyp
Stage I
Stage I
151 total depth (ft)
LIRASA
Yucca Mesa No. 4
Depth (ft)
Bags
Stage II
Stage I
Stage I
Stage I
Stage I
Stage I
Stage I
Stage I
LIRASA
Yucca Mesa No. 4
(continued)
Depth (ft)
Stage I
fr filled with calcite
Stage I
Stage I
Stage I
Stage I
250 total depth (ft)
LIRASA
Yucca Mesa No. 5
Depth (ft)
Bags
Stage II
Bags
Stage I
Bags
Stage I
Bags
Stage I
Horizontal laminations
Stage I
Bags
Stage I
Stage I

OAa3292

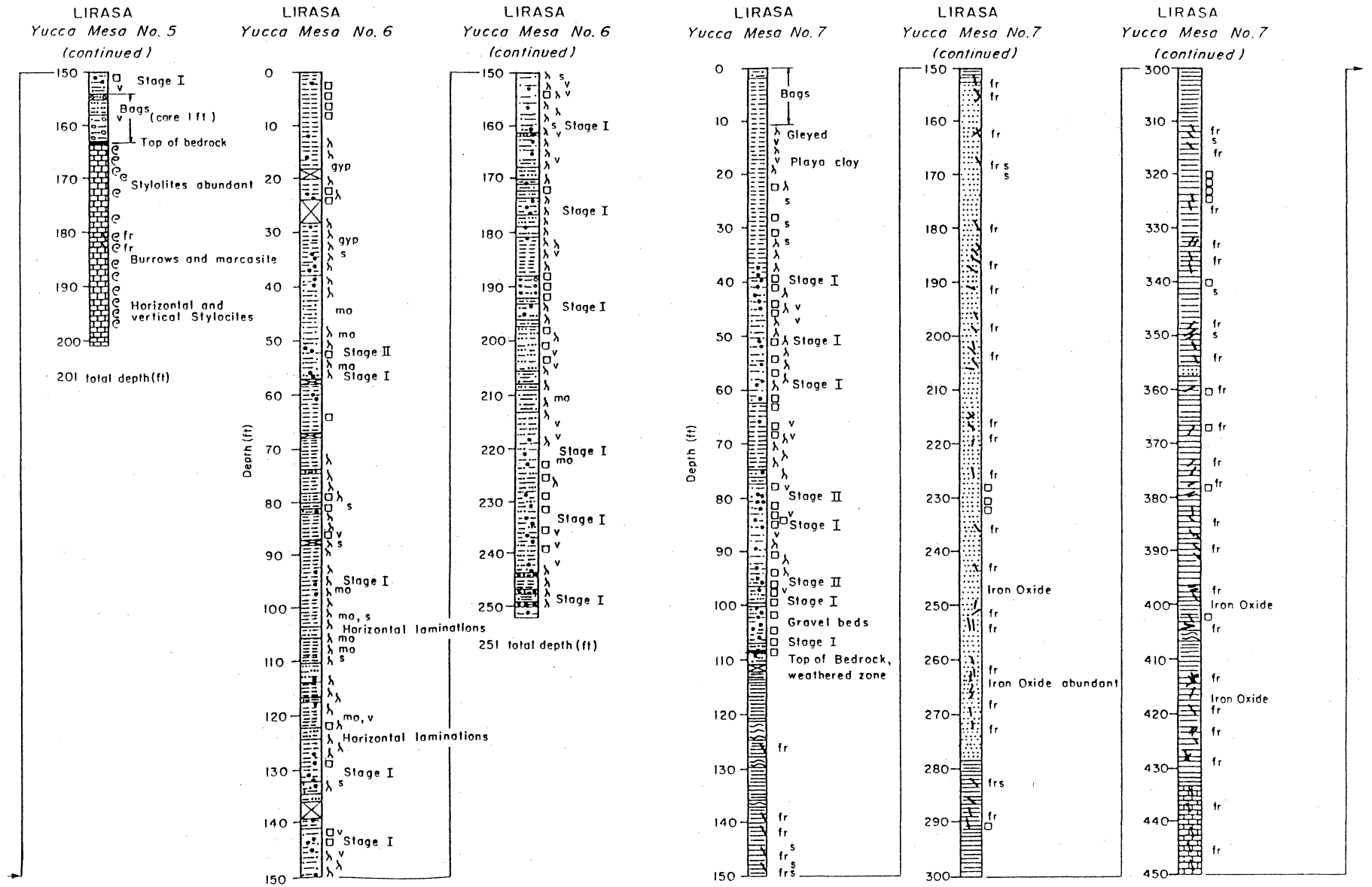
LIRASA
Yucca Mesa No. 5
(continued)
Stage I
Bags
(core 1 ft)
Top of bedrock
Stylolites abundant
Burrows and marcasite
Horizontal and vertical Stylocites
201 total depth(ft)
LIRASA
Yucca Mesa No. 6
Depth (ft)
gyp
Stage II
Stage I
Horizontal laminations
LIRASA
Yucca Mesa No. 6
(continued)
251 total depth (ft)
LIRASA
Yucca Mesa No. 7
Bags
Gleyed
Playa clay
Gravel beds
Top of Bedrock, weathered zone
LIRASA
Yucca Mesa No. 7
(continued)
Iron Oxide
Iron Oxide abundant
LIRASA
Yucca Mesa No. 7
(continued)
Iron Oxide

QAa3293

LIRASA
Yucca Mesa No. 7
(continued)

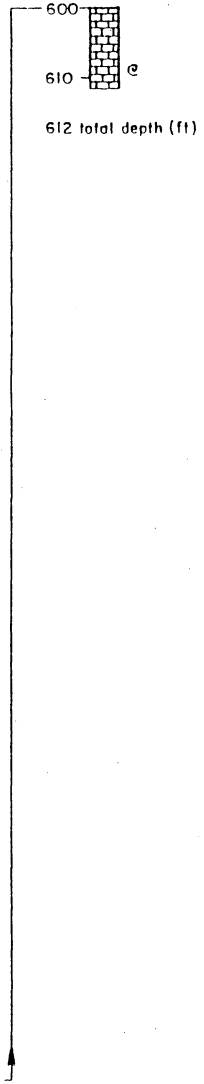

LIRASA
Yucca Mesa No. 8

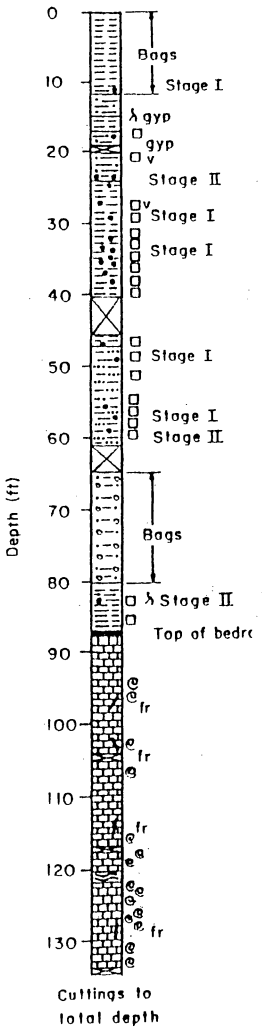

LIRASA
Yucca Mesa No. 9

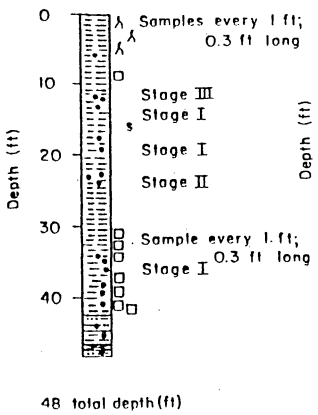

LIRASA
Yucca Mesa No. 10

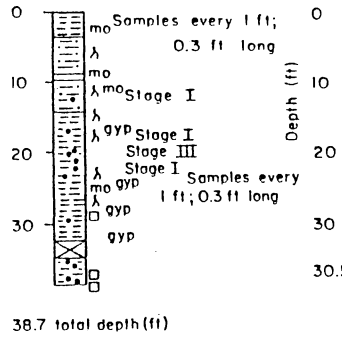

LIRASA
Yucca Mesa No. 11

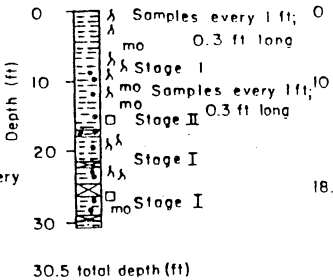

LIRASA
Yucca Mesa No. 12

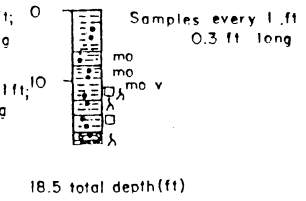

QAa3294

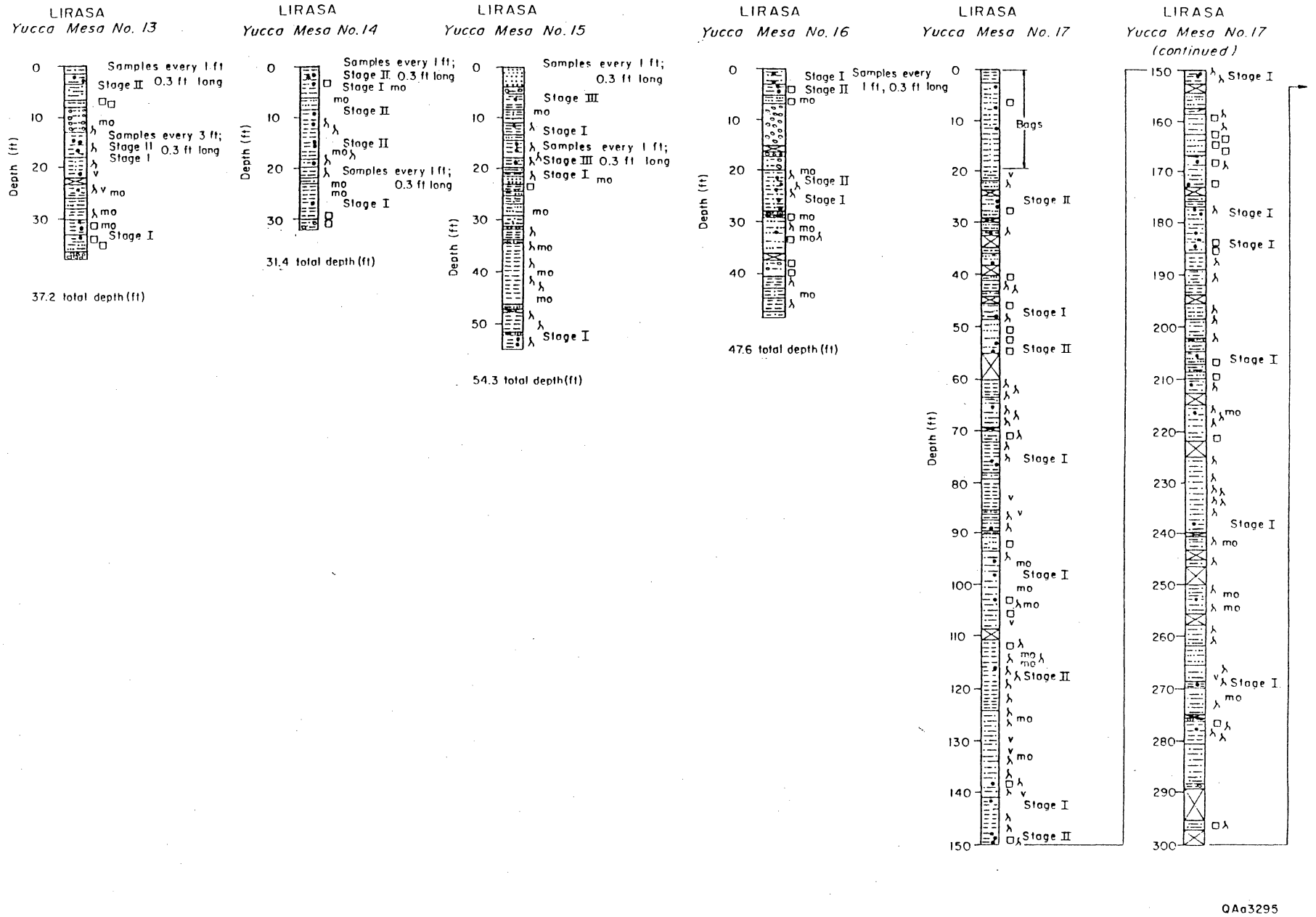
LIRASA
Yucca Mesa No. 13
Depth (ft)
Samples every 1 ft
Stage II 0.3 ft long
Samples every 3 ft;
Stage II 0.3 ft long
Stage I
mo
37.2 total depth (ft)
LIRASA
Yucca Mesa No. 14
Samples every 1 ft;
Stage II 0.3 ft long
Stage I mo
Stage II
Samples every 1 ft;
0.3 ft long
31.4 total depth (ft)
LIRASA
Yucca Mesa No. 15
Samples every 1 ft;
0.3 ft long
Stage III
Stage I
Samples every 1 ft;
Stage III 0.3 ft long
54.3 total depth (ft)
LIRASA
Yucca Mesa No. 16
Stage I Samples every
Stage II 1 ft, 0.3 ft long
47.6 total depth (ft)
LIRASA
Yucca Mesa No. 17
Bags
Stage I
Stage II
LIRASA
Yucca Mesa No. 17
(continued)
Stage I
Stage II
QAa3295

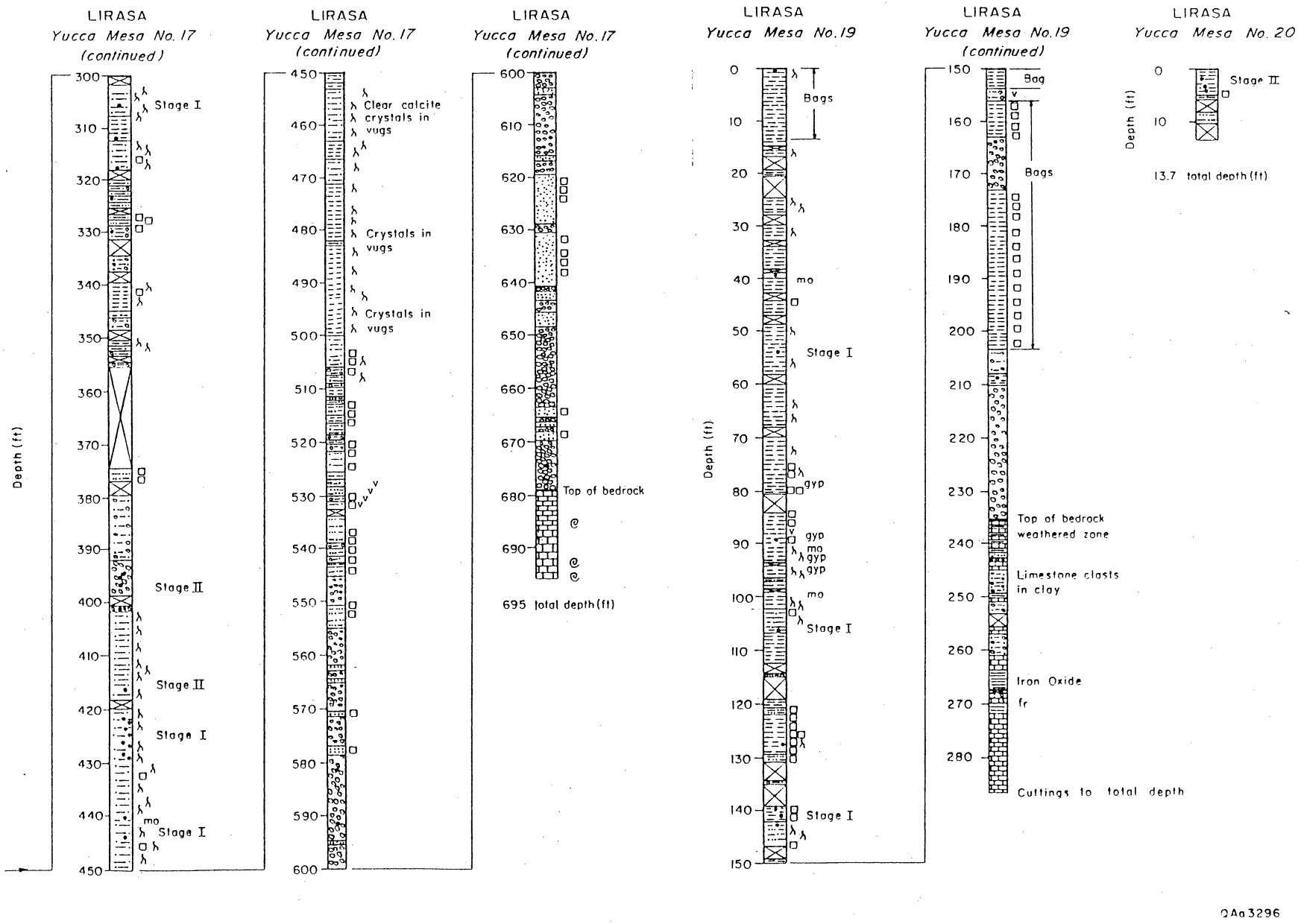
LIRASA
Yucca Mesa No. 17
(continued)
Depth (ft)
300
310
320
330
340
350
360
370
380
390
400
410
420
430
440
450
Stage I
Stage II
Stage II
Stage I
mo
Stage I
LIRASA
Yucca Mesa No. 17
(continued)
450
460
470
480
490
500
510
520
530
540
550
560
570
580
590
600
Clear calcite crystals in vugs
Crystals in vugs
Crystals in vugs
LIRASA
Yucca Mesa No. 17
(continued)
600
610
620
630
640
650
660
670
680
690
Top of bedrock
695 total depth (ft)
LIRASA
Yucca Mesa No. 19
Depth (ft)
0
10
20
30
40
50
60
70
80
90
100
110
120
130
140
150
Bags
mo
Stage I
gyp
gyp
mo
gyp
gyp
mo
Stage I
Stage I
LIRASA
Yucca Mesa No. 19
(continued)
150
160
170
180
190
200
210
220
230
240
250
260
270
280
Bag
Bags
Top of bedrock weathered zone
Limestone clasts in clay
Iron Oxide
fr
Cuttings to total depth
LIRASA
Yucca Mesa No. 20
Depth (ft)
0
10
Stage II
13.7 total depth (ft)

QAa3296

LIRASA
Yucca Mesa No. 21

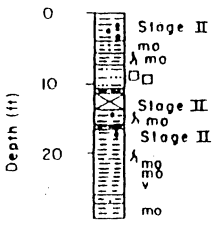

28.8 total depth (ft)

LIRASA
Yucca Mesa No. 22

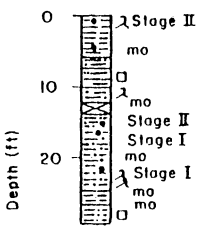

29 total depth (ft)

LIRASA
Yucca Mesa No. 23

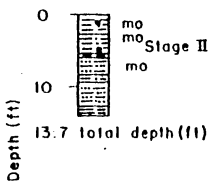

13.7 total depth (ft)

LIRASA
Yucca Mesa No. 27

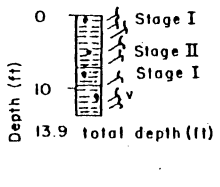

13.9 total depth (ft)

LIRASA
Yucca Mesa No. 28

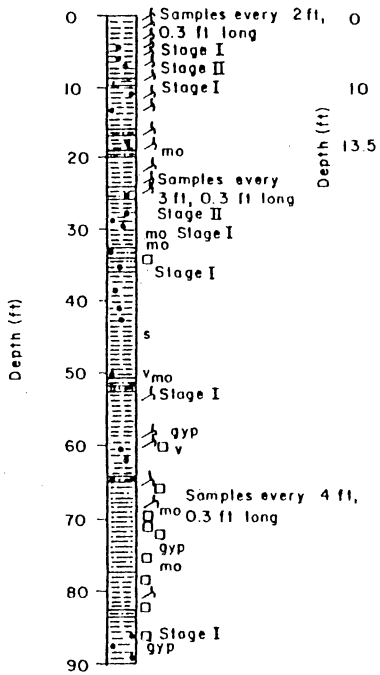

90 total depth (ft)

LIRASA
Yucca Mesa No. 29

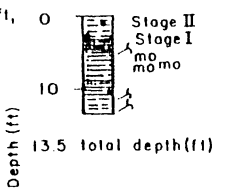

13.5 total depth (ft)

QAa3297

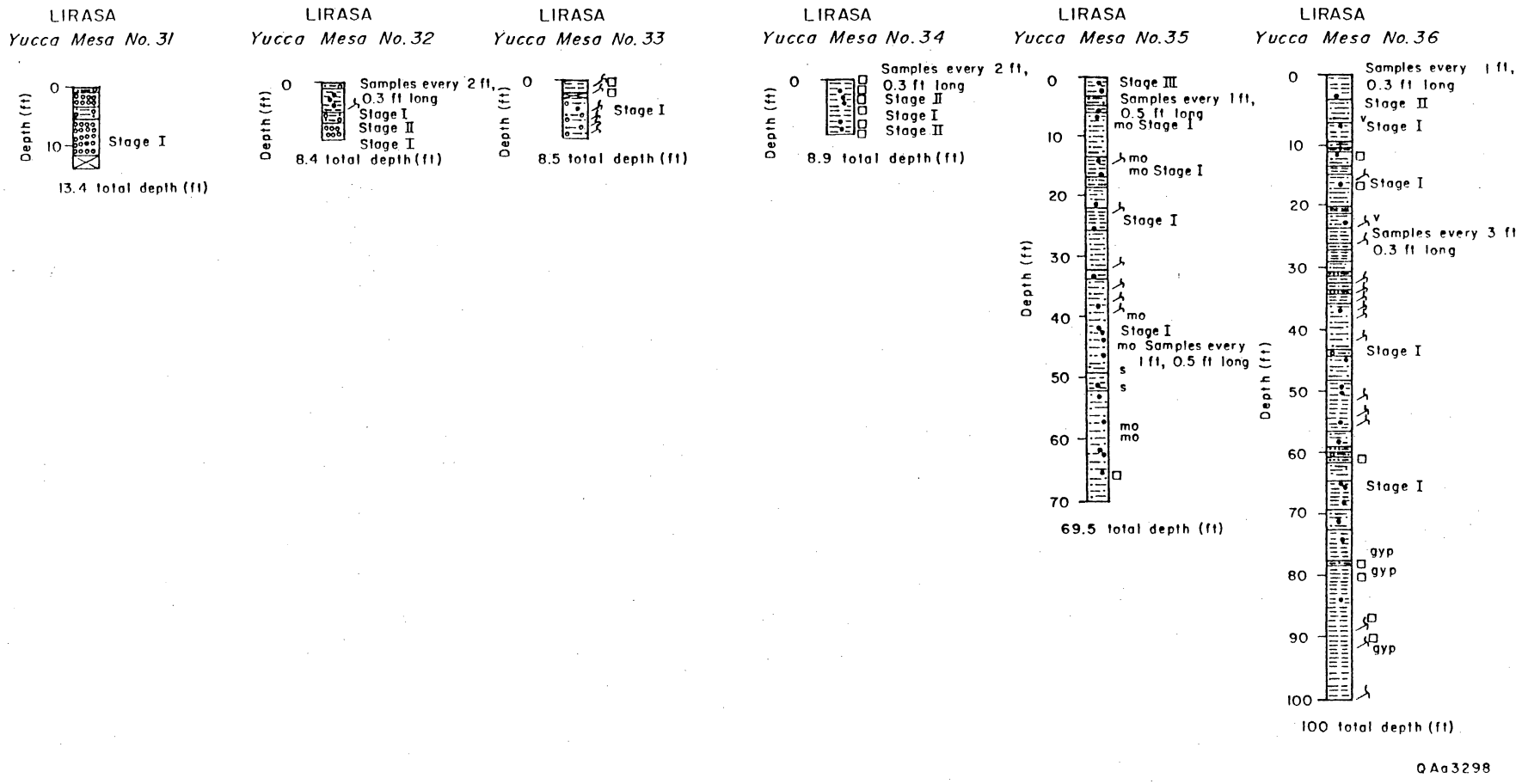
LIRASA
Yucca Mesa No. 31
Depth (ft)
0
10
Stage I
13.4 total depth (ft)
LIRASA
Yucca Mesa No. 32
Depth (ft)
0
Samples every 2 ft,
0.3 ft long
Stage I
Stage II
Stage I
8.4 total depth (ft)
LIRASA
Yucca Mesa No. 33
Depth (ft)
0
Stage I
8.5 total depth (ft)
LIRASA
Yucca Mesa No. 34
Depth (ft)
0
Samples every 2 ft,
0.3 ft long
Stage II
Stage I
Stage II
8.9 total depth (ft)
LIRASA
Yucca Mesa No. 35
Depth (ft)
0
10
20
30
40
50
60
70
Stage III
Samples every 1 ft,
0.5 ft long
mo Stage I
mo
mo Stage I
Stage I
mo
Stage I
mo Samples every
1 ft, 0.5 ft long
s
s
mo
mo
69.5 total depth (ft)
LIRASA
Yucca Mesa No. 36
Depth (ft)
0
10
20
30
40
50
60
70
80
90
100
Samples every 1 ft,
0.3 ft long
Stage II
v Stage I
Stage I
v
Samples every 3 ft
0.3 ft long
Stage I
Stage I
gyp
gyp
gyp
100 total depth (ft)
QAa3298

LIRASA
Yucca Mesa No. 37

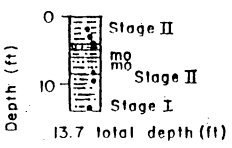

13.7 total depth (ft)

LIRASA
Yucca Mesa No. 38

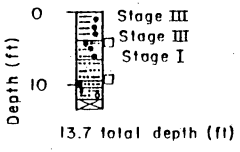

13.7 total depth (ft)

LIRASA
Yucca Mesa No. 39

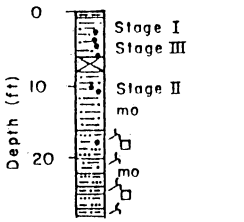

28.8 total depth (ft)

LIRASA
Yucca Mesa No.40

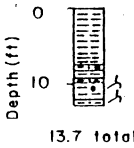

13.7 total depth (ft)

LIRASA
Yucca Mesa No. 41

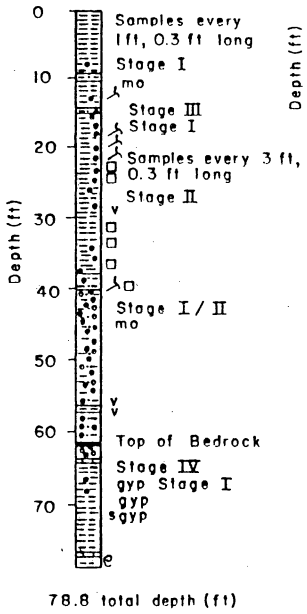

78.8 total depth (ft)

LIRASA
Yucca Mesa No. 42

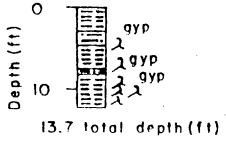

13.7 total depth (ft)

OAa3299

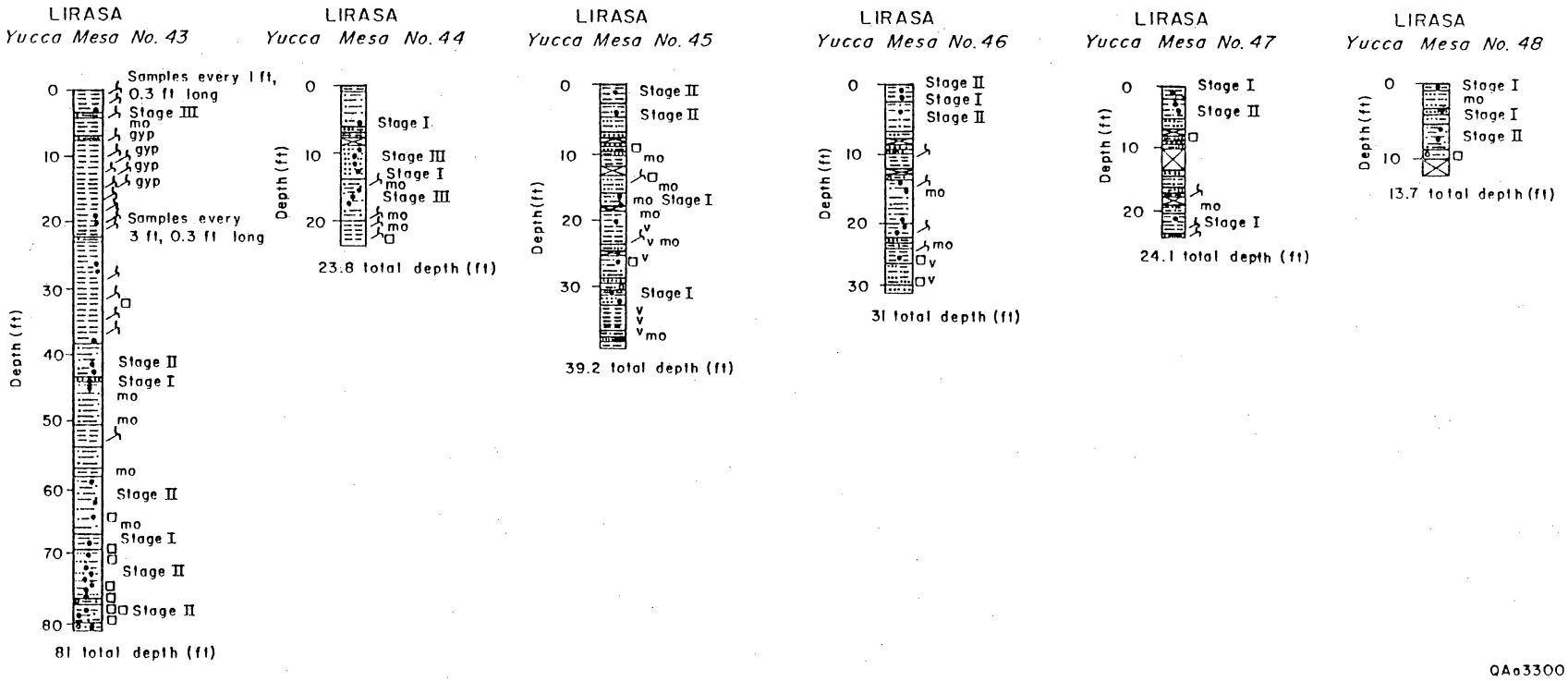
LIRASA
Yucca Mesa No. 43
Samples every 1 ft, 0.3 ft long
Stage III
mo
gyp
gyp
gyp
gyp
Samples every 3 ft, 0.3 ft long
Stage II
Stage I
mo
mo
mo
Stage II
mo
Stage I
Stage II
Stage II
Depth (ft)
0
10
20
30
40
50
60
70
80
81 total depth (ft)
LIRASA
Yucca Mesa No. 44
Stage I
Stage III
Stage I
mo
Stage III
mo
mo
Depth (ft)
0
10
20
23.8 total depth (ft)
LIRASA
Yucca Mesa No. 45
Stage II
Stage II
mo
mo
mo Stage I
mo
v
v mo
v
Stage I
v
v
v mo
Depth (ft)
0
10
20
30
39.2 total depth (ft)
LIRASA
Yucca Mesa No. 46
Stage II
Stage I
Stage II
mo
mo
v
v
Depth (ft)
0
10
20
30
31 total depth (ft)
LIRASA
Yucca Mesa No. 47
Stage I
Stage II
mo
Stage I
Depth (ft)
0
10
20
24.1 total depth (ft)
LIRASA
Yucca Mesa No. 48
Stage I
mo
Stage I
Stage II
Depth (ft)
0
10
13.7 total depth (ft)

QA:3300

LIRASA
Yucca Mesa No. 51

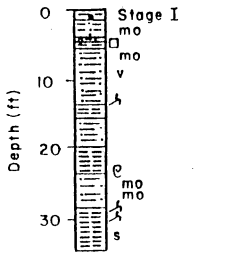

34.1 total depth (ft)

LIRASA
Yucca Mesa No. 52

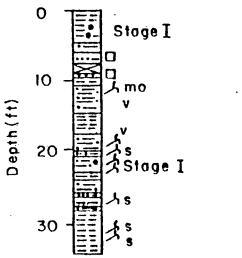

34.2 total depth (ft)

LIRASA
Yucca Mesa No. 53

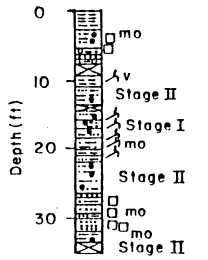

34 total depth (ft)

LIRASA
Yucca Mesa No. 54

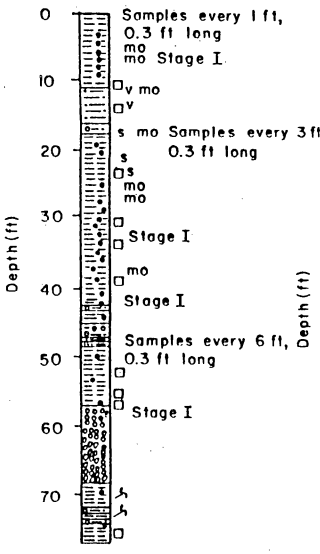

77.6 total depth (ft)

LIRASA
Yucca Mesa No. 59

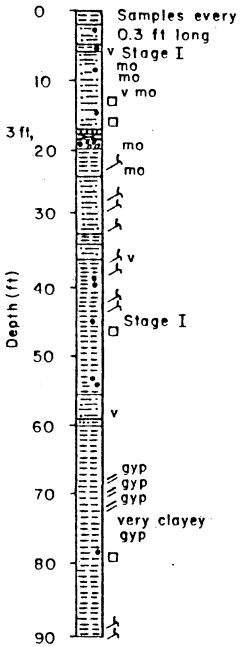

90.2 total depth (ft)

LIRASA
Yucca Mesa No. 62

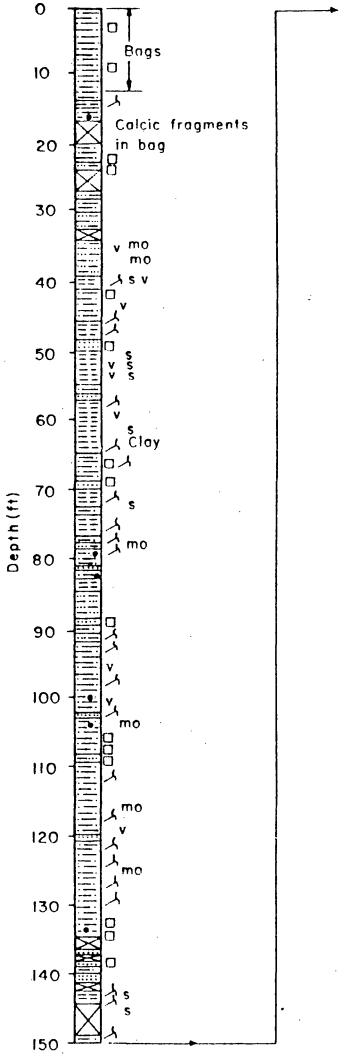

QAa3301

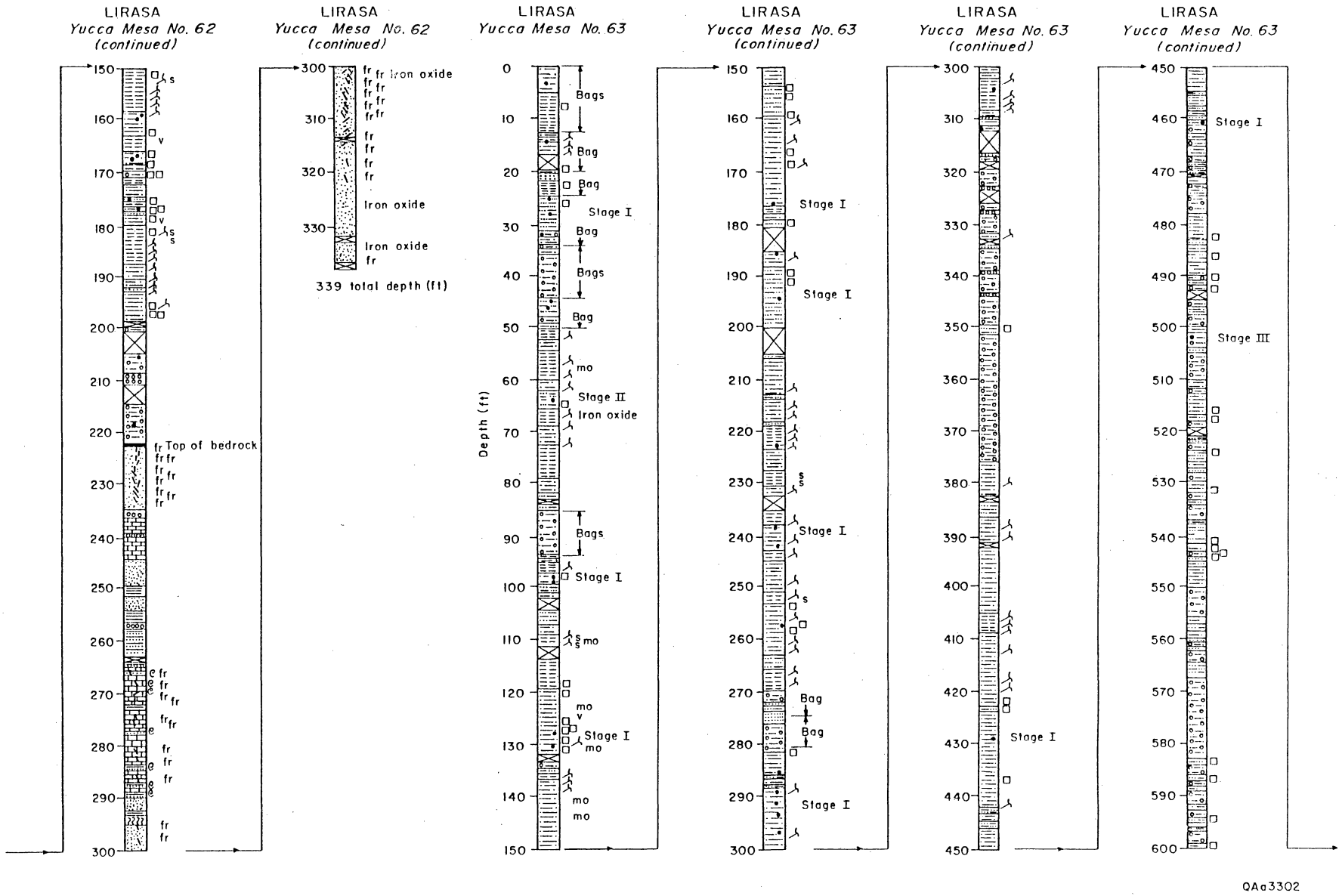
LIRASA
Yucca Mesa No. 62
(continued)
LIRASA
Yucca Mesa No. 62
(continued)
LIRASA
Yucca Mesa No. 63
LIRASA
Yucca Mesa No. 63
(continued)
LIRASA
Yucca Mesa No. 63
(continued)
LIRASA
Yucca Mesa No. 63
(continued)
Depth (ft)
Top of bedrock
Iron oxide
Iron oxide
339 total depth (ft)
Bags
Bag
Stage I
Stage II
Iron oxide
Stage III
QAa3302

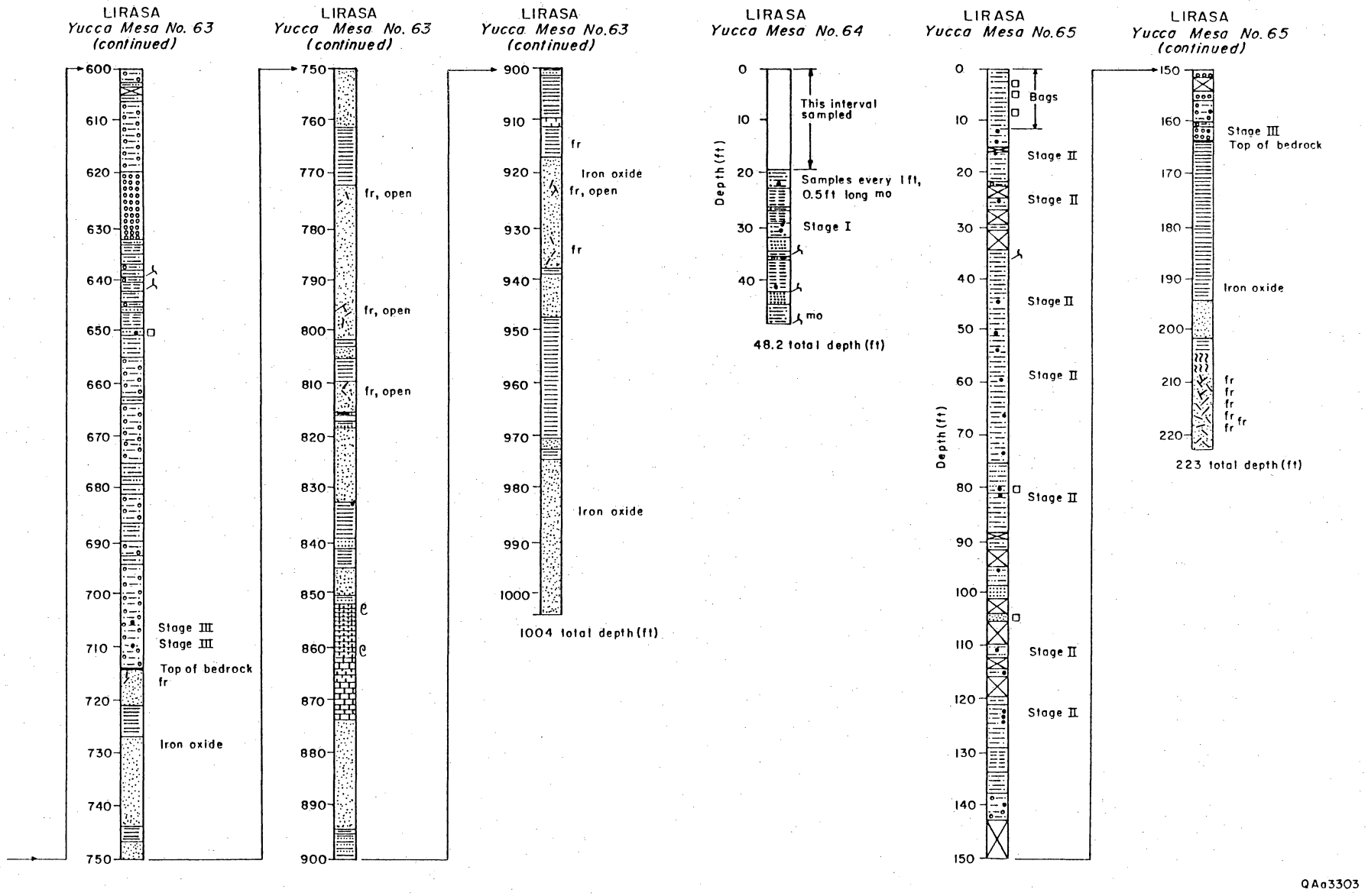
LIRASA
Yucca Mesa No. 63
(continued)
600
610
620
630
640
650
660
670
680
690
700
710
720
730
740
750
Stage III
Stage III
Top of bedrock
fr
Iron oxide
LIRASA
Yucca Mesa No. 63
(continued)
750
760
770
780
790
800
810
820
830
840
850
860
870
880
890
900
fr, open
fr, open
fr, open
c
c
LIRASA
Yucca Mesa No.63
(continued)
900
910
920
930
940
950
960
970
980
990
1000
fr
Iron oxide
fr, open
fr
Iron oxide
1004 total depth (ft)
LIRASA
Yucca Mesa No.64
0
10
20
30
40
Depth (ft)
This interval
sampled
Samples every 1 ft,
0.5 ft long mo
Stage I
mo
48.2 total depth (ft)
LIRASA
Yucca Mesa No.65
0
10
20
30
40
50
60
70
80
90
100
110
120
130
140
150
Depth (ft)
Bags
Stage II
Stage II
Stage II
Stage II
Stage II
Stage II
LIRASA
Yucca Mesa No.65
(continued)
150
160
170
180
190
200
210
220
Stage III
Top of bedrock
Iron oxide
fr
fr
fr
fr
fr fr
223 total depth (ft)
QAa3303

LIRASA
Yucca Mesa No. 65
(continued)

LIRASA
Yucca Mesa No. 66

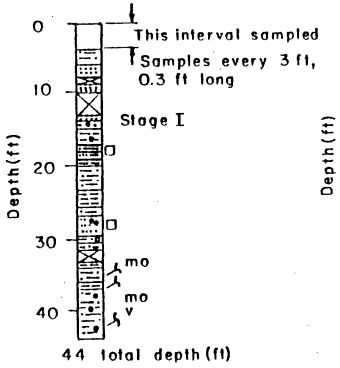

44 total depth (ft)

LIRASA
Yucca Mesa No. 70

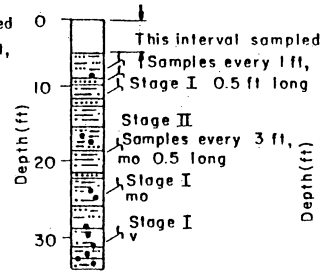

34.1 total depth(ft)

LIRASA
Yucca Mesa No. 71

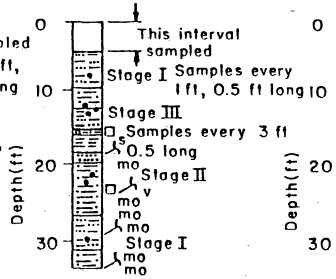

34 total depth(ft)

LIRASA
Yucca Mesa No. 72

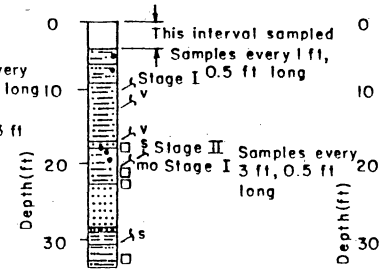

34.1 total depth (ft)

LIRASA
Yucca Mesa No. 73

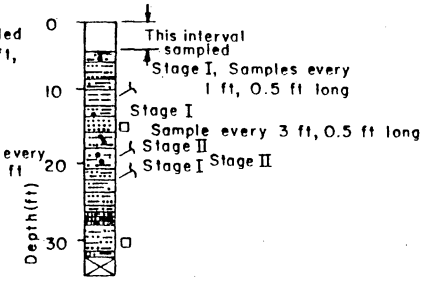

34.2 total depth(ft)

QAa3404

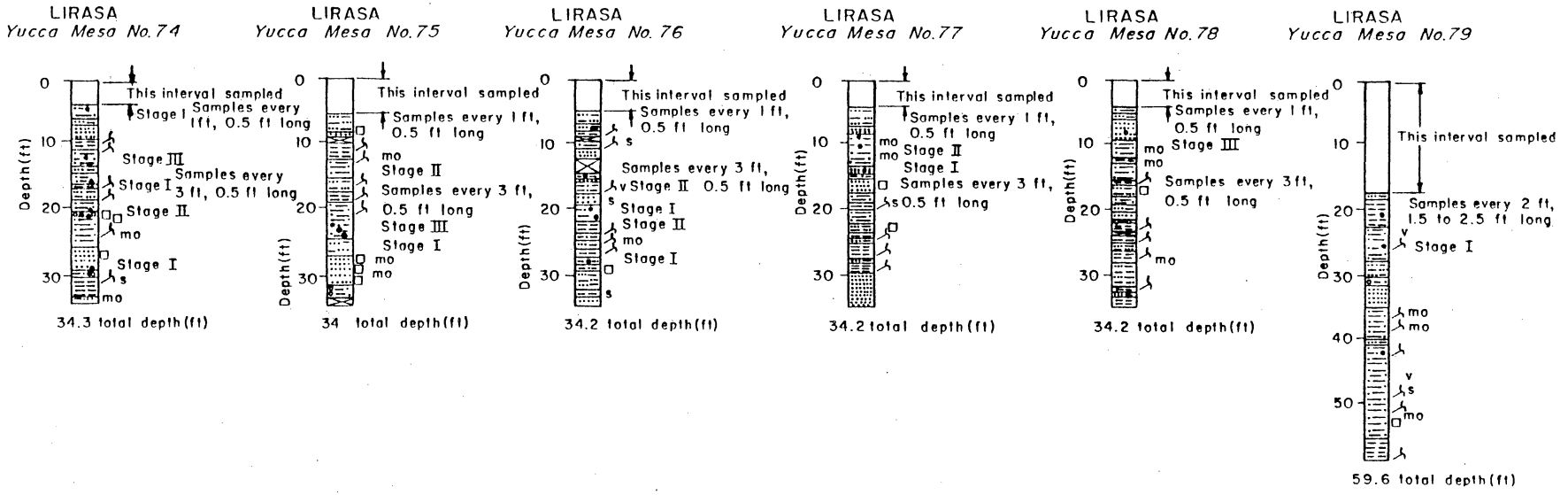
LIRASA
Yucca Mesa No. 74
This interval sampled
Stage I Samples every 1 ft, 0.5 ft long
Stage III
Samples every 3 ft, 0.5 ft long
Stage I
Stage II
mo
Stage I
s
mo
Depth(ft)
0
10
20
30
34.3 total depth(ft)
LIRASA
Yucca Mesa No. 75
This interval sampled
Samples every 1 ft, 0.5 ft long
mo
Stage II
Samples every 3 ft, 0.5 ft long
Stage III
Stage I
mo
mo
34 total depth(ft)
LIRASA
Yucca Mesa No. 76
This interval sampled
Samples every 1 ft, 0.5 ft long
s
Samples every 3 ft,
v Stage II 0.5 ft long
s
Stage I
Stage II
mo
Stage I
s
34.2 total depth(ft)
LIRASA
Yucca Mesa No. 77
This interval sampled
Samples every 1 ft, 0.5 ft long
mo
mo Stage II
Stage I
Samples every 3 ft,
s 0.5 ft long
34.2 total depth(ft)
LIRASA
Yucca Mesa No. 78
This interval sampled
Samples every 1 ft, 0.5 ft long
mo Stage III
mo
Samples every 3 ft, 0.5 ft long
mo
34.2 total depth(ft)
LIRASA
Yucca Mesa No. 79
This interval sampled
Samples every 2 ft, 1.5 to 2.5 ft long
v
Stage I
mo
mo
v
s
mo
40
50
59.6 total depth(ft)

QAa3305

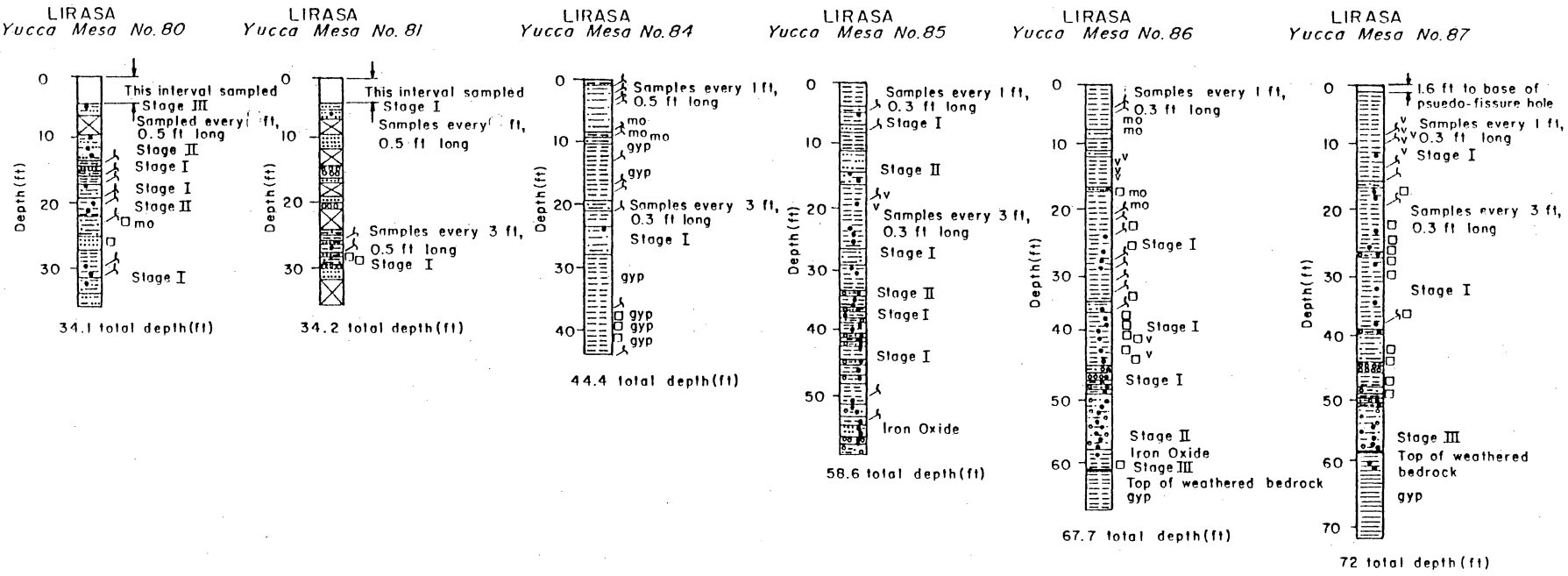
LIRASA
Yucca Mesa No. 80
Depth(ft)
This interval sampled
Stage III
Sampled every ft,
0.5 ft long
Stage II
Stage I
Stage I
Stage II
mo
Stage I
34.1 total depth(ft)
LIRASA
Yucca Mesa No. 81
Depth(ft)
This interval sampled
Stage I
Samples every ft,
0.5 ft long
Samples every 3 ft,
0.5 ft long
Stage I
34.2 total depth(ft)
LIRASA
Yucca Mesa No. 84
Depth(ft)
Samples every 1 ft,
0.5 ft long
mo
mo
mo
gyp
gyp
Samples every 3 ft,
0.3 ft long
Stage I
gyp
gyp
gyp
gyp
44.4 total depth(ft)
LIRASA
Yucca Mesa No. 85
Depth(ft)
Samples every 1 ft,
0.3 ft long
Stage I
Stage II
v
v
Samples every 3 ft,
0.3 ft long
Stage I
Stage II
Stage I
Stage I
Iron Oxide
58.6 total depth(ft)
LIRASA
Yucca Mesa No. 86
Depth(ft)
Samples every 1 ft,
0.3 ft long
mo
mo
v
v
mo
mo
Stage I
Stage I
v
v
Stage I
Stage II
Iron Oxide
Stage III
Top of weathered bedrock
gyp
67.7 total depth(ft)
LIRASA
Yucca Mesa No. 87
Depth(ft)
1.6 ft to base of
psuedo-fissure hole
v
v
v
Samples every 1 ft,
0.3 ft long
Stage I
Samples every 3 ft,
0.3 ft long
Stage I
Stage III
Top of weathered
bedrock
gyp
72 total depth(ft)
QAa3776

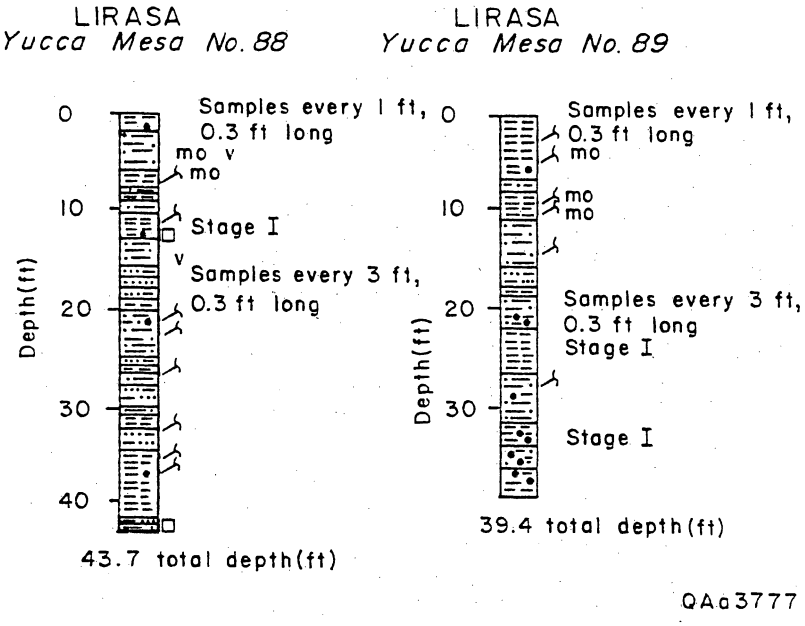
LIRASA
Yucca Mesa No. 88
LIRASA
Yucca Mesa No. 89
Depth(ft)
0
10
20
30
40
Samples every 1 ft,
0.3 ft long
mo v
mo
Stage I
v
Samples every 3 ft,
0.3 ft long
43.7 total depth(ft)
Samples every 1 ft,
0.3 ft long
mo
mo
mo
Samples every 3 ft,
0.3 ft long
Stage I
Stage I
39.4 total depth(ft)
QAa3777

Appendix B. Textural data from core, trench, and surface samples on Faskin Ranch.

Table B-1. Unified soil (Lambe and Whitman, 1969) and approximately equivalent geologic textural classifications.

Unified soil classification	Group symbols	Geologic textural classification (see explanation used in appendix A)
Well graded gravels, gravel-sand mixtures, little or no fines	GW	Gravel (≥50% pebbles and cobbles, sandy matrix)
Poorly graded gravels, gravel-sand mixtures, little or no fines	GP	Gravel (≥50% pebbles and cobbles, sandy matrix)
Silty gravels, poorly graded gravel-sand-silt mixtures	GM	Muddy and sandy gravel (<50% gravel)
Clayey gravels, poorly graded gravel-sand-clay mixtures	GC	Muddy and sandy gravel (<50% gravel)
Well graded sands, gravelly sands, little or no fines	SW	Sand (>80% sand)
Poorly graded sands, gravelly sands, little or no fines	SO	Sand (>80% sand)
Silty sands, poorly graded sand-silt mixtures	SM	Muddy sand (50–80% sand)
Clayey sands, poorly graded sand-clay mixtures	SC	Muddy sand (50–80% sand)
Inorganic silts and very fine sands, rock flour, silty or clayey fine sands with slight plasticity	ML	Sandy mud (20–49% sand)
Inorganic clays of low to medium plasticity, gravelly clays, sandy clays, silty clays, lean clays	CL	Sandy mud (20–49% sand) or mud (silt and clay)
Organic silts and organic silt-clays of low plasticity	OL	Mud (silt and clay)
Inorganic silts, micaceous or diatomaceous fine sandy or silty soils, elastic silts	MH	Mud (silt and clay)
Inorganic clays of high plasticity, fat clays	CH	Mud (silt and clay)
Organic clays of medium to high plasticity	OH	Mud (silt and clay)

Table B-2. Core sample depths and textural data. Sand is 2 to 0.0625 mm, silt is 0.0625 to 0.0039 mm, and clay is <0.0039 mm. Gravel content less than 2% of each sample, except for samples L2YM-1 and L4YM-1 (not plotted on figure 6). The dominant color of the basin-fill sediments is 5YR 4/4, moderate brown. Calcic-rich strata range from 10YR 5/4, moderate yellowish brown, to 10YR 7/4, grayish orange (color codes from Goddard and others, 1948).

Sample no.	Depth (ft)	Total sand (%)	Total silt (%)	Total clay (%)
Core 1				
L1YM-3	21.4	39	24	37
Core 2				
L2YM-1	2.5–5, bag	30	36	20
L2YM-2	18.6	21	55	22
L2YM-3	35.1	27	30	43
Core 3				
L3YM-1	11.4	13	32	55
L3YM-2	60.5	20	27	53
L3YM-3	68.1	30	42	28
Core 4				
L4YM-1	10–12, bag	19	3	7
L4YM-2	20			
part A		25	62	13
part B		27	27	46
L4YM-3	22.3			
L4YM-4	25.8			
part A		22	59	19
part B		23	52	25
L4YM-5	39.5	64	29	7
L4YM-6	47.5	4	75	19
L4YM-7	72.5	42	40	17
L4YM-8	150.0	46	19	35
Core 5				
L5YM-1	12.9	53	17	29
L5YM-2	39.3	11	31	58
L5YM-3	33–34, bag	86	8	5
L5YM-4	53.6	3	45	52
L5YM-5	88.5	71	14	15
Core 6				
L6YM-1	15.8	27	27	45
L6YM-2	29.1	14	36	49
L6YM-3	36.8	41	31	28
L6YM-4	47.5	12	58	29
Core 7				
L7YM-1	11	0	73	27
L7YM-2	29.5	6	30	65
L7YM-3	44.9	33	28	39
Core 11				
L11YM-1A	0.5 (treated)	analysis incomplete		

Table B-2 (cont.)

L11YM-1B	0.5 (not treated)	11	59	30
Core 13				
L13YM-1	1.2	44	25	31
L13YM-2	6.1	76	13	10
L13YM-3	12.0	96	0	4
Core 15				
L15YM-1	0.3	94	1	5
Core 17				
L17YM-1	26.7	44	17	39
L17YM-2	40.5	6	48	45
L17YM-3	51.8	64	12	24
L17YM-4	100.2	20	25	55
L17YM-5	386.5	83	7	11
L17YM-6	430.7	19	37	44
Core 27				
L27YM-1	0.7	21	28	51
Core 43				
L43YM-1	3.6	44	38	18
L43YM-2	6.6	10	63	28
L43YM-3	8.7	3	27	70
L43YM-4	12.7	4	30	66
Core 44				
LYM44-1	3.5	75	10	15
LYM44-2	1.5	69	13	19
LYM44-3	9	84	6	10
LYM44-4	14.3	13	33	54

Table B-3. Trench and surface sample depths and textural data. Sand is 2 to 0.0625 mm, silt is 0.0625 to 0.0039 mm, and clay is <0.0039 mm. Gravel content less than 2% of each sample.

Sample no.	Depth (cm)	Total sand (%)	Total silt (%)	Total clay (%)
trench 1				
T1-1	10	34.8	25.8	39.4
T1-2	120	11.2	27.5	61.3
T1-3	40	18.6	33.3	48.1
T1-4	60	7.8	32.9	59.3
trench 2				
T2-1	5	67.1	15.8	17.1
T2-2	20	63.2	20.2	16.6
T2-3	40	65.8	13.1	21.0
T2-4	60	55.8	18.3	25.9
T2-5	80	56.6	15.5	27.9
T2-6	100	48.7	21.1	30.2
T2-7	120	48.0	23.3	28.7
T2-8	60	51.4	18.0	30.5
T2-9	70	47.8	19.7	32.5
T2-10	60	72.4	12.5	15.0
trench 9				
T9-1	30	35.0	32.7	32.3
T9-2	140	80.8	11.7	7.5
T9-3	70	30.6	31.7	37.7
T9-4	110	53.8	18.2	27.9
T9-5	50	40.7	32.1	27.2
T9-6	110	51.2	36.4	12.3
T9-7	210	61.5	19.2	19.3
T9-8	240	20.2	27.5	52.4
trench 12				
T12-1	20	16.6	36.8	46.6
T12-2	40	14.8	36.3	48.9
T12-3	70	14.8	34.0	51.2
T12-4	90	20.1	30.5	49.4
T12-5	120	28.3	30.8	40.9
trench 17				
T17-1	130	41.3	22.2	36.5
T17-2	40	82.6	6.1	11.4
T17-3	40	10.7	39.4	49.8
T17-4	60	83.6	5.2	11.2
T17-5	80	82.6	9.1	8.3
trench 18				
T18-1	analyses incomplete			
T18-2				
T18-3				
T18-4				
T18-5				
T18-6				

Table B-3 (cont.)

Sample no.	Depth (cm)	Total sand (%)	Total silt (%)	Total clay (%)
T18-7				
T18-8				
Surface engineering samples				
BW-0	60 cm deep at BW-1	20.2	46.4	33.4
TW-0	7.5 cm deep at TW-1	26.5	26.2	47.3
Sand dunes, Fort Hancock area				
CL-1	surface	96	7	0.04
CL-2	surface	90.2	3.6	6.2

Table B-4. Core, trench, and surface sample textural data from Faskin Ranch. See tables B-2 and B-3 for sample depths. Gravel = -2 to -1 phi, sand = –1 to 3 phi, silt = 4 to 9 phi, and clay = 10 to 14 phi.

Grain size (phi)	Sample no. L1YM-3	L2YM-1	L2YM-2	L2YM-3	L3YM-1	L3YM-2	L3YM-3	L4YM-1	L4YM-3	L4YM-5	L4YM-6	L4YM-7	L4YM-8
-2	27	15	1	2	0	1	3	75	0	0	1	0	0
-1	1	0	0	1	0	0	0	10	0	8	0	0	0
0	2	6	1	5	0	3	3	4	0	5	0	0	0
1	2	4	1	5	0	5	5	1	3	14	0	0	0
2	4	5	3	8	3	7	9	2	9	15	0	0	7
3	3	3	3	6	10	6	9	0	2	2	0	0	6
4	5	37	30	6	10	5	12	3	46	34	15	62	39
5	6	5	14	4	5	5	8	1	10	8	25	7	4
6	6	4	11	6	7	6	9	1	10	8	25	6	3
7	4	5	12	7	6	6	7	1	5	5	6	3	2
8	3	0	0	6	4	5	5	0	0	0	0	0	0
9	0	4	5	0	0	0	0	0	2	1	4	3	1
10 to 14	37	20	22	43	55	53	28	7	14	7	17	16	33

Grain size (phi)	Sample no. L5YM-1	L5YM-2	L5YM-3	L5YM-4	L5YM-5	L6YM-1	L6YM-2	L6YM-3	L6YM-4	L7YM-1	L7YM-2	L7YM-3	L11YM-1B
-2	0	0	0	0	1	0	1	1	0	0	0	0	0
-1	0	0	0	0	2	0	0	0	0	0	0	4	0
0	1	0	2	0	1	0	0	0	0	0	0	3	0
1	13	2	48	0	14	1	2	3	0	0	1	5	0
2	24	4	30	1	37	4	7	15	0	0	2	10	3
3	16	5	3	2	16	22	5	21	0	0	3	12	8
4	6	8	10	10	7	11	5	19	13	3	5	13	5
5	4	6	1	12	2	3	7	4	16	3	4	6	12
6	3	8	2	12	2	4	11	4	25	9	15	6	20
7	3	6	2	7	2	5	9	3	14	11	5	3	17
8	1	4	0	4	1	5	5	2	0	3	0	0	4
9	0	0	0	0	0	0	0	0	3	0	3	0	0
10 to 14	29	58	5	52	15	45	49	28	30	72	65	39	30

Table B-4 (cont.)

Grain size (phi)	Sample no. L13YM-1	L13YM-2	L13YM-3	L15YM-1	L17YM-1	L17YM-2	L17YM-3	L17YM-4	L17YM-5	L17YM-6	L27YM-1	L43YM-1	L43YM-2
-2	0	0	1	8	4	0	1	0	51	0	0	0	0
-1	0	0	1	0	0	0	0	0	5	0	0	0	1
0	1	0	8	4	0	0	2	0	9	1	0	0	0
1	10	6	56	47	10	1	17	2	10	4	1	1	0
2	22	29	28	32	17	3	29	8	4	7	4	4	0
3	11	41	1	3	12	2	15	10	3	7	16	38	9
4	9	10	0	0	2	6	4	12	0	4	10	33	27
5	4	2	0	0	3	13	3	3	1	11	5	1	16
6	7	1	0	0	3	19	2	3	3	17	5	2	11
7	4	1	0	0	6	9	2	4	1	5	4	2	7
8	1	0	0	0	2	1	0	1	0	0	4	1	2
9	0	0	0	0	0	0	0	0	0	0	0	0	0
10 to 14	31	10	4	5	39	45	24	55	11	44	51	18	28

Grain size (phi)	Sample no. L43YM-3	L43YM-4	L44YM-1	L44YM-2	L44YM-3	L44YM-4	T1-1	T1-2	T1-3	T1-4	T2-1	T2-2	T2-3	T2-4
-2	0	0	0	0	0	0	0	0	0	0	1	1	3	0
-1	0	0	0	0	0	0	0	0	0	0	0	0	0	1
0	0	0	0	1	0	0	0	0	0	0	2	1	1	1
1	0	0	12	12	4	2	1	1	1	0	9	7	8	8
2	1	1	35	32	36	5	7	2	3	1	22	20	22	19
3	1	3	27	24	44	7	26	9	15	7	33	34	32	26
4	3	7	5	6	5	2	13	9	11	11	6	7	3	8
5	3	5	2	4	1	4	4	5	7	4	4	5	2	4
6	9	7	1	1	0	8	3	4	6	9	3	3	5	2
7	11	9	1	1	0	11	3	4	5	6	2	3	2	2
8	1	2	1	1	0	7	3	5	4	4	2	2	1	2
9	0	0	0	0	0	0	0	0	0	0	0	0	0	0
10 to 14	70	66	15	19	10	54	39	61	48	59	17	17	21	26

Table B-4 (cont.)

Grain size (phi)	Sample no. T2-5	T2-6	T2-7	T2-8	T2-9	T2-10	T9-1	T9-2	T9-3	T9-4	T9-5	T9-6	T9-7	T9-8
-2	0	0	0	1	1	1	0	4	0	0	0	0	1	0
-1	0	0	0	0	1	0	0	5	0	0	2	0	0	0
0	4	0	0	1	2	1	1	7	0	1	2	2	1	0
1	7	5	4	7	6	11	2	9	1	3	4	4	6	1
2	15	14	12	16	15	24	7	23	4	10	9	12	17	5
3	30	30	31	26	23	35	25	33	25	39	24	34	36	14
4	3	10	11	10	11	10	10	5	16	12	11	24	9	9
5	3	3	3	2	3	1	7	2	6	3	8	5	3	4
6	4	3	4	2	3	1	8	2	4	2	6	4	3	5
7	2	2	3	2	2	1	7	2	4	2	5	2	3	7
8	3	2	3	2	2	1	1	1	2	0	2	1	1	2
9	0	0	0	0	0	0	0	0	0	0	0	0	0	0
10 to 14	28	30	29	31	32	15	32	8	38	28	27	12	19	52

Grain size (phi)	Sample no. T12-1	T12-2	T12-3	T12-4	T12-5	T17-1	T17-2	T17-3	T17-4	T17-5	BW-0	TW-0	CL-1	CL-2
-2	0	0	0	0	0	1	0	0	3	0	0	0	0	0
-1	0	0	0	0	0	0	0	0	3	0	0	0	0	0
0	0	0	0	0	0	0	0	0	3	0	1	0	2	1
1	0	1	1	1	1	6	10	3	24	12	3	1	15	10
2	3	3	3	4	7	18	34	4	34	40	7	5	41	38
3	13	11	11	14	20	16	39	3	18	31	15	14	16	41
4	14	16	14	12	16	8	2	9	2	6	4	21	22	3
5	7	7	6	6	5	4	1	5	1	1	3	6	1	0
6	6	6	11	6	5	3	1	7	1	1	14	14	0	0
7	7	6	3	5	4	3	1	9	1	1	5	5	1	0
8	2	2	0	2	1	3	1	10	1	1	1	1	0	0
9	0	0	0	0	0	0	0	0	0	0	0	0	0	0
10 to 14	47	49	51	49	41	37	11	50	11	8	47	33	0	6

Appendix C. X-ray analyses of core samples, Faskin Ranch.

Table C-1. X-ray diffraction analyses of different-sized fractions of samples from core YM-4.

Clay-sized fraction

Sample no.	Minerals identified
L4YM-9	Illite-Montmorillonite (mixed-layer), Kaolinite, Quartz, Feldspar
L4YM-10	Illite-Montmorillonite (mixed-layer), Kaolinite, Quartz, Feldspar
L4YM-12	Illite-Montmorillonite (mixed-layer), Kaolinite, Quartz, Feldspar
L4YM-13	Illite-Montmorillonite (mixed-layer), Kaolinite, Quartz, Feldspar
L4YM-15	Illite-Montmorillonite (mixed-layer), Kaolinite, Quartz, Feldspar
L4YM-16	Illite-Montmorillonite (mixed-layer), Kaolinite, Quartz, Feldspar

Silt-sized fraction

Sample no.	Minerals identified
L4YM-9	Quartz, K-spar, Albite, Illite, Kaolinite, Smectitie, Amphibole (tr)
L4YM-10	Quartz, Albite, Kaolinite, Illite-Smectite
L4YM-12	Quartz, Albite, Microcline, Kaolinite, Illite-Smectite
L4YM-13	Quartz, Feldspar, Kaolinite
L4YM-15	Quartz, Plagioclase (Oligoclase, Albite), K-spar (Microline), Kaolinite
L4YM-16	Quartz, Plagioclase (Oligoclase), Kaolinite

Sand-sized fraction

Sample no.	Minerals identified
L4YM-9	Quartz, Microcline, Albite, Amphibole (tr)
L4YM-10	Quartz, Microcline, Albite
L4YM-12	Quartz, Microcline, Albite
L4YM-13	Quartz, Microcline, Albite, Calcite, Amphibole (tr)
L4YM-15	Quartz, Albite, Calcite (tr), Oligoclase (?)
L4YM-16	Quartz, Microcline, Albite, Calcite

Table C-2. X-ray diffraction analyses of oriented samples of clay extracted from cores YM-4, YM-44, and YM-62.

Sample no.	Minerals identified
L-4YM-9	Illite-Montmorillonite (mixed-layer), Kaolinite
L-4YM-10	Illite-Montmorillonite (mixed-layer), Kaolinite
L-4YM-11	Illite-Montmorillonite (mixed-layer), Kaolinite
L-4YM-12	Illite-Montmorillonite (mixed-layer), Kaolinite
L-4YM-13	Illite-Montmorillonite (mixed-layer), Kaolinite
L-4YM-15	Illite-Montmorillonite (mixed-layer), Kaolinite
L-4YM-16	Illite-Montmorillonite (mixed-layer), Kaolinite
L-4YM-17	Illite-Montmorillonite (mixed-layer), Kaolinite
L-4YM-18	Illite-Montmorillonite (mixed-layer), Kaolinite
L-44YM-5	Illite-Montmorillonite (mixed-layer), Kaolinite
L-44YM-6	Illite-Montmorillonite (mixed-layer), Kaolinite
L-44YM-7	Illite-Montmorillonite (mixed-layer), Kaolinite
L-44YM-8	Illite-Montmorillonite (mixed-layer), Kaolinite
L-44YM-9	Illite-Montmorillonite (mixed-layer), Kaolinite
L-62YM-1	Illite-Montmorillonite (mixed-layer), Kaolinite
L-62YM-2	Illite-Montmorillonite (mixed-layer), Kaolinite
L-62YM-3	Illite-Montmorillonite (mixed-layer), Kaolinite
L-62YM-4	Illite-Montmorillonite (mixed-layer), Kaolinite
L-62YM-5	Illite-Montmorillonite (mixed-layer), Kaolinite
L-62YM-6	Illite-Montmorillonite (mixed-layer), Kaolinite
L-62YM-7	Illite-Montmorillonite (mixed-layer), Kaolinite
L-62YM-8	Illite-Montmorillonite (mixed-layer), Kaolinite
L-62YM-9	Illite-Montmorillonite (mixed-layer), Kaolinite
L-62YM-10	Illite-Montmorillonite (mixed-layer), Kaolinite
L-62YM-11	Illite-Montmorillonite (mixed-layer), Kaolinite

APPENDIX D
PALEOMAGNETIC DATA

SAMPLE (Depth)	INCL. (^{o})	kappa	a95	NRM Intens. ($x10^{-5}$ A/m)	SI Susceptibility Bulk Sus ($x10^{-4}$)	Sus/gm ($x10^{-5}$)
YM#1						
11.8	42.9	22.8	13.62	26.10	17.02	6.754
15.4	48.5	118.6	4.84	11.10	11.28	6.337
16.8	-7.1	176.4	5.58	12.10	15.13	5.980
21.2	62.2	28.7	14.02	3.39	9.497	3.134
YM#2						
17.4	-29.2	19.4	20.56	2.43	13.59	5.373
18.9	-25.6	9.5	21.33	1.54	9.343	3.767
20.6	-38.0	19.6	27.30	1.84	1.133	4.443
23.2	-19.2	211.5	3.96	6.60	12.15	4.418
24.4	-7.7	367.8	3.86	25.80	10.78	3.891
25.9	-8.1	1464.8	1.50	14.30	8.528	3.807
28.2	25.2	38.6	10.40	4.85	7.260	3.408
32.0	67.0	1478.1	1.81	6.28	16.82	6.347
33.0	45.1	10.6	20.32	1.60	10.18	4.757
35.5	84.5	261.1	5.67	3.53	15.51	5.119
38.0	47.6	214.8	5.06	2.44	10.98	3.826
YM#3						
12.3	59.5	161.3	4.15	4.01	18.26	5.947
15.1	65.5	1083.7	2.25	3.67	12.36	5.373
17.1	-22.4	1437.1	1.70	3.95	14.54	5.466
19.2	18.1	68.7	6.97	1.93	15.46	5.992
22.5	-19.6	88.3	4.86	1.30	15.25	5.980
25.2	-34.7	249.3	3.33	2.20	11.63	5.169
30.7	-43.8	43.0	11.36	3.23	14.78	5.394
33.9	-21.6	1041.0	2.15	2.81	15.03	6.423
36.3	40.1	15.9	16.41	2.34	12.66	5.481
40.0	34.5	20.3	12.95	2.00	13.50	5.555
42.6	-37.3	33.9	15.49	1.40	12.57	4.743
45.8	-75.5	83.8	6.43	1.87	16.89	5.906
50.8	-38.1	734.1	2.12	2.06	18.88	6.865
51.9	-38.9	124.9	5.16	2.73	19.03	7.048
56.7	22.2	288.8	3.39	4.34	17.66	6.819
59.3	35.1	1040.3	1.63	3.23	13.98	5.376
62.1	81.8	1385.2	1.73	7.96	14.47	5.359
64.3	56.3	103.3	7.31	1.74	15.70	5.322
67.3	50.0	66.3	7.94	3.42	15.42	5.711
70.1	37.1	373.9	2.36	2.31	14.25	5.588
74.4	59.7	241.3	4.48	6.09	15.32	6.383
76.9	45.4	3520.4	0.97	10.30	15.03	6.109
80.8	65.1	465.0	3.44	2.71	15.71	6.685
83.3	-27.4	61.9	8.20	1.04	17.04	6.579
85.8	39.4	156.3	7.18	1.41	13.06	4.984
90.3	11.9	45.8	9.5	1.75	12.43	5.650
93.7	5.4	445.0	2.13	28.20	13.88	5.277
102.3	-14.3	92.6	9.33	12.30	19.89	6.906

103.3	-24.3	880.5	1.94	7.70	19.08	7.482
SAMPLE (Depth)	INCL. (^{o})	kappa	a95	NRM Intens. ($x10^{-5}$ A/m)	SI Susceptibility Bulk Sus ($x10^{-4}$)	Sus/gm ($x10^{-5}$)
YM#4						
14.9	33.7	1583.6	1.45	2.88	8.524	3.674
17.6	50.6	67.7	6.43	2.45	6.293	2.784
22.6	-50.9	592.7	2.00	3.39	14.40	6.050
24.5	5.2	107.4	4.70	1.12	10.88	4.792
29.1	-48.9	2111.5	0.99	5.01	13.96	4.762
34.3	47.1	94.1	5.44	1.41	8.955	3.731
43.6	-46.3	41.1	10.11	2.44	12.19	4.653
46.7	-33.7	317.8	2.41	0.98	9.511	4.423
50.1	-23.1	1764.7	1.02	8.84	9.910	5.475
52.1	-45.2	148.5	4.00	0.561	9.287	4.091
60.3	-23.1	269.6	3.92	1.34	10.09	3.709
63.5	-54.4	150.6	4.30	1.07	8.955	3.927
65.8	-51.9	130.5	4.27	0.968	8.112	3.671
68.9	-25.5	518.5	2.14	0.829	12.64	5.333
72.5	-34.1	500.6	2.35	2.97	14.55	6.113
76.2	41.0	205.1	3.40	2.24	6.534	3.913
80.3	74.3	142.0	6.25	2.20	9.490	5.243
83.1	53.4	206.3	3.67	3.40	16.07	5.366
86.4	-51.9	49.1	9.24	0.387	9.091	3.953
89.1	-36.6	46.8	7.73	6.43	10.02	3.914
92.7	59.6	44.3	13.56	14.90	13.27	4.807
98.0	53.6	259.2	4.00	4.88	15.29	5.131
99.4	38.9	167.4	3.32	4.30	17.20	5.714
103.3	-38.0	22.4	15.80	13.80	13.07	6.438
107.0	-21.8	83.5	7.05	1.28	19.25	6.395
110.2	-59.6	100.2	6.45	0.816	11.98	5.055
113.5	-8.9	16.0	18.73	0.745	14.73	6.012
116.7	58.2	390.0	1.97	5.06	14.26	6.094
120.1	45.0	646.2	2.26	1.95	14.69	5.083
122.6	-22.3	411.9	3.65	0.845	12.54	4.804
127.7	53.5	70.2	6.91	2.04	9.962	4.000
130.3	42.6	153.8	4.65	2.20	15.50	4.754
131.4	67.9	218.4	3.31	3.23	15.22	4.756
134.3	42.7	114.1	5.40	2.27	16.01	5.555
139.2	57.0	294.2	3.36	2.65	14.11	6.271
141.8	16.3	200.7	3.22	3.02	10.28	5.874
145.0	59.2	278.8	3.86	2.74	16.82	6.596
148.6	-12.1	90.7	7.79	1.69	16.71	7.021
153.3	-29.0	383.8	2.68	1.21	13.30	6.456
156.5	-15.0	74.4	10.41	1.73	11.57	5.235
160.9	-34.8	56.5	8.59	3.27	16.94	6.368
161.5	69.1	111.0	5.04	1.10	13.91	5.701
164.0	-42.5	165.2	6.98	9.38	15.40	6.676
165.4	-11.6	70.3	6.29	0.747	17.37	6.785
168.9	-29.3	112.8	3.84	1.28	19.86	8.241
173.9	-46.7	10.7	23.19	4.24	15.44	7.568
176.6	42.7	75.2	6.66	0.869	17.41	6.964
179.0	-37.5	170.7	3.49	0.898	14.05	7.025
182.3	-42.2	312.0	3.26	1.77	16.79	5.954

185.4	24.2	2.9	31.53	0.703	10.62	5.503
190.5	-9.1	18.6	13.51	1.01	23.20	8.992
YM#4 cont.						
193.4	-28.6	40.5	7.70	2.09	27.58	12.04
194.9	-18.0	29.9	13.64	1.28	26.19	8.394
198.4	-38.7	193.0	4.15	1.28	17.36	6.551
201.5	-27.9	166.5	4.47	4.22	20.13	7.863
205.5	33.7	22.8	13.60	2.62	20.86	9.525
210.5	51.2	49.4	7.54	1.65	26.96	9.594
213.9	75.0	139.6	4.51	4.87	17.05	7.893
214.4	64.4	223.9	4.31	3.24	24.20	9.201
218.8	-42.1	27.4	11.11	1.67	20.12	9.104
222.4	-34.4	100.4	5.76	1.97	17.00	8.673
226.3	-15.8	28.5	38.67	5.79	18.47	8.434
230.3	-27. 3	1285.7	1.36	5.33	22.37	9.130
233.0	-54.8	114.8	8.38	0.906	22.42	7.424
235.3	-7.6	85.9	6.95	11.80	19.54	8.496
240.0	-34.0	238.5	4.17	8.04	21.52	7.319
242.9	-27.4	638.4	2.08	4.16	19.73	7.046
244.9	-55.8	1024.3	1.80	3.47	20.37	7.957
249.5	-35.2	175.3	3.98	1.76	25.94	8.853

SAMPLE (Depth)	INCL. (^{o})	kappa	a95	NRM Intens. ($x10^{-5}$ A/m)	SI Susceptibility Bulk Sus ($x10^{-4}$)	Sus/gm ($x10^{-5}$)
YM#5						
11.6	75.3	34.3	10.61	5.12	8.077	4.038
13.2	55.8	129.4	4.64	1.18	7.430	3.302
14.4	34.6	3.6	32.95	1.57	6.517	3.325
34.4	-15.8	367.0	2.38	2.28	14.99	6.220
36.3	-9.2	140.6	10.10	1.50	7.381	3.989
38.4	-23.5	57.3	6.97	1.60	12.46	5.990
40.3	-22.4	190.1	3.82	0.869	6.544	3.480
41.5	-24.5	364.3	3.37	2.06	15.38	6.687
55.3	-57.8	36.9	12.30	0.633	8.696	4.064
57.8	-31.6	75.9	5.60	2.63	10.78	4.473
60.1	-32.5	296.2	2.65	3.96	10.26	5.343
70.7	-21.4	240.7	3.39	1.20	10.51	4.418
72.3	-44.2	192.1	4.16	0.751	8.843	4.171
76.2	0.0	71.6	14.18	2.38	16.73	8.898
77.2	22.3	9.3	24.86	3.19	12.97	6.862
86.9	2.6	21.1	16.29	2.27	15.16	8.106
90.3	-25.4	62.6	8.16	0.998	14.12	7.550
92.7	76.6	296.8	6.96	2.07	12.57	6.785
96.9	-55.7	41.6	10.06	1.32	14.87	7.548
100.0	-16.4	6.4	48.58	4.33	16.19	7.359
103.5	59.7	702.2	1.98	4.80	16.89	8.617
104.9	65.6	160.2	3.87	3.88	16.60	8.783
107.2	59.7	122.5	3.70	7.37	16.68	7.981
110.2	-28.2	211.0	5.10	4.57	21.54	9.488
112.9	-17.9	6541.9	0.71	7.64	17.27	9.284
118.4	-11.4	923.3	2.12	3.57	17.40	10.057
123.5	-27.0	268.6	3.51	2.10	15.07	7.176
125.1	-38.1	402.4	2.62	4.02	17.20	7.022
130.3	51.3	94.5	5.43	2.60	15.19	7.482
133.2	70.4	102.6	6.40	4.61	16.99	7.517
135.2	69.9	309.4	3.28	3.33	16.79	7.429
137.3	47.5	26.8	12.56	3.96	15.39	8.456
138.8	67.6	145.7	6.15	5.45	15.45	8.049
142.9	14.7	28.7	13.91	1.30	15.83	7.837
144.7	-25.3	46.3	9.49	11.00	19.32	8.781
149.1	42.6	1092.3	2.24	4.51	14.21	8.509
152.5	84.4	854.4	2.00	5.46	7.584	4.790
154.2	59.3	178.4	4.82	4.33	17.25	7.500

SAMPLE (Depth)	INCL. (^{o})	kappa	a95	NRM Intens. ($x10^{-5}$ A/m)	SI Susceptibility Bulk Sus ($x10^{-4}$)	Sus/gm ($x10^{-5}$)
YM#6						
11.1	43.0	231.9	2.99	3.21	12.20	3.609
12.4	36.5	482.7	2.39	4.18	16.66	5.764
13.0	-29.9	778.0	1.54	2.00	11.96	5.009
13.4	-11.8	64.2	11.22	1.94	11.44	4.486
14.9	-28.6	123.0	4.40	3.45	15.64	5.708
16.3	-60.3	39.4	10.37	2.33	16.15	5.192
17.1	-29.5	37.0	10.63	1.55	13.54	5.167
21.0	-22.9	86.4	5.67	0.974	11.41	5.048
22.2	-27.2	101.0	4.85	1.63	8.869	4.768
23.7	61.3	59.8	11.64	2.01	7.619	4.354
28.6	-51.3	32.1	7.31	1.48	7.500	3.456
30.4	69.8	12512.8	0.41	5.16	9.182	4.231
32.0	-26.4	522.8	2.13	0.935	7.370	3.560
34.7	-25.7	127.7	5.10	1.08	7.290	3.169
39.7	-16.2	139.1	5.46	1.63	12.42	4.210
43.6	-43.8	18.6	13.58	1.43	11.94	4.175
44.9	-9.9	1359.7	2.01	1.72	12.21	4.522
49.5	-15.8	33.6	12.85	0.839	11.89	5.380
52.2	61.2	49.1	8.31	1.21	8.693	3.294
56.1	-28.2	128.3	4.65	0.452	7.699	3.019
59.0	-24.9	194.4	3.27	0.963	10.73	3.959
63.3	1.8	4019.2	0.77	6.23	10.86	5.402
66.5	16.7	8.1	15.59	1.15	9.992	5.072
69.3	37.5	112.9	4.96	2.39	14.46	4.804
73.2	61.0	48.9	6.24	2.92	16.85	6.149
78.1	48.8	340.0	2.85	2.54	12.52	4.145
80.5	58.4	1226.6	1.39	3.74	13.79	4.269
83.1	20.0	19.4	20.56	1.17	19.81	6.390
86.4	75.1	195.8	4.62	2.01	12.96	5.122
90.4	-45.1	114.2	6.94	0.513	14.226	5.288
93.8	45.3	29.8	11.89	0.799	14.12	5.348
96.5	30.1	34.1	4.65	3.21	12.916	5.689
100.2	38.9	931.2	1.02	5.98	14.86	5.992
103.7	17.4	30.6	6.77	4.82	16.15	6.358
106.6	49.3	82.3	4.51	2.62	15.00	5.905
110.9	41.6	75.0	3.86	3.65	16.435	6.346
113.9	43.2	29.6	7.58	2.19	15.115	4.723
116.0	44.2	906.8	1.42	8.74	16.365	7.023
120.9	28.9	22.1	8.02	1.53	14.65	5.613
123.8	14.7	432.6	1.87	4.51	18.63	6.849
125.9	-64.5	748.1	1.67	1.39	16.15	5.401
130.7	-37.9	51.3	6.03	0.358	15.972	6.191
132.8	-21.3	25.1	9.80	0.646	16.388	6.471
140.0	-44.9	77.0	4.91	1.04	8.63	3.649
142.9	-35.6	244.8	2.28	3.25	18.44	6.105
146.8	-56.2	54.7	5.87	0.220	14.583	5.608
150.5	-44.3	373.6	2.52	1.07	16.597	6.311
153.5	-54.7	68.6	4.36	0.693	16.736	5.041
156.7	-44.7	183.9	3.59	1.01	18.98	6.347
160.3	-46.6	124.2	4.38	1.45	17.638	6.732

163.4	-50.4	74.3	4.18	1.31	20.90	7.411
YM#6 cont.						
166.1	-21.0	57.6	6.44	0.928	15.85	5.661
170.9	-45.0	39.0	11.93	2.60	17.06	6.462
173.3	-13.3	39.7	10.26	3.29	21.48	7.406
175.7	78.6	98.6	9.14	5.15	21.75	7.823
180.9	53.9	214.5	3.94	4.96	20.648	8.292
183.1	54.2	115.4	6.00	1.02	16.36	5.681
186.8	55.1	1441.3	1.38	3.89	19.44	7.018
190.7	39.4	70.7	8.83	1.32	21.92	9.171
193.7	59.6	182.1	2.56	4.72	22.10	8.983
195.7	47.9	240.3	2.94	2.66	19.67	8.833
203.6	-25.1	273.7	2.08	2.10	19.49	7.218
206.7	-21.1	49.3	6.97	1.83	21.36	8.215
210.5	-1.4	1243.0	1.29	1.71	17.82	6.363
213.7	-17.1	112.9	5.43	0.749	16.50	6.735
216.4	-56.9	45.3	17.86	0.0604	17.06	7.935
220.3	19.2	52.0	5.98	1.21	19.72	8.016
223.5	61.1	73.1	5.38	3.09	18.58	7.011
226.4	48.8	15.5	10.71	2.20	20.55	7.667
230.4	58.1	268.9	2.78	2.33	20.32	8.683
233.7	-40.2	88.0	3.82	1.31	22.68	8.217
235.6	-6.7	575.1	4.99	2.96	20.83	10.415
240.1	-16.7	66.2	5.29	1.75	22.33	8.003
243.5	-40.0	61.4	4.58	1.88	24.46	8.019
248.1	53.5	77.5	7.03	4.89	19.67	7.312
250.5	43.1	161.8	3.59	4.81	19.09	6.942

SAMPLE (Depth)	INCL. (^{o})	kappa	a95	NRM Intens. ($x10^{-5}$ A/m)	SI Susceptibility Bulk Sus ($x10^{-4}$)	Sus/gm ($x10^{-5}$)
YM#7						
11.2	73.9	186.6	3.88	0.767	2.266	1.574
13.0	52.9	1473.6	1.50	1.25	5.373	2.499
14.6	59.2	418.4	2.82	0.973	6.237	2.784
15.6	65.7	334.2	2.88	1.33	5.929	2.935
17.3	63.1	645.3	2.27	1.57	5.719	2.672
18.3	52.1	155.4	4.23	1.17	4.607	2.588
20.3	44.8	331.7	2.89	1.31	5.166	2.719
21.9	40.7	24.4	9.35	1.15	5.306	3.139
23.2	51.1	84.1	7.04	2.31	5.905	2.907
24.5	53.7	160.0	5.86	4.01	6.286	3.096
26.5	-6.0	300.2	5.17	4.19	7.342	3.529
27.6	-21.0	40.6	14.14	3.31	7.612	3.557
29.5	49.7	112.4	3.85	2.98	8.542	4.098
30.0	-75.1	228.2	4.28	2.42	9.088	4.709
31.2	40.6	49.2	9.22	1.58	10.02	5.246
33.2	-44.8	55.3	10.00	4.01	15.36	6.707
36.2	22.7	40.0	9.15	3.37	14.10	7.085
39.2	-34.2	2848.1	1.20	3.14	14.54	7.418
43.3	-46.5	259.8	3.58	1.63	17.77	7.253
47.1	-46.4	34.1	11.11	2.22	15.17	7.056
50.5	-19.7	74.5	10.41	3.63	15.24	6.896
52.2	-1.7	385.8	6.09	3.77	14.04	7.029
55.5	-24.2	40.8	7.17	2.37	15.10	6.681
56.4	-10.3	725.2	4.44	2.07	13.84	7.025
59.4	41.4	161.2	3.06	1.91	14.37	2.543
63.5	28.9	205.9	3.18	8.34	19.76	8.743
67.4	-29.8	283.0	3.82	1.06	20.11	8.344
72.7	-37.1	56.4	9.90	0.995	17.13	8.565
76.0	-27.1	319.8	3.22	3.59	22.40	10.228
77.7	-38.5	263.3	3.24	1.41	15.66	8.199
80.3	-19.1	459.3	3.45	3.96	15.97	7.129
84.4	45.9	407.4	2.61	4.80	13.72	6.628
88.5	41.4	146.2	4.77	6.83	20.82	8.936
90.2	33.2	1332.2	1.33	4.07	12.29	7.063
93.2	27.7	15.7	18.95	2.41	13.99	8.229
96.8	-30.2	137.5	5.49	1.75	18.51	8.154
103.4	72.9	185.6	6.60	0.911	15.10	6.565
105.3	64.7	63.8	7.28	2.35	9.392	4.388
107.0	55.3	486.1	2.39	3.07	11.98	5.209
114.4	-25.7	95.4	12.27	5.48	3.449	1.455
116.8	-12.7	231.1	5.90	0.103	1.042	0.624

SAMPLE (Depth)	INCL. (^{o})	kappa	a95	NRM Intens. ($x10^{-5}$ A/m)	SI Susceptibility Bulk Sus ($x10^{-4}$)	Sus/gm ($x10^{-5}$)
YM#17						
20.0	53.4	187.0	4.32	2.79	5.281	4.059
20.7	57.8	3374.3	1.54	2.07	6.078	4.675
21.2	45.7	1173.4	2.16	1.69	5.372	3.921
22.0	56.6	138.2	6.31	1.31	5.078	4.454
23.0	35.4	42.0	8.94	1.44	5.104	4.325
25.2	68.6	133.3	10.38	0.53	5.729	3.508
28.5	65.9	360.6	6.30	1.96	3.485	3.189
30.5	49.9	2733.7	1.10	6.05	5.981	4.463
31.3	-38.4	1991.6	2.01	1.38	5.402	3.650
36.0	27.6	13.0	25.23	2.18	5.340	3.841
36.8	64.9	1071.1	2.74	2.67	6.448	3.931
38.0	-6.2	312.8	6.77	2.43	5.172	4.879
40.4	-42.7	8826.4	0.79	0.145	7.061	5.230
41.4	-44.0	222.4	6.01	0.574	7.270	5.385
42.4	-28.9	164.9	4.10	1.24	8.023	5.278
43.5	-1.2	64.2	14.97	2.34	7.500	5.172
45.8	-7.1	192.7	8.63	0.287	6.880	4.617
47.2	-28.0	11.5	35.93	0.619	7.452	4.600
49.5	-52.1	5.5	53.49	1.05	6.901	4.792
50.4	-49.8	25.2	14.93	0.505	6.615	4.864
51.4	-18.0	29.0	38.35	0.006	6.134	4.477
53.1	-27.8	8.0	43.45	0.499	5.604	3.761
54.1	-4.8	15.5	30.76	0.405	4.491	3.034
54.6	-0.7	3.3	70.24	0.888	5.563	4.183
60.6	-42.6	95.2	5.92	0.551	7.668	4.564
61.6	-29.9	675.0	7.90	0.462	6.615	4.973
62.5	-42.4	50.5	12.67	0.299	5.451	5.241
63.4	-24.4	649.8	2.90	1.71	7.284	4.699
64.3	-27.8	4293.0	1.37	2.72	7.236	4.020
65.3	-46.3	80.1	6.45	0.456	4.984	3.560
66.6	-19.1	504.4	5.33	2.53	6.964	3.499
67.8	44.2	4.2	34.23	1.98	8.484	4.200
70.6	-56.7	472.0	2.96	1.05	6.092	4.034
71.5	28.8	35.5	12.50	0.78	6.789	4.332
72.4	-38.5	228.7	5.93	0.779	7.452	4.006
72.8	-29.1	260.4	7.42	0.731	6.253	4.034
74.6	36.5	3251.4	1.57	2.13	9.125	4.854
75.6	-39.7	226.0	5.96	0.963	8.943	5.962
77.0	-9.9	453.4	5.62	1.32	7.863	4.182
78.1	40.9	19.2	12.20	2.58	9.933	5.808
79.3	72.0	872.9	3.03	2.55	9.076	4.052
80.6	47.3	432.8	3.56	1.84	8.135	4.470
81.9	63.8	1637.9	1.83	3.03	8.344	5.026
83.1	47.9	1642.0	1.83	3.22	8.943	4.968
84.6	58.6	695.9	1.99	3.26	8.713	5.095
85.4	-41.1	65.7	11.09	1.86	8.009	4.739
86.6	-45.4	213.5	6.14	1.97	10.20	5.368
87.7	-44.8	1438.9	2.36	1.48	9.606	5.787
88.6	-30.5	48.8	10.64	2.33	9.954	5.266
90.7	50.2	33.4	9.21	1.58	6.525	4.321

91.5	67.7	104.4	7.28	1.44	5.082	3.322
YM#17	cont.					
93.0	-43.2	154.4	5.97	0.461	6.253	4.060
94.2	-43.8	156.0	5.16	0.998	7.117	3.826
95.8	-59.2	1280.6	1.80	0.622	5.890	4.237
97.1	-41.6	84.6	5.73	1.43	5.437	3.939
98.5	-36.6	157.5	5.13	0.169	5.834	4.138
99.5	-19.0	92.8	6.69	0.452	6.071	4.275
100.8	54.0	59.5	9.64	2.63	9.891	6.553
102.0	51.0	148.1	7.37	1.72	8.191	4.654
103.3	57.7	32.5	9.38	1.58	8.191	5.056
104.6	51.8	467.6	4.14	1.97	9.250	6.752
107.9	41.4	122.7	6.70	2.91	12.83	6.682
111.1	36.7	824.9	2.58	2.49	8.874	5.955
112.7	40.1	82.6	9.88	2.79	12.92	6.729
114.0	-58.8	42.0	8.21	0.393	9.996	6.247
114.9	-41.5	181.5	4.78	0.902	10.53	5.428
115.6	-19.3	346.3	3.98	0.848	10.58	6.531
117.0	-45.6	60.5	9.56	0.805	11.79	6.046
118.4	-50.9	40.6	14.15	0.604	10.99	5.387
119.8	-40.9	495.0	4.03	0.289	8.999	5.388
121.8	-14.5	520.9	9.00	1.24	13.19	8.244
123.6	47.8	145.3	6.15	5.09	12.22	6.943
124.5	-35.8	5548.0	0.99	0.596	12.71	7.894
125.5	24.0	35.8	12.44	1.62	10.40	16.00
126.9	52.0	379.7	2.96	2.705	8.957	4.789
128.3	56.3	155.9	5.94	2.34	10.36	6.24
129.5	-19.5	7.8	43.91	0.559	8.630	4.903
131.1	-40.9	421.4	3.13	1.15	7.877	4.189
132.2	-36.6	169.0	4.43	0.386	7.716	5.673
133.9	15.6	46.0	9.52	0.936	12.30	7.028
135.8	39.8	107.0	7.17	4.18	12.99	5.799
137.1	54.0	1147.0	2.19	2.85	9.682	4.632
138.5	39.3	213.9	4.40	3.14	7.710	4.331
139.4	52.1	124.2	4.38	2.98	8.428	4.682
141.2	57.8	199.1	6.36	3.10	12.65	7.354
142.5	59.2	198.8	4.57	2.563	11.90	7.727
144.1	44.3	60.6	9.55	3.21	12.46	8.038
145.8	48.5	380.8	4.59	2.31	8.197	5.614
147.1	49.2	20.1	11.95	1.91	8.574	6.915
148.5	40.5	1649.2	1.82	1.59	6.915	4.020
150.0	57.9	151.3	5.24	1.05	8.783	6.016
151.6	12.6	360.3	3.39	2.05	12.49	7.262
152.6	50.7	17.6	21.64	0.707	10.62	9.000
155.3	-28.2	24.3	10.77	0.528	10.21	6.807
156.8	50.9	33.3	11.24	0.702	7.082	4.659
158.5	-49.6	68.6	6.99	1.12	13.11	6.757
159.8	-53.9	115.3	5.38	1.16	8.518	4.280
161.8	-48.4	98.0	6.51	0.948	9.201	5.576
164.1	-35.9	37.5	9.47	0.888	8.818	5.068
166.0	-27.0	294.4	5.22	0.448	9.243	6.121
168.9	-40.4	121.0	10.89	0.674	7.326	4.139
171.0	52.5	133.1	6.43	0.849	11.07	5.984
172.3	-14.6	36.9	10.64	0.760	10.76	5.198

175.5	-40.4	393.1	6.04	0.566	9.410	5.032
YM#17	cont.					
176.6	-39.1	523.3	3.24	3.10	10.57	6.181
178.7	-15.9	7.0	28.89	2.13	12.28	6.429
180.1	-18.6	39.0	19.26	2.09	9.452	6.518
181.5	65.8	36.8	10.79	6.54	12.06	6.852
182.5	-35.4	52.0	10.31	4.05	11.24	6.279
184.3	5.6	299.3	5.92	2.31	10.62	7.426
186.4	-45.0	117.4	5.95	5.47	10.34	6.893
188.6	77.8	94.0	7.77	5.09	12.75	10.991
190.4	-37.6	115.8	8.34	1.95	13.47	6.668
191.5	-38.7	29.0	16.77	0.355	7.096	5.217
192.6	-27.0	138.4	10.18	0.592	13.74	7.676
195.8	12.7	211.1	5.10	0.834	10.23	6.475
196.9	52.0	37.4	14.76	0.576	8.685	5.497
198.5	-33.0	46.1	8.52	0.840	14.08	6.802
199.5	-34.3	172.3	9.12	3.33	15.52	8.126
201.7	-22.4	387.1	4.56	0.457	10.05	7.179
203.0	-32.5	59.0	7.52	3.41	13.11	8.798
204.1	-27.2	106.7	6.24	0.887	13.75	10.826
205.8	-31.6	16.0	22.72	0.684	9.473	6.112
207.3	-43.6	313.8	6.76	1.63	14.43	10.090
208.5	33.4	125.6	8.01	1.75	11.86	8.352
209.9	72.9	219.9	8.08	1.19	10.34	7.833
211.2	69.4	60.3	8.39	2.22	15.58	9.617
212.4	62.8	3432.3	1.10	3.23	11.44	8.474
215.6	52.1	117.7	6.84	1.93	11.29	9.567
217.2	60.3	333.9	4.91	2.59	16.81	10.066
218.6	46.6	9620.0	0.75	5.39	15.25	11.213
219.9	55.1	648.9	3.52	2.25	14.32	8.574
221.3	48.9	501.6	3.31	1.96	14.66	8.726
225.5	39.7	860.3	1.96	4.19	15.89	10.664
227.7	16.7	69.5	10.78	1.61	14.56	10.041
228.9	14.4	31.1	13.37	1.35	13.95	9.362
230.6	-47.4	31.3	11.60	1.53	13.14	10.197
232.2	-10.5	40.9	11.63	1.45	16.45	10.894
233.5	-54.8	132.6	5.01	3.66	14.54	11.099
236.1	-27.6	67.0	10.98	0.963	16.67	13.126
237.3	-28.9	498.1	2.58	3.99	15.76	10.794
238.7	21.6	91.7	7.75	3.88	19.53	10.731
240.7	-35.1	85.1	8.05	1.68	14.94	11.233
242.2	-35.8	69.0	6.35	1.71	15.01	9.265
245.5	-40.3	1529.7	1.64	9.82	10.10	6.273
251.0	65.8	348.7	6.41	3.07	14.23	9.882
252.9	-33.7	82.6	8.17	0.726	11.03	7.902
254.1	-7.6	75.3	13.82	3.09	15.38	11.223
257.6	-31.9	3088.6	1.16	9.47	9.734	6.365
258.9	-58.0	903.6	2.98	1.55	13.67	7.948
260.5	-48.3	44.6	13.48	1.06	14.90	8.713
261.7	7.8	34.3	9.89	7.28	15.59	9.335
262.8	47.8	45.5	9.59	1.54	14.99	17.430
264.4	11.4	70.8	7.66	0.187	19.26	10.299
265.4	46.5	689.2	4.56	6.48	11.95	8.852
266.3	29.3	445.3	5.67	7.09	12.08	8.507

268.8	35.5	745.4	4.38	7.69	16.55	8.803
YM#17	cont.					
270.1	31.2	36.8	10.66	4.73	15.71	10.135
271.6	47.0	43.1	11.34	3.98	10.80	6.792
272.9	36.3	429.2	5.78	2.40	13.17	10.885
273.8	31.6	2038.7	2.65	6.32	13.09	8.555
275.9	41.7	78.0	8.41	3.28	20.62	12.129
277.2	69.4	47.4	13.15	1.89	13.14	10.429
278.7	15.5	251.5	4.06	1.06	19.67	9.835
280.2	-30.3	135.7	7.70	1.57	16.55	8.359
281.5	-48.7	2367.0	1.52	3.29	15.22	8.139
282.7	-25.7	39.1	8.46	1.64	15.78	12.232
284.2	-43.4	88.9	6.12	1.81	16.26	9.795
285.9	-38.2	145.9	7.43	2.09	19.21	10.672
287.2	-20.1	131.2	6.52	0.860	20.37	12.811
295.5	66.3	112.4	11.31	2.35	17.95	10.379
301.6	46.5	62.4	9.41	2.06	13.13	8.206
302.9	44.8	105.1	5.14	2.79	15.38	10.253
304.6	36.4	1967.3	2.02	3.12	15.36	9.722
306.8	35.5	258.7	4.61	2.68	10.87	7.445
308.5	61.9	495.1	4.03	2.17	11.45	8.740
309.8	50.5	4936.8	1.05	5.06	12.86	7.477
310.9	49.7	284.0	3.82	2.66	15.29	9.101
311.5	43.2	870.6	2.51	2.26	11.38	7.795
312.5	39.9	838.6	2.56	2.42	13.38	7.352
314.3	59.7	383.0	4.58	1.61	15.02	3.779
315.7	55.9	73.3	8.68	1.93	12.50	8.449
317.4	82.3	376.5	6.18	2.14	11.99	7.735
318.6	41.6	26.6	12.59	1.67	11.31	7.158
319.7	18.0	63.5	11.28	3.49	15.31	8.057
320.4	24.9	152.3	9.71	1.83	13.14	8.644
321.5	26.2	54.8	16.22	2.65	14.76	10.888
325.9	7.2	53.6	8.82	2.52	11.65	9.873
326.7	-56.8	429.3	5.78	2.90	16.12	12.693
328.3	64.6	45.6	30.53	3.09	10.98	11.902
330.5	78.4	92.5	7.85	6.07	16.56	9.517
340.5	53.1	743.0	2.11	4.21	14.08	8.697
342.1	59.3	355.2	4.76	2.87	15.66	7.909
343.7	37.7	44.0	13.58	5.22	16.07	9.343
344.8	63.3	62.9	11.36	1.59	18.73	10.405
347.2	56.5	52.3	10.29	1.58	10.89	7.949
350.4	-43.4	159.4	4.57	1.41	11.56	7.136
351.4	-53.9	96.7	7.55	0.871	11.97	8.489
352.3	-41.6	4180.9	1.14	1.96	12.44	7.494
353.7	20.6	10.0	28.99	1.07	9.327	8.479
375.9	-25.1	114.5	8.39	4.51	18.22	9.110
380.2	-43.0	25.4	10.56	1.72	15.22	10.353
382.0	-20.4	3.3	52.46	2.68	17.39	11.829
383.3	18.1	109.0	8.60	1.79	7.284	5.436
384.8	45.1	258.4	4.61	2.67	10.69	9.991
386.3	61.8	113.0	8.45	0.299	26.65	14.723
387.7	-38.9	17.7	13.91	5.54	26.47	12.545
388.9	-30.7	2974.7	2.19	3.99	8.671	7.888
393.1	66.6	74.4	10.44	1.87	9.104	6.794

393.7	-53.4	35.6	20.18	0.421	2.767	2.635
YM#17	cont.					
395.7	26.5	57.5	11.86	1.78	5.381	2.599
396.7	-4.7	99.3	5.79	2.89	15.50	8.708
398.2	-22.3	2598.7	4.03	1.96	9.843	3.673
400.5	-1.6	67.8	14.57	1.09	6.364	4.714
402.0	-26.4	179.1	8.95	0.631	3.729	2.361
403.7	30.4	1612.7	1.84	1.22	6.085	5.464
404.6	-56.3	196.2	6.40	1.41	9.898	5.592
405.6	-52.7	219.9	5.00	1.434	9.194	4.552
407.2	-8.4	21.8	44.35	2.54	10.67	5.831
408.1	18.1	55.6	16.10	2.17	10.69	5.539
410.4	-11.9	384.7	4.57	1.61	9.557	9.562
411.6	-39.6	409.9	3.66	0.628	7.842	5.724
412.8	-22.3	321.8	11.45	0.911	8.678	6.675
413.7	-16.1	28.6	13.94	0.701	12.50	6.614
415.7	-26.9	598.8	3.03	2.32	13.47	7.127
416.7	-46.7	705.4	2.79	1.76	10.52	7.735
417.8	-42.0	5356.7	1.22	2.11	14.42	8.956
421.0	-37.0	258.3	7.45	0.845	10.25	7.374
422.2	-26.2	82.3	13.22	0.393	8.532	5.469
423.7	49.2	2111.5	1.61	2.76	10.16	6.195
424.6	33.8	411.5	3.65	4.78	12.51	6.482
426.3	61.8	156.1	5.16	1.50	9.431	7.241
427.6	22.9	496.1	2.89	3.17	12.64	6.618
430.2	42.1	5306.6	1.02	5.50	8.539	4.824
431.1	57.9	991.1	2.85	2.51	9.905	6.229
432.7	49.9	145.3	6.15	2.00	11.00	6.145
434.2	40.2	64.5	14.95	1.98	8.386	4.570
435.3	12.9	19.4	20.54	1.17	11.29	8.122
436.5	-27.3	461.8	5.57	1.19	11.88	7.071
437.8	52.8	606.3	3.01	0.999	9.727	8.843
438.9	7.3	568.6	3.76	0.778	7.647	6.069
440.6	61.8	102.6	4.84	2.75	10.90	6.374
441.6	1.5	148.6	6.08	1.22	9.905	8.465
442.5	60.5	1090.0	2.24	2.29	11.98	7.779
443.6	-35.0	7211.7	0.87	3.32	12.32	6.659
445.1	-42.5	1135.8	2.20	2.07	13.54	7.481
445.9	-49.5	30.0	9.72	0.764	11.69	7.742
447.5	-58.5	477.1	3.39	2.13	12.14	8.203
448.6	-33.4	3091.3	1.33	3.80	15.17	8.156
449.9	-38.1	1161.5	2.17	2.99	14.14	7.899
451.3	-40.0	3080.4	1.33	4.31	15.29	8.942
453.6	-40.2	227.8	5.94	1.52	12.99	6.984
454.4	49.6	50.1	12.72	1.64	12.57	8.216
456.2	-52.3	1427.4	1.96	4.89	12.73	8.160
457.2	-48.1	502.0	3.30	4.30	16.99	9.184
457.9	-34.2	135.6	6.37	2.33	16.81	9.606
459.5	-51.9	349.3	3.08	5.79	14.66	8.189
460.9	-40.2	304.1	3.69	4.31	9.613	8.011
462.2	-50.9	182.0	5.49	1.31	15.70	9.752
463.7	13.4	107.5	7.15	1.60	12.48	8.376
464.7	37.8	3072.8	1.62	10.68	12.58	7.028
466.3	50.4	121.5	8.14	3.82	9.675	7.220

467.4	-31.4	40.2	14.20	0.775	13.11	7.994
YM#17	cont.					
468.4	-43.9	7324.2	0.75	11.61	9.341	5.527
469.8	-44.6	53.2	12.34	0.436	12.35	7.485
471.8	26.4	1184.8	2.15	6.39	11.46	9.024
472.7	29.4	171.4	4.92	1.37	11.11	7.407
473.9	41.5	1346.7	2.02	5.16	11.01	7.541
475.2	51.0	3869.3	1.44	4.09	13.45	7.819
476.9	32.0	999.0	3.79	2.28	12.09	7.153
478.0	47.0	4895.3	1.06	7.82	9.773	6.225
479.8	52.0	2223.1	1.36	5.67	9.856	8.013
480.8	40.2	3091.3	1.33	9.10	11.98	7.441
482.4	77.5	76.4	10.39	2.15	14.54	8.706
483.2	-25.5	4002.2	1.89	7.85	11.08	6.882
484.4	-34.7	6990.5	1.07	5.12	12.35	8.179
485.6	-52.8	276.2	3.87	3.06	9.424	6.590
487.0	-28.3	2335.4	1.53	7.28	12.41	7.132
488.0	-38.6	186.5	5.43	2.99	14.14	8.417
490.0	-8.7	1236.2	2.55	22.74	12.06	8.676
490.8	43.7	12.2	21.67	12.68	9.989	5.644
492.3	38.9	31.2	10.40	8.87	11.05	7.436
493.0	48.8	1527.1	3.06	5.85	10.73	7.451
495.0	68.0	774.4	4.30	4.07	12.75	8.121
496.7	37.5	5964.4	0.96	9.16	11.98	7.349
497.8	-1.7	663.2	2.50	2.68	12.53	7.119
498.9	50.2	402.1	2.62	2.68	8.957	5.932
500.6	38.6	3059.3	1.62	2.91	12.79	7.308
501.6	44.7	7565.5	0.85	5.57	10.81	6.177
503.3	43.6	366.5	3.87	3.96	15.60	7.326
504.8	40.6	71.8	10.61	2.40	11.13	7.420
505.9	49.0	264.5	7.36	3.31	10.59	7.457
508.7	53.8	95.9	9.17	2.98	16.10	7.666
510.7	50.9	2477.0	1.29	3.96	8.358	5.804
513.5	-38.3	190.4	4.66	2.79	14.28	8.073
516.5	46.3	222.9	6.01	2.50	12.56	8.103
519.8	8.5	49.5	8.21	3.94	11.88	7.244
521.8	16.5	626.3	4.78	1.16	13.93	7.782
524.1	29.9	1096.5	2.26	3.21	15.57	7.462
526.4	44.5	1227.6	2.11	7.74	12.39	6.883
529.6	45.6	504.7	5.33	2.82	13.91	7.358
532.0	10.8	125.1	6.63	1.78	8.093	5.951
536.4	52.3	193.1	6.45	3.71	9.787	5.468
538.7	32.1	232.3	5.88	1.78	11.31	7.204
541.1	47.1	4053.8	1.01	11.76	17.22	8.610
542.3	61.0	1032.7	2.30	7.13	13.89	7.847
544.8	27.3	84.2	7.02	2.37	9.250	5.968
548.0	-37.0	103.8	11.77	0.150	2.251	1.407
551.5	31.0	249.7	7.58	1.56	12.11	7.475
554.0	-2.1	64.3	9.26	0.879	10.82	6.936
555.2	67.4	95.8	12.26	1.42	12.39	6.961
558.2	58.9	280.5	7.15	1.54	13.81	8.124
561.0	37.3	5.8	38.85	0.636	10.68	5.235
563.3	75.5	142.5	7.54	0.627	13.06	8.214
567.4	49.6	8.3	32.05	2.55	8.142	5.733

570.4	14.1	48.1	9.31	0.611	10.25	6.529
YM#17	cont.					
572.4	-27.0	178.3	15.00	0.156	7.758	5.388
577.2	-38.5	4069.5	1.01	3.41	9.989	5.946
582.3	-58.4	13.1	33.72	1.99	10.40	5.810
586.9	-2.7	104.0	11.75	1.09	8.065	4.505
592.8	7.0	9.1	25.07	1.34	7.103	4.028
595.0	-23.1	9.8	38.94	0.578	7.933	5.433
596.6	-58.2	120.4	8.18	0.820	17.72	10.011
599.2	-24.7	140.4	6.25	0.853	6.964	4.352
602.8	-54.1	32.4	13.12	0.551	5.144	3.622
603.7	-47.3	89.6	12.67	0.989	9.543	5.927
609.4	-49.9	54.4	8.76	1.13	6.901	5.434
613.7	10.5	114.1	6.94	2.82	10.07	6.333
616.7	8.0	63.0	9.36	0.592	8.637	6.039
619.8	38.8	141.0	6.24	1.91	12.70	7.888
624.4	-29.7	27.1	14.33	0.416	5.744	3.616
628.8	-37.1	190.2	3.82	2.81	10.30	7.007
629.2	15.1	155.1	5.17	0.532	10.49	6.856
632.2	50.8	55.9	12.04	1.79	11.94	6.708
634.5	34.7	223.0	4.31	2.21	10.02	5.726
637.5	62.9	49.0	12.89	4.63	15.38	8.268
639.9	17.1	848.1	2.21	6.20	13.95	8.454
642.4	30.6	151.1	5.24	3.68	13.97	7.592
645.9	48.0	997.1	2.34	2.55	8.372	5.896
648.2	51.7	1529.0	1.89	4.92	11.98	6.925
650.4	36.6	35.8	20.11	0.757	10.35	6.235
658.2	-20.0	23.6	18.58	0.437	2.112	1.040
661.8	26.0	46.2	8.51	1.01	8.365	6.062
663.8	37.8	13.9	14.44	0.827	10.64	6.527
666.7	23.6	80.1	8.29	3.03	11.14	7.427
672.2	-59.8	2283.2	1.87	1.15	7.493	3.345

SAMPLE (Depth)	INCL. (^{o})	kappa	a95	NRM Intens. ($x10^{-5}$ A/m)	SI Susceptibility Bulk Sus ($x10^{-4}$)	Sus/gm ($x10^{-5}$)
YM#53						
.4	59.4	2910.7	0.97	0.992	8.608	4.597
1.4	60.8	170.7	3.74	0.087	6.942	3.364
2.9	-19.4	917.2	1.90	0.942	5.080	3.654
4.0	-42.9	143.7	4.81	0.860	5.018	3.610
5.2	-57.8	252.9	7.53	0.272	6.711	4.726
8.7	42.8	736.9	1.79	3.39	5.150	4.087
10.0	41.0	371.6	2.73	0.137	4.416	3.371
11.6	53.1	139.8	10.14	0.992	7.243	5.249
14.4	52.5	31.5	8.25	1.66	6.795	4.300
15.9	45.8	100.4	5.76	0.137	3.534	2.618
16.3	16.5	92.6	7.71	0.131	3.450	3.165
17.7	42.6	69.7	6.32	0.163	7.474	4.917
19.3	61.4	1068.9	1.61	0.209	4.178	3.289
20.5	44.9	112.4	4.60	5.23	7.138	4.224
22.0	63.2	34.6	9.13	1.00	5.955	4.194
23.0	51.2	670.9	2.22	0.514	4.962	3.121
24.4	63.3	243.0	4.13	0.677	5.213	2.979
25.8	56.0	286.0	4.38	0.575	4.752	4.483
26.8	7.7	23.0	12.13	3.10	7.649	4.421
27.9	56.6	274.0	7.23	0.189	5.066	3.838
29.2	31.2	209.7	3.36	0.660	4.563	3.709
31.7	-60.3	915.2	1.61	0.254	7.649	4.636

SAMPLE (Depth)	INCL. (^{o})	kappa	a95	NRM Intens. ($x10^{-5}$ A/m)	SI Susceptibility Bulk Sus ($x10^{-4}$)	Sus/gm ($x10^{-5}$)
TREN#17						
1.0	59.2	23.2	6.31	0.963	6.325	3.628
2.0	57.6	18.4	8.83	0.665	5.299	3.284
3.0	58.4	27.0	7.14	0.859	7.485	4.629
4.0	45.9	17.4	9.57	0.681	4.885	3.015
4.8	40.1	9.5	14.51	3.029	4.299	2.755
5.8	29.8	46.9	4.34	1.837	8.018	5.309
6.8	47.5	42.8	4.28	1.655	5.651	3.724
8.0	43.0	84.1	2.77	3.090	6.100	3.297
9.0	51.0	41.6	3.95	3.264	8.293	5.327
10.0	42.3	21.5	6.91	4.608	6.718	4.764
11.0	35.8	24.6	5.20	3.785	7.373	4.444
12.0	48.6	40.9	4.59	2.724	3.724	2.470
13.0	31.8	435.3	1.54	4.106	6.325	3.628
14.0	25.6	19.8	6.28	2.790	6.277	3.753